Remotely-sensed sea-ice and chlorophyll a variability in the Beaufort Sea from 1998 to 2020

Ryan Galley, Emmanuel Devred, Andrea Hilborn, and Christine Michel

Fisheries and Oceans Canada
Freshwater Institute
501 University Cresent
Winnipeg, Manitoba
Canada, R3T 2N6

2022

Canadian Technical Report of Hydrography and Ocean Sciences 339

Fisheries and Oceans Canada | Pêches et Océans Canada

Canada

Canadian Technical Report of Hydrography and Ocean Sciences

Technical reports contain scientific and technical information of a type that represents a contribution to existing knowledge but which is not normally found in the primary literature. The subject matter is generally related to programs and interests of the Oceans and Science sectors of Fisheries and Oceans Canada.

Technical reports may be cited as full publications. The correct citation appears above the abstract of each report. Each report is abstracted in the data base *Aquatic Sciences and Fisheries Abstracts.*

Technical reports are produced regionally but are numbered nationally. Requests for individual reports will be filled by the issuing establishment listed on the front cover and title page.

Regional and headquarters establishments of Ocean Science and Surveys ceased publication of their various report series as of December 1981. A complete listing of these publications and the last number issued under each title are published in the *Canadian Journal of Fisheries and Aquatic Sciences*, Volume 38: Index to Publications 1981. The current series began with Report Number 1 in January 1982.

Rapport technique canadien sur l'hydrographie et les sciences océaniques

Les rapports techniques contiennent des renseignements scientifiques et techniques qui constituent une contribution aux connaissances actuelles mais que l'on ne trouve pas normalement dans les revues scientifiques. Le sujet est généralement rattaché aux programmes et intérêts des secteurs des Océans et des Sciences de Pêches et Océans Canada.

Les rapports techniques peuvent être cités comme des publications à part entière. Le titre exact figure au-dessus du résumé de chaque rapport. Les rapports techniques sont résumés dans la base de données *Résumés des sciences aquatiques et halieutiques*.

Les rapports techniques sont produits à l'échelon régional, mais numérotés à l'échelon national. Les demandes de rapports seront satisfaites par l'établissement auteur dont le nom figure sur la couverture et la page de titre.

Les établissements de l’ancien secteur des Sciences et Levés océaniques dans les régions et à l'administration centrale ont cessé de publier leurs diverses séries de rapports en décembre 1981. Vous trouverez dans l'index des publications du volume 38 du *Journal canadien des sciences halieutiques et aquatiques*, la liste de ces publications ainsi que le dernier numéro paru dans chaque catégorie. La nouvelle série a commencé avec la publication du rapport numéro 1 en janvier 1982.

Canadian Technical Report of
Hydrography and Ocean Sciences 339

2022

REMOTELY-SENSED SEA-ICE AND CHLOROPHYLL *a* VARIABILITY IN THE BEAUFORT SEA FROM 1998 TO 2020

by
Ryan Galley, Emmanuel Devred, Andrea Hilborn, and Christine Michel

Fisheries and Oceans Canada
Freshwater Institute
501 University Crescent
Winnipeg, Manitoba
Canada, R3T 2N6

Cat. No. Fs.97-18/339E-PDF ISBN 978-0-660-41332-7 ISSN 1488-5417

Correct Citation for this publication:

Galley, R., Devred, E., Hilborn, A, Michel, C. 2022. Remotely-sensed sea-ice and chlorophyll *a* variability in the Beaufort Sea from 1998 to 2020. Can. Tech. Rep. Hydrogr. Ocean Sci. 339: x + 90 p.

CONTENTS

List of Figures

ABSTRACT

Galley, R., Devred, E., Hilborn, A., Michel, C. 2022. Remotely-sensed sea-ice and chlorophyll *a* variability in the Beaufort Sea from 1998 to 2020. Can. Tech. Rep. Hydrogr. Ocean Sci. 339: x + 90 p.

Physical and biological systems in Canada's western marine Arctic are changing rapidly; satellite information can aid in the assessment of status and trends in marine ecosystems, and help illuminate their response to climate change. A 23-year time series (1998-2020) of chlorophyll *a* concentration derived from ocean colour satellites, namely Sea-viewing Wide Field-of-view Sensor (SeaWIFs, 1998 - 2002) and the MODerate resolution Imaging Spectroradiometer (MODIS, 2003-2020), is presented in this report for the Canadian Beaufort Sea, Amundsen Gulf, M'Clure Strait, and Dolphin and Union Strait, extending from Northwest Territories to Nunavut. The intercalibration of these data from two different sensors is explained, and the images of chlorophyll *a* concentration for the entire time series are binned in annual and 8-week composites. Chlorophyll *a* biomass is analysed in the context of the annual evolution of sea ice in the study region by stage of development (old ice, first-year sea ice, and young-plus-new sea ice) over the same 23-year period at the same spatial resolution using the Canadian Ice Service digital archive. Two subregions of particular interest are considered, one offshore in the Canada Basin, and one adjoining the west coast of Banks Island. Bathymetry, sea-ice properties and processes differ significantly between these two areas, which impact the phenology and biomass of primary producers which also differ in these two regions. Inter-annual, intra-annual, and spatial variability in chlorophyll *a* concentration, and in sea-ice concentration and type are high in the study region and the two subregions presented.

RÉSUMÉ

Galley, R., Devred, E., Hilborn, A., Michel, C. 2022. Remotely-sensed sea-ice and chlorophyll *a* variability in the Beaufort Sea from 1998 to 2020. Can. Tech. Rep. Hydrogr. Ocean Sci. 339: x + 90 p.

Les systèmes physiques et biologiques de l'Arctique marin occidental du Canada évoluent rapidement; l'information satellitaire peut contribuer à l'évaluation de l'état et des tendances des écosystèmes marins et à la compréhension de leur réponse au changement climatique. Une série temporelle de 23 ans (1998-2020) de la concentration en chlorophylle *a* dérivée des satellites de couleur de l'océan, à savoir le Sea-viewing Wide Field-of-view Sensor (SeaWIFs, 1998 - 2002) et le MODerate resolution Imaging Spectroradiometer (MODIS, 2003-2020), est présentée dans ce rapport pour la région canadienne de la mer de Beaufort, le golfe d'Amundsen, le détroit de M'Clure et les détroits de Dolphin et d'Union, des Territoires du Nord-Ouest au Nunavut. L'intercalibration de ces données provenant de deux capteurs différents est expliquée, et les concentrations en chlorophylle *a* pour l'ensemble de la série temporelle sont regroupées en composites annuelles et de 8 semaines. La biomasse chlorophyllienne est analysée dans le contexte de l'évolution annuelle de la glace de mer dans la région étudiée en utilisant les données des archives numériques par stade de développement (vieille glace, glace de mer de première année et glace de mer jeune + nouvelle) sur la même période de 23 ans à la même résolution spatiale obtenues du Service Canadien des glaces. Deux sous-régions d'intérêt particulier sont considérées, l'une au large du bassin Canadien, et l'autre jouxtant la côte ouest de l'île Banks. La bathymétrie, les propriétés et les processus de la glace de mer diffèrent considérablement dans ces deux zones, ce qui a un impact sur la phénologie et la biomasse des producteurs primaires qui diffère également dans ces deux régions. La variabilité inter-annuelle, intra-annuelle et spatiale de la concentration en chlorophylle *a*, ainsi que de la concentration et du type de glace de mer est élevée dans la région d'étude et les deux sous-régions présentées.

1 Introduction

The Arctic is warming three times faster than the rest of the world and its ecosystems are rapidly changing (AMAP, 2021). Sea ice declines expose large areas of the Arctic Ocean to open water conditions and extend the open water phytoplankton growth period (e.g., Kahru et al., 2016). Conversely, intensification of the surface stratification, linked to increasing freshwater content, tends to isolate surface primary producers from nutrients at depth, impacting species composition and potential productivity (e.g., Li et al., 2009; Coupel et al., 2015; Ardyna and Arrigo, 2020). In marine ecosystems, fisheries productive capacity is directly linked to the amount of primary production. In the Arctic Ocean, the extreme phenological and spatial variations in the distribution of primary producers are even more critical for energy transfers to higher trophic levels than at temperate latitudes. Therefore, sustainable management of current and future potential fisheries resources requires a better understanding of changes in the amount, type, seasonality, and distribution of primary producers. Current satellite-based estimates show increasing trends in primary productivity over the past two decades in all regions of the Arctic Ocean, although the trend was not significant for the Beaufort Sea region (Frey et al., 2020; Lewis et al., 2020). Satellite-derived estimates also show a northward expansion and increase in spring primary production (Renaut et al., 2018). Many pan-Arctic scale studies of primary production, and of sea ice, consider some or all of the Canada Basin and the Beaufort Sea area as a single subregion within the Arctic Ocean (e.g., Arrigo and van Dijken, 2011, 2015). Conversely, process studies of smaller Arctic marine regions are more typically done using *in situ* data (e.g., Ardyna et al., 2017).

Marine ecosystems throughout Canada's Arctic, including the Beaufort Sea have undergone major changes over the past decades (Michel, 2013; Niemi et al., 2019). Most evident over the past 40 years are changes to the sea-ice scape of the Beaufort Sea/Canada Basin that impact the area's primary productivity. Changes in the melt season length (Stroeve et al., 2014) and decreasing sea-ice season length (Parkinson, 2014) have been recently documented. The region has also experienced substantial changes to the predominant sea-ice stages of development, the duration of the open water season, and a delay in annual

freeze up timing (Galley et al., 2016). These changes affect the amount of solar energy that reaches the ocean surface, which is relevant for both photosynthesis and the heat budget that in turn influence sea-ice melt and freeze up (Perovich et al., 2011; Babb et al., 2016). Freshwater inputs from both runoff and increasing sea-ice melt in the Beaufort Sea specifically influence the strength of the upper ocean stratification which initially favors primary production, before reducing the ability of nutrients at depth to be mixed to the surface layer for use by primary producers (McLaughlin and Carmack, 2010; Jackson et al., 2011; Nummelin et al., 2016). Understanding and quantifying changes in sea-ice regime and the marine ecosystem at regional scales requires the use of adapted tools such as satellite remote sensing, which provide a synoptic view of the marine ecosystem with high revisit frequency.

This report presents medium-resolution remotely-sensed chlorophyll *a* concentration and sea-ice datasets from 1998 to 2020 in the Canadian Beaufort Sea. Data visualization depicts the phenology of primary producers and seasonal evolution of the sea-ice cover, informing changes in primary production in the Beaufort Sea in relation to sea-ice conditions and seasonal dynamics over the past two decades.

2 Data and Methods

2.1 Study Region

The geographic extent of the study region is 67.5ºN - 76ºN, and 142ºW - 110ºW (Figure 1). The region contains several Ecologically and Biologically Significant Areas (EBSAs) identified for the Western Arctic Region (DFO, 2014) and overlaps with the Beaufort Sea Large Ocean Management Area (Cobb et al., 2008). Within this study area, two sub-regions were identified for a more focused analysis: the Offshore Beaufort Sea subregion and the Western Banks Island subregion (Figure 1). The offshore Beaufort Sea subregion was created using a neural network analysis of all the Moderate Resolution Imaging Spectroradiometer (MODIS) imagery between 2003 and 2019 at 1.1-km resolution for sea-surface temperature (SST), suspended particulate matter (SPM) and chlorophyll *a* concentration (A. Hilborn, pers.

comm.), while the geographic extent of the Western Banks Island EBSA (DFO, 2014) is used to delineate the Western Banks Island subregion.

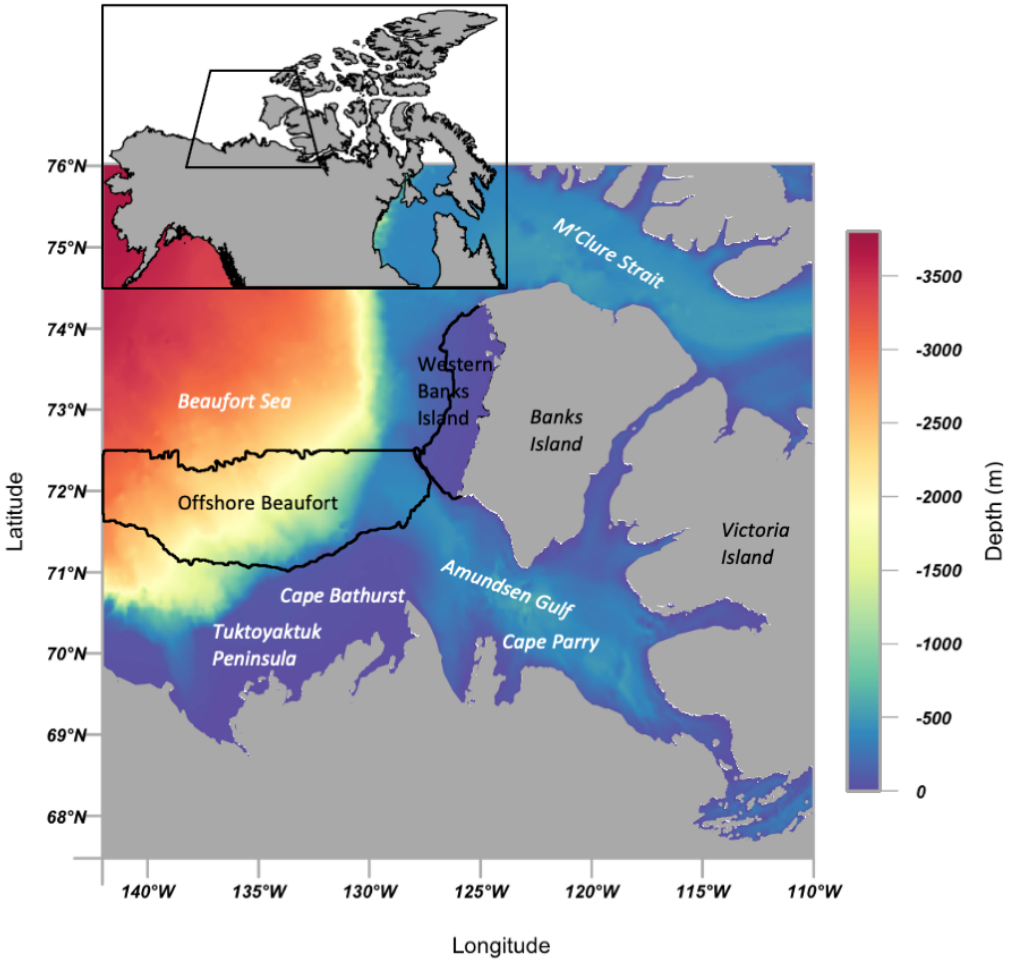

Figure 1: ETOPO1 (NOAA, 2009) bathymetric map (*in meters*) of the study region within Canada's western marine Arctic bioregion. The offshore Beaufort Sea and Western Banks Island sub-regions are delineated in black.

2.2 Satellite Data

2.2.1 Chlorophyll a concentration

Chlorophyll *a* concentrations (chl *a*, mg m^{-3}) reported here (1998-2020) were derived from remote-sensing analysis of the Sea-viewing Wide Field-of-view Sensor (SeaWiFS, 1998-2002) and the MODIS instrument aboard the Aqua satellite (MODIS-Aqua, 2003-2020) (Figure 2a). Images intersecting the region 67.5°N to 76°N and 142°W to 110°W (Figure 1) were identified by querying the EARTHDATA Common

Metadata Repository Search site (https://cmr.earthdata.nasa.gov/search/) using the R packages *httr* and *jsonlite*, and downloaded from the NASA Ocean Biology Processing Group (OBPG) website (https://oceancolor.gsfc.nasa.gov). Images with very low data coverage (< 100 pixels) were discarded.

SeaWiFS data at 1.1 km resolution (merged local area coverage, MLAC) were acquired for the study region at processing level 2 (i.e. geophysical variables and remote sensing reflectance (Rrs)), with Rrs already calculated using the near-infrared atmospheric correction method. Processing flags associated with the OBPG files were used to remove pixels (i) intersecting land (LAND flag), (ii) under high satellite zenith angle conditions, where the satellite is tilted greater than 60° from zenith (HISATZEN flag), and (iii) containing the standard OBPG flag for high solar zenith angle (HISOLZEN flag), which restricts data collection to sun angle less than 70° from zenith. Grid cells with negative Rrs at 555 and 670 nm were also removed. The resulting images were gridded and daily composites were created. SeaWiFS data (1998-2002) reported here consisted of 3,656 level-2 images (i.e., single satellite pass) yielding 725 total daily composites between March and October in 1998-2002. The average days per year where a daily composite was created using SeaWiFS data was 145.

Unprocessed full-resolution MODIS-Aqua instrument data were acquired from the OBPG and processed to level 2 (28899 images) with the *l2gen* program distributed with open-source SeaDAS software (https://seadas.gsfc.nasa.gov, last accessed on November 26th, 2021) using the near-infrared/shortwave-infrared switching atmospheric correction algorithm (Wang and Shi, 2007). All MODIS images with pixels at the direct outlet of the Mackenzie River were processed twice (after Doxaran et al., 2015), using a raised maximum cloud albedo threshold of 0.4 (instead of the recommended 0.027 cloud albedo threshold) to recover pixels in high suspended particulate matter (SPM) conditions that are typically removed due to brightness in the near-infrared bands. Images with raised cloud albedo were cropped to retain only the pixels near the Delta, and later combined with their counterpart when creating the daily composites. The resulting processed satellite images contained atmospherically-corrected Rrs and other parameters (e.g., SST, Kd_{490}), as well as the solar zenith angle at each pixel. The solar zenith angle layer was employed to remove grid cells whose sun angle exceeded 74° (IOCCG, 2015), and grid cells with negative Rrs at 555 and 667 nm

were also removed. The MODIS data (2003-2020) yielded 2,941 daily composites between March and October in 2003-2020. The average days per year where a daily composite was created with MODIS data was 163.

Chlorophyll *a* from both instruments was calculated from the filtered level 2 Rrs using a recently calibrated empirical algorithm for the Arctic Ocean (referred to as AOEmp; Lewis and Arrigo, 2020). Chl *a* from the SeaWiFS Rrs data was calculated in Python v.3.7.3 using the 443, 490 and 555 nm bands, while chl *a* from MODIS used Rrs at 443, 488 and 547 nm. All processed images were projected on a regular grid at 1.1 km resolution using the Generic Mapping Tools (GMT) software (Wessel et al., 2013; https://www.generic-mapping-tools.org), and all individual satellite passes on any given day were combined using R software into daily composites using the median value at each grid cell, with chl *a* range restricted from 0.05 to 40 mg m^{-3} (https://www.r-project.org).

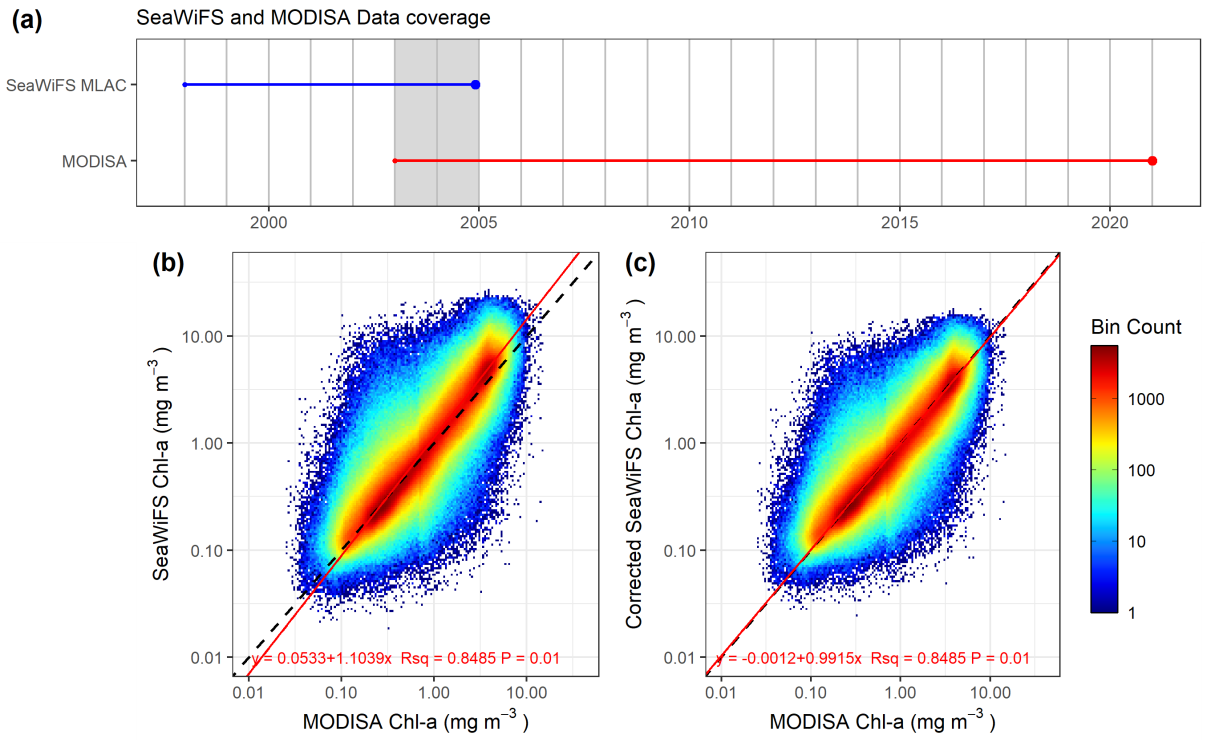

Figure 2: (a) SeaWiFS and MODIS-Aqua 1.1 km resolution records from 1998 through 2020 showing overlap for the years 2003 and 2004; (b) linear type 2 major axis regression between concurrent SeaWiFS and MODIS-Aqua chlorophyll *a* (chl *a*) pixels before correction, and (c) regression after adjustment of the SeaWiFS chl *a* data. Regressions are in $\log_{10}$ space, the 1:1 line is shown dashed in black, and the slope of the regression is in red in panels b and c.

2.2.2 SeaWiFS and MODIS-Aqua chlorophyll a intercalibration

Inherent differences in chl *a* derived from different ocean colour sensors exist due to differences in satellite characteristics (e.g., atmospheric correction scheme, wavebands, and calibration approach) such that ocean colour satellites require intercalibration to obtain continuous, climate compatible time series. We assessed the agreement between chl *a* using concurrent pixels from MODIS and SeaWiFS in all daily composites between 2003 and 2004 when both sensors were collecting data (N = 248, Figure 2a). MODIS chl *a* were used as the reference since MODIS is the longest running time series. A pre-quality control included discarding pixels containing the upper and lower 1% of chl *a* in every daily composite (i.e., potential outliers). A linear type-2 major-axis regression (*lmodel2* R package) of SeaWiFS chl *a* against MODIS chl *a* was carried out to determine potential bias in SeaWiFS data (slope 1.1039 ± 0.0005 and intercept 0.0533 ± 0.0001, with confidence intervals at 2.5 and 97.5%). This analysis indicated SeaWiFS chl *a* were slightly lower than MODIS chl *a* below 1.0 mg m^{-3} and slightly higher than MODIS-derived values above 1.0 mg m^{-3} (Figure 2b). The SeaWiFS daily composites of chl *a* were then adjusted using the regression model which improved statistics when compared to MODIS chl *a* (slope 0.9915 ± 0.0004, intercept -0.0012 ± 0.00004 in $\log_{10}$ space, Figure 2c). We assumed that this relationship improved the SeaWiFS chl *a* estimates from 1998 through 2002, and used the adjusted values in this analysis.

Each daily composite image was assigned its year-week (YW) using the ISO 8601 date convention. The top and bottom 1% of the chl *a* concentration data were removed from all (1998-2020) daily images prior to any further computation. The mean chl *a* concentration in each 1.1 km resolution grid cell (n = 507559) was calculated for each two-YW interval beginning at YW18-19 (roughly the last two weeks of April), and ending at YW40-41 (roughly the first two weeks of October) in each year, and the number of occurrences of chl *a* in each grid cell was recorded for each two-YW interval. The chl *a* weighted means in each grid cell for the annual period (YW18-19 to YW40-41) and the three 8-YW periods; YW18-25 (mid-April to mid-June), YW26-33 (mid-June to early August), and YW34-41 (mid-August to early October), were computed using the 2-YW mean chl *a* during that period weighted by the occurrence data in each grid

cell in the period. These mean chl *a* were mapped on a $\log_{10}$ scale for the entire study region (Appendix A, Figures A.1 to A.23) with two subregions, Offshore Beaufort (53721 grid cells), and western Banks Island (14610 grid cells) outlined in a solid black line. White areas indicate the absence of chl *a* data in those grid cells in the period of interest, which may be due to sea-ice cover and/or cloud cover. The chl *a* standard deviation (mg m^{-3}) for each year (YW18-19 to YW40-41) and in the same three periods of eight year-weeks (YW18-25, YW26-33, and YW34-41) in each grid cell in each year were also calculated and mapped in the entire study region (Appendix B, Figures B.1 to B.23).

2.2.3 Regional Sea-Ice Concentration

The Canadian Ice Service (CIS) digital archive data used for sea-ice analysis was downloaded from the CIS digital archive (https://iceweb1.cis.ec.gc.ca/Archive/page1.xhtml?lang=en) for the western Arctic region between 1998 and 2020. These charts are created manually by expert interpretation of remotely-sensed, ship, and airborne observations (Fequet, 2005) and are made freely available as projected vector files of sea-ice concentration. Polygons within these data files include total concentration (in tenths) and up to three partial concentrations (in tenths) that are categorized by their stage of development using the World Meteorological Organization egg code. Historically, these charts were operational products, and as such have not been created for each week of each year. Before 2012 a combination of monthly, bi-weekly, and weekly charts was made available by the CIS. Since 2012 weekly charts have been produced. Each polygonal chart, in its original Lambert Conformal Conic projection, was gridded at 1.1 km using the centroids of the MODIS grid cells. The year-week for each chart was calculated using the ISO 8601 date convention.

Annual stacked bar charts of the regional proportion of three sea-ice stages of development, namely old ice, first-year sea ice, and young-plus-new sea ice (< 30cm thick), were created (Appendix C, Figure C.1 panel a for example). For each year-week, the individual grid cell concentrations were summed for each stage of development and the result was then divided by the number of grid cells in the region

multiplied by 10 (i.e. the maximum possible sea-ice concentration in the region) yielding the decimal fraction of the region covered by each stage of development at each YW in each year.

The minimum sea-ice concentration in each grid cell in each of the three 8-YW chl *a* periods used (YW18-25, YW26-33, and YW34-41) was also mapped to provide information on the open water area in the region and highlight missing chl *a* pixels that might be caused by cloud cover (Appendix C, Figure C.1, panels b, c, and d for example).

3 Results and Discussion

3.1 Annual mean chlorophyll *a* concentration

The regional mean chl *a* maps in Appendix A provide a comparative assessment of the magnitude and distribution of chl *a* for each year in the entire study region, and in the two subregions. The eight-YW periods show the spatio-temporal evolution of chl *a* in each year, elucidating the seasonality and phenology of the productive season within each annual cycle. Note that the approximate location of the Cape Bathurst flaw lead polynya complex may be reliably inferred from the mean chl *a* map for YW18-25 in many of the 23 years presented here (e.g., Figure A.9 panel b in 2006).

In the Offshore Beaufort subregion, chl *a* was highly variable annually and inter-annually. In some years the subregion almost completely lacked chl *a* data (eg., Figure A.16), which may have been due to sea ice like in 2013 (Figure C.16), or cloud cover in some other years or periods. In other years the subregion exhibited persistent, high chl *a* values (e.g., 2012, Figure A.15), which was due to very low sea-ice cover in the region (Figure C.15). Intrusion of the Mackenzie River plume into the Offshore Beaufort subregion has also been variable inter-annually. For example, in 2006 (Figure A.9) high chl *a* values extending from the nearshore Mackenzie River plume were present in the YW34-41 period, whereas the influence of the river on the surface appeared to be more constrained in other years (e.g., 2004, Figure A.7).

Influence of the Mackenzie River was undetected in the Western Banks Island subregion, contrasting it with the Offshore Beaufort subregion. This subregion overlaps substantially with the proposed

Banks Island Westerly Gradient eco-unit, which lacks river influence (DFO, 2015). The Western Banks Island subregion contains a meridional portion of the regional flaw lead system, especially in the YW18-25 period (e.g., Figure A.12), a time of year when comparatively little chl *a* data exist in the region. The Western Banks Island subregion typically contained chl *a* data in the second and third 8-YW periods (YW26-41), though in 2018 the subregion contained almost no chl *a* data throughout the study period (Figure A.21) due to high sea-ice cover (Figure C.21). In this subregion, the chl *a* values were typically higher close to the coast of Banks Island than farther offshore.

3.2 Annual chlorophyll *a* standard deviation

The standard deviation maps document the spatio-temporal variability in chl *a*, which may reflect episodically high chl *a* values (possibly phytoplankton blooms) in individual years, or within the three 8-YW periods. Much of the variability in chl *a* occurred along the continental shelf and slope north of the Mackenzie River Delta and the Tuktoyaktuk Peninsula, but chl *a* variability was also substantial in some years and periods around Cape Bathurst (Figure B.15d), in Franklin Bay (Figure B.19c), in eastern Amundsen Gulf (Figure B.20d), and in M'Clure Strait in 1998 (Figure B.1b).

The chl *a* standard deviation for each year, and in the 8-YW periods annually, was generally low in both the Offshore Beaufort and Western Banks Island subregions. In the Offshore Beaufort subregion, elevated chl *a* standard deviations occurred towards the southwestern boundary of the region (e.g., Figure B.8d, B.11c, B. 15c). In the Western Banks Island subregion, high standard deviations occurred mainly towards the southwest coast of Banks Island (e.g., Figure B.9d, B.15d) but were also observed in the northernmost area of the subregion (e.g., Figure B.2c).

3.3 Annual sea-ice coverage

The annual variability of old sea-ice coverage (Appendix C, panel a in Figures C.1 to C.23) indicates in part the prevalence of dynamic and/or thermodynamic sea-ice processes within the region each year. Annual increases in regional old ice coverage (e.g., Figures C.1a, C.13a) typically indicate old ice has

been imported into the study region, usually from the north (e.g., Galley et al., 2013). An abrupt increase in old ice coverage in autumn is a function of the first-year sea ice in the region that has survived the summer, which is reclassified as old ice in the fall as it begins to undergo its second annual thermodynamic cycle (Fequet, 2005). Dramatic reductions in the percent coverage of old ice within years (e.g., Figure C.15a) have also occurred, which have been attributed to thermodynamic melt in place within the region, and/or dynamic export out of the study region, usually to the west (Perovich et al., 2011; Galley et al., 2013; Babb et al., 2016). Within the sea-ice concentration bar charts (Figures C.1 to C.23, panel a), the interplay between thicker first-year sea ice, and the thinner new-plus-young sea-ice stages of development also offers some insight into the evolution of physical processes at the surface in the region. In the winter and spring (~ prior to YW 20, or Mid-May) there was almost no interannual or annual variation in the sea-ice cover. However, the presence and persistence of the young-plus-new sea ice stage of development prior to the onset of melt is a good proxy indicator for the extent and duration of the flaw lead polynya system, a physically and biologically significant component of the ecosystem in the region (Carmack and Macdonald, 2002). In the late summer and fall, (after about YW 37, the beginning of September) the increasing percent cover of young-plus-new sea ice is indicative of the start of regional freeze up, and the total sea-ice coverage composed of the three stages of development indicate the speed with which the region becomes completely ice covered. Young-plus-new sea ice is reclassified as first-year sea ice once its thickness exceeds 30 cm, resulting in the typical autumnal increase in the coverage of the first-year stage of development denoting thickening.

Within any year, the minimum sea-ice concentration maps for each of the 8-YW periods (YW18-25, YW26-33, and YW34-41, Figures C.1 to C.23, panels b, c, and d respectively) show the seasonal evolution of the open water area within the study region including the two subregions. Inter-annually, the maps provide a basis to compare the timing and spatial extent of open water in the region in the spring, summer, and fall in each year and aid interpretation of chl *a* dynamics.

The mean total sea-ice concentrations for each YW in each year are presented in line plots for each of the 23 years in the Offshore Beaufort (53731 grid cells) (Figure D.1), and Western Banks Island (14610

grid cells) subregions (Figure D.2). These yearly plots show the intra- and inter-annual variability of the sea ice cover within the two subregions over the time series presented here, and lend some insight into both the dynamic and thermodynamic processes that variably affect it.

4 Conclusion

This report provides a compilation and preliminary analysis of 23 years of satellite remote-sensing data on chlorophyll *a* and sea ice in Canada's western marine Arctic and presents in detail the methodology used to create this first-order analysis. Regional maps of annual and 8-weeks averages of chl *a* are presented together with standard deviations for the same periods, providing insights into spatial, annual, and inter-annual variability in primary production processes. Sea ice conditions are summarized via regional maps and annual trends in average sea ice concentration and sea ice type. Minimum sea ice concentration maps over 8-week periods are also presented, informing changes and variability in open water conditions and linking to estimates of chl *a*. The regional analysis presented reveals high annual and inter-annual variability in both the physical and biological datasets, and points to important linkages between the two systems. Further, spatial differences and mesoscale variability within the Beaufort Sea study region, highlighted here by the Offshore Beaufort and western Banks Island subregions, emphasizes the importance of elucidating regional responses in order to understand and predict the impacts of climate change on Arctic Ocean productivity.

5 Acknowledgements

This study was supported by DFO's Results Funds to CM and ED. Some satellite processing code and parts of the satellite dataset presented here were generated during the 2019-2022 Arctic Science Fund project entitled, "Measuring the impact of permafrost thaw and river export on the health of the coastal arctic ecosystem using satellite observation of Ocean Colour and hydrodynamic simulation: case study of MPAs in the Southern Beaufort Sea".

6 References

AMAP, 2021. Arctic Climate Change Update 2021: Key Trends and Impacts. Summary for Policy-makers. Arctic Monitoring and Assessment Programme (AMAP), Tromsø, Norway. 16 pp.

Ardyna, M., Babin, M., Devred, E., Forest, A., Gosselin, M., Raimbault, P., and Tremblay, J.-E. 2017. Shelf-basin gradients shape ecological phytoplankton niches and community composition in the coastal Arctic Ocean (Beaufort Sea). Limnology and Oceanography, 62, doi: 10.1002/lno.10554.

Ardyna, M., and Arrigo, K. R. 2020. Phytoplankton dynamics in a changing Arctic Ocean. Nature Climate Change, 10, 892-903, doi: 10.1038/s41558-020-0905-y.

Arrigo, K. R., and van Dijken, G. L. 2011. Secular trends in Arctic Ocean net primary production. Journal of Geophysical Research, 116, C09011, doi: 10.1029/2011JC007151.

Arrigo, K. R., and van Dijken, G. L. 2015. Continued increases in Arctic Ocean primary production. Progress in Oceanography, 136, 60-70, doi: 10.1016/j.pocean.2015.05.002.

Babb, D. G., Galley, R. J., Barber, D. G., and Rysgaard, S. 2016. Physical processes contributing to an ice-free Beaufort Sea during September 2012. Journal of Geophysical Research, 121, doi: 10.1002/2015JC010756.

Carmack. E. C., and Macdonald, R. W. 2002. Oceanography of the Canadian Shelf of the Beaufort Sea: A setting for marine life. Arctic, 55(supp. 1), 29-45, doi: 10.14430/arctic733.

Cobb, D., Fast, H., Papst, M. H., Rosenberg, D., Rutherford, R., and Sareult, J. E. (Editors). 2008. Beaufort Sea Large Ocean Management Area: Ecosystem Overview and Assessment Report. Can. Tech. Rep. Fish. Aquat. Sci. 2780: ii-ix + 188 p.

Coupel, P., Ruiz-Pino, D., Sicre, M.-A., Chen, J. F., Lee, S. H., Schiffrine, N., Li, L., and Gascard, J.-C. 2015. The impact of freshening on phytoplankton production in the Pacific Arctic Ocean. Progress in Oceanography, 131, 113-125, doi: 10.1016/j.pocean.2014.12.003.

DFO. 2014. Re-evaluation of ecologically and biologically significant areas (EBSAs) in the Beaufort Sea. DFO Can. Sci. Advis. Sec. Sci. Advis. Rep. 2014/052.

DFO. 2015. Eco-units and potential Priority Conservation Areas in the Western Arctic Bioregion. DFO Can. Sci. Advis. Sec. Sci. Advis. Rep. 2015/021.

Doxaran, D., Devred, E., and Babin, M. 2015. A 50% increase in the mass of terrestrial particles delivered by the Mackenzie River into the Beaufort Sea (Canadian Arctic Ocean) over the last 10 years. Biogeosciences, 12, 3551-3565. doi:10.15194/bg-12-3551-2015.

Fequet, D. 2005. Manual of Standard Procedures for Observing and Reporting Ice Conditions (9th ed.). Ottawa: Canadian Ice Service, Environment Canada.

Frey, K. E., Comiso, J. C., Cooper, L. W. Grebmeier J. M., and Stock, L.V. 2019. Arctic Ocean primary productivity: the response of marine algae to climate warming and sea ice decline. *In:* Richter-Menge, J., M.L. Druckenmiller and M. Jeffries (eds.). Arctic Report Card 2019. www.arctic.noaa.gov/Report-Card, doi: 10.25923/vtdn-2198.

Galley, R. J. Else, B. G. T., Prinsenberg, S. J., Babb, D., and Barber, D. G. 2013. Summer sea ice concentration motion, and thickness near areas of proposed offshore oil and gas development in the Canadian Beaufort Sea – 2009. Arctic, 66(1): 105-115, doi: 10.14430/arctic4270.

Galley, R. J., Babb, D. G., Ogi, M., Else, B. G. T., Geifus, N. X., Crabeck, O., Barber, D. G., and Rysgaard, S. 2016. Replacement of multiyear sea ice and changes in the open water season duration in the Beaufort Sea since 2004. Journal of Geophysical Research: Oceans, 121, doi: 10.1002/2015JC011583.

IOCCG. 2015. Ocean Colour Remote Sensing in Polar Seas. Babin, M., Arrigo, K., Bélanger, S. and Forget, M-H. (eds.), Reports of the International Ocean-Colour Coordinating Group, No. 16, IOCCG, Dartmouth, Canada.

Jackson, J. M., Allen, S. E., Mclaughlin, F. A., Woodgate, R. A., and Carmack, E. C. 2011. Changes to the near-surface waters in the Canada Basin, Arctic Ocean from 1993-2009: A basin in transition. Journal Geophysical Research, 116, doi: 10.1029/2011JC007069.

Kahru, M., Lee, Z., Mitchell B. G., and Nevison, C. D. 2016. Effects of sea ice cover on satellite-detected primary production in the Arctic Ocean. Biology Letters, 12:20160223, doi: 10.1098/rsbl.2016.0223.

Lewis, K. M., van Dijken, G. L., and Arrigo, K. R. 2020. Changes in phytoplankton concentration now drive increased Arctic Ocean primary production. Science, 369(6500), 198-202, doi: 10.1126/science.aay8380.

Lewis, K. M., and Arrigo, K. R. 2020. Ocean Color Algorithms for Estimating Chlorophyll *a*, CDOM Absorption, and Particle Backscattering in the Arctic Ocean. Journal of Geophysical Research - Oceans, 125(6), doi:10.1029/2019JC015706.

Li, W. K., McLaughlin, F. A., Lovejoy, C., and Carmack, E. C. 2009. Smallest algae thrive as the Arctic Ocean freshens, Science, 326(5952), 539, doi: 10.1126/science.1179798.

McLaughlin, F. A. and Carmack, E. C. 2010. Deepening of the nutricline and chlorophyll maximum in the Canada Basin interior, 2003-2009. Geophysical Research Letters, 37, doi: 10.1029/2010GL045459.

Michel, C. 2013. Chapter 14: Marine Ecosystems, *In*: Arctic Biodiversity Assessment.Status and Trends in Biodiversity. H. Meltofte (ed.). Conservation of Arctic Flora and Fauna, Akureyri, pp. 486-526.

Niemi, A., Ferguson, S., Hedges, K., Melling, H., Michel, C., Ayles, B., Azetsu-Scott, K., Coupel, P., Deslauriers, D., Devred, E., Doniol-Valcroze, T., Dunmall, K., Eert, J., Galbraith, P., Geoffroy, M., Gilchrist, G., Hennin, H., Howland, K., Kendall, M., Kohlbach, D., Lea, E., Loseto, L., Majewski, A., Marcoux, M., Matthews, C., McNicholl, D., Mosnier, A., Mundy, C.J., Ogloff, W., Perrie, W., Richards, C., Richardson, E., Reist, R., Roy, V., Sawatzky, C., Scharffenberg, K., Tallman, R., Tremblay, J-É., Tufts, T., Watt, C., Williams, W., Worden, E., Yurkowski, D., and Zimmerman, S. 2019. State of Canada's Arctic Seas. Can. Tech. Rep. Fish. Aquat. Sci. 3344: xv + 189 p.

NOAA National Geophysical Data Center. 2009. ETOPO1 1 Arc-Minute Global Relief Model. NOAA National Centers for Environmental Information.

Nummelin, A., Illicak, M., Li, C., and Smedsrud, L. H. 2016. Consequences of future increased Arctic runoff on Arctic Ocean stratification, circulation, and sea ice cover. Journal of Geophysical Research, 121, doi: 10.1002/2015JC011156.

Parkinson, C. L. 2014. Spatially mapped reductions in the length of the Arctic sea ice season. Geophysical Research Letters, 41, doi: 10.1002/2014GL060434.

Perovich, D. K., Richter-Menge, J. A., Jones, K. F., Light, B., Elder, B. C., Polashenski, C., Laroche, D., Markus, T., and Lindsay, R. 2011. Arctic sea-ice melt in 2008 and the role of solar heating. Annals of Glaciology, 52(57), 355-359, doi: 10.3189/172756411795931714.

Renaut, S., Devred, E., and Babin, M. 2018. Northward expansion and intensification of phytoplankton growth during the early ice-free season in Arctic. Geophysical Research Letters, 45(19), 10590-10598, doi: 10.1029/2018GL078995.

Stroeve, J., Markus, T., Boisvert, L., Miller, J., and Barrett, A. 2014. Changes in Arctic melt season and implications for sea ice loss. Geophysical Research Letters, 41, doi: 10.1002/2013GL05855.

Wang, M., and Shi, W. 2007. The NIR-SWIR combined atmospheric correction approach for MODIS ocean color data processing. Opt. Express 15(24), 15722-15733, doi: 10.1364/OE.15.015722.

Wessel, P., Smith, W. H. F., Scharroo, R., Luis, J. F, and Wobbe, F. 2013. Generic Mapping Tools: Improved Version Released, EOS Trans. AGU, 94(45), 409–410, doi:10.1002/2013EO450001.

A Average chlorophyll *a* concentration in the study region by year

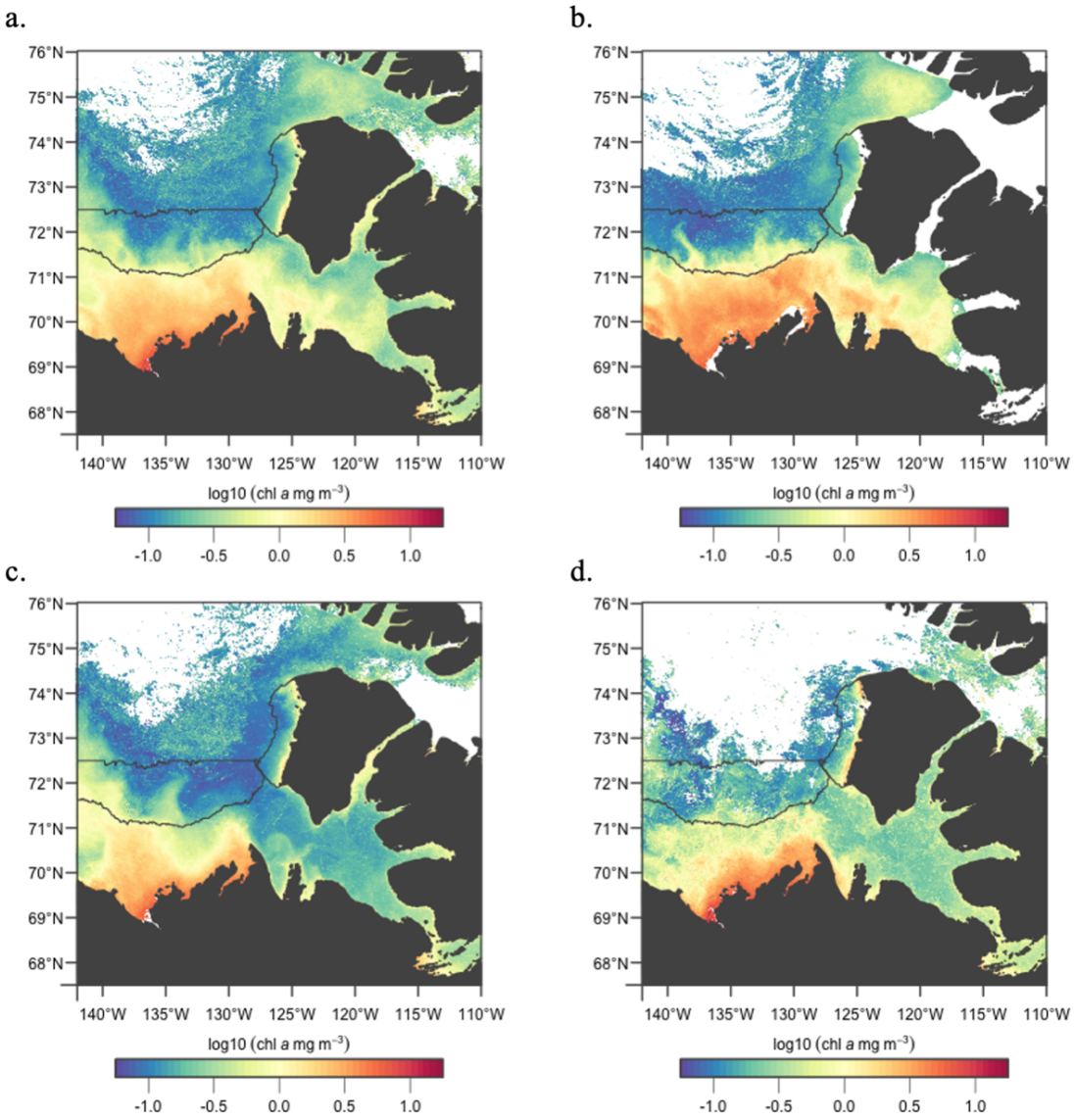

Figure A.1: Mean chlorophyll *a* concentration in **(a)** year-weeks 18 to 41, **(b)** year-weeks 18 to 25, **(c)** year-weeks 26 to 33, **(d)** year-weeks 34 to 41 in 1998.

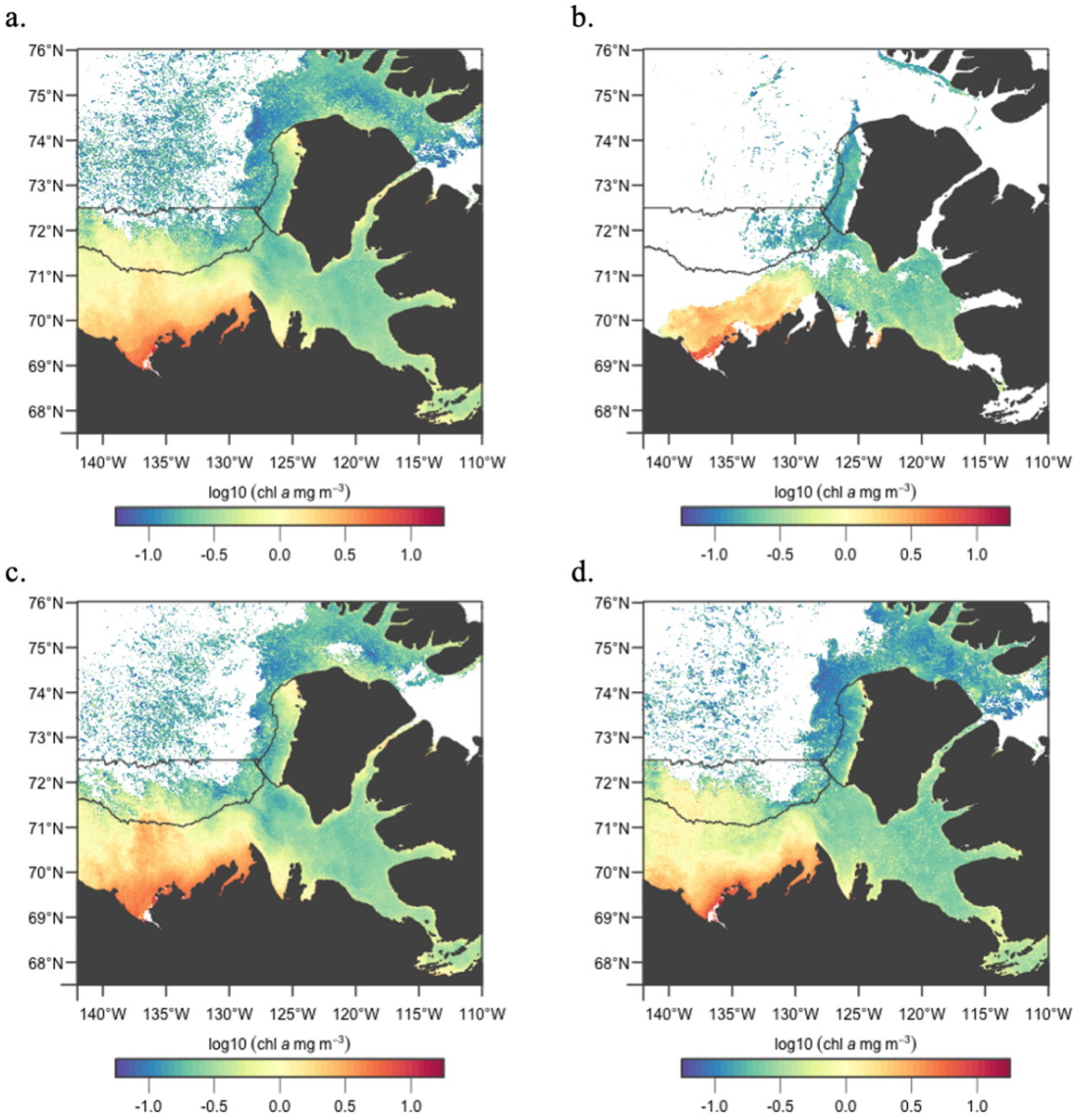

Figure A.2: Mean chlorophyll *a* concentration in **(a)** year-weeks 18 to 41, **(b)** year-weeks 18 to 25, **(c)** year-weeks 26 to 33, **(d)** year-weeks 34 to 41 in 1999.

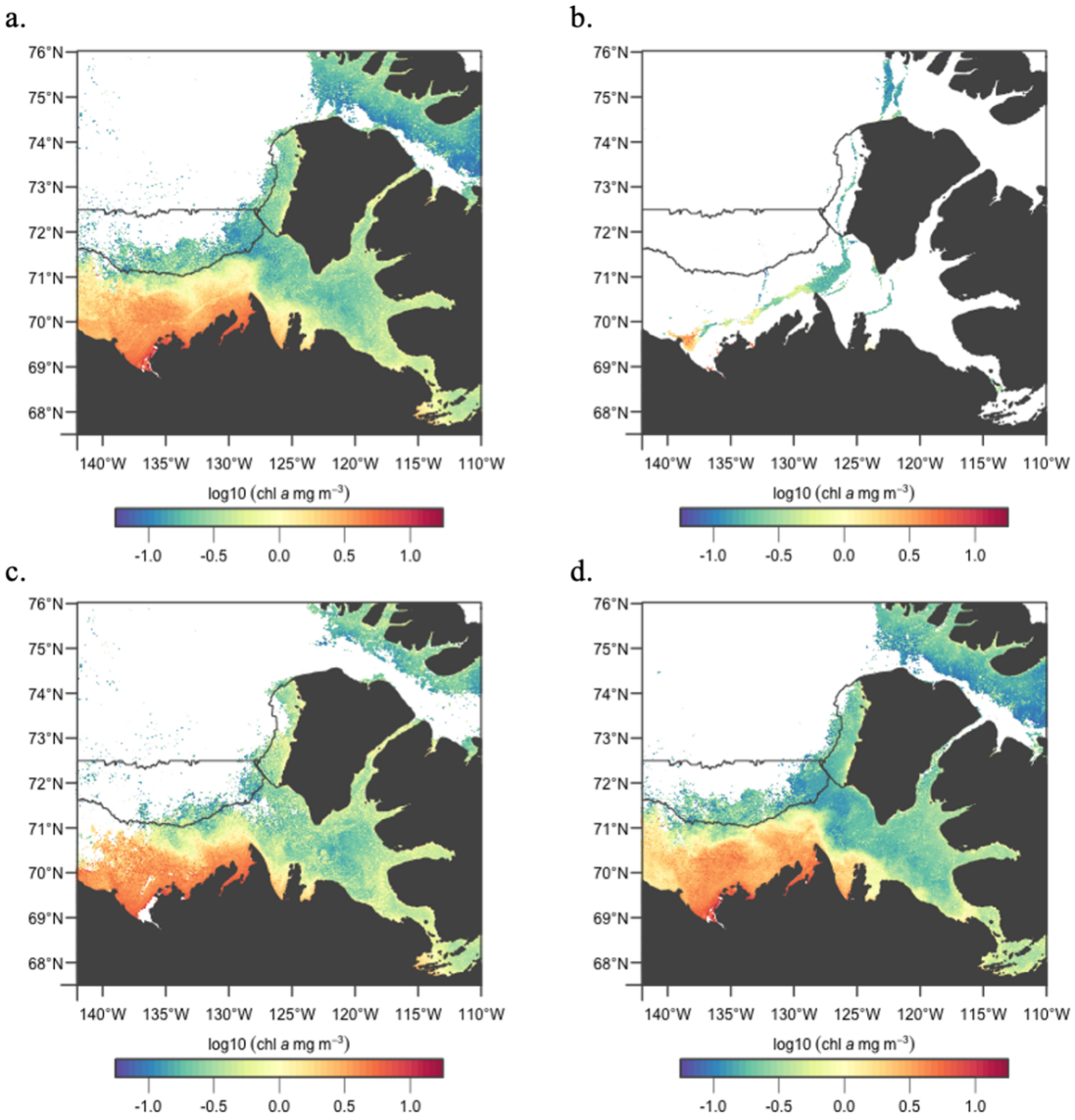

Figure A.3: Mean chlorophyll *a* concentration in **(a)** year-weeks 18 to 41, **(b)** year-weeks 18 to 25, **(c)** year-weeks 26 to 33, **(d)** year-weeks 34 to 41 in 2000.

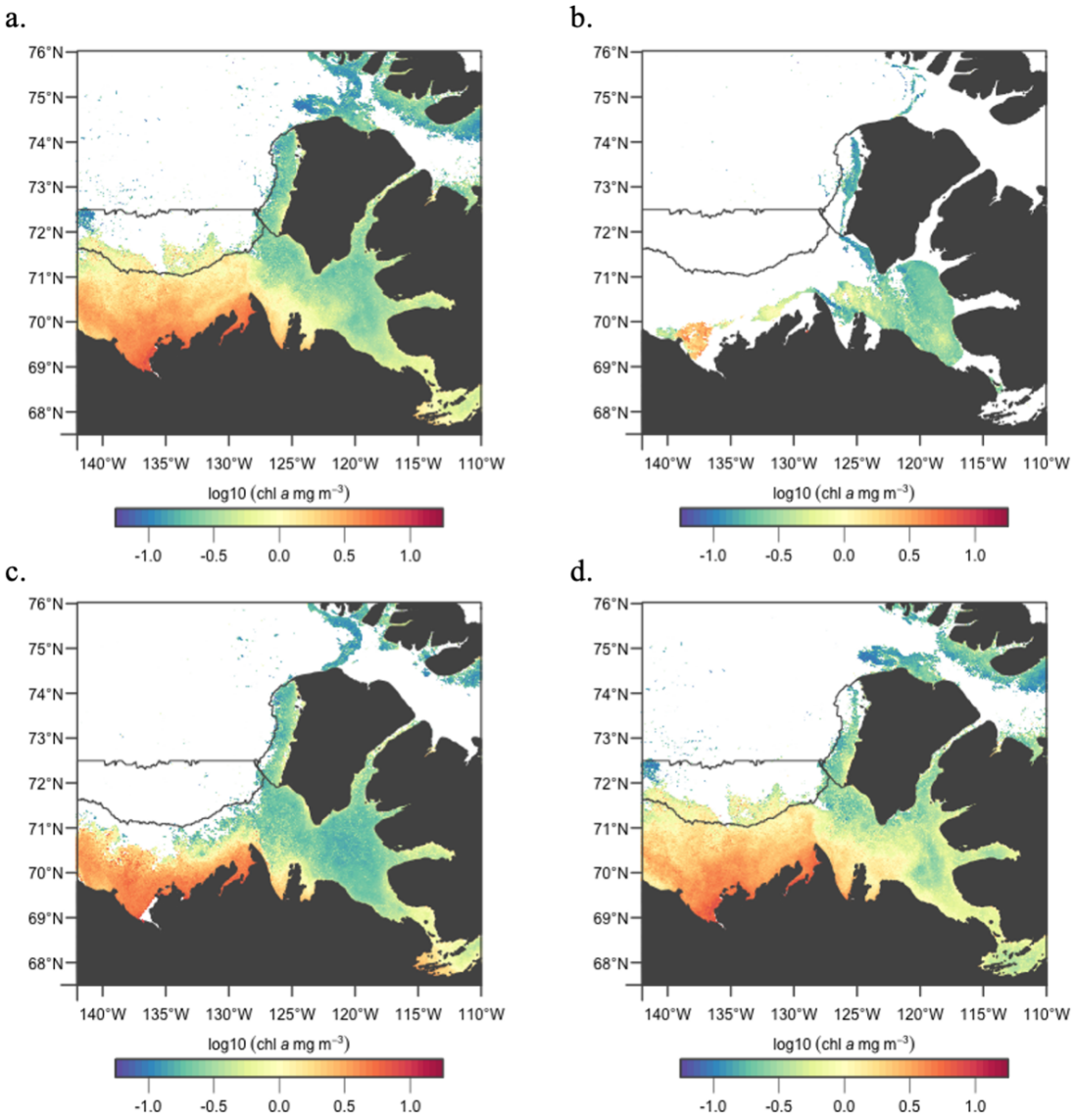

Figure A.4: Mean chlorophyll *a* concentration in **(a)** year-weeks 18 to 41, **(b)** year-weeks 18 to 25, **(c)** year-weeks 26 to 33, **(d)** year-weeks 34 to 41 in 2001.

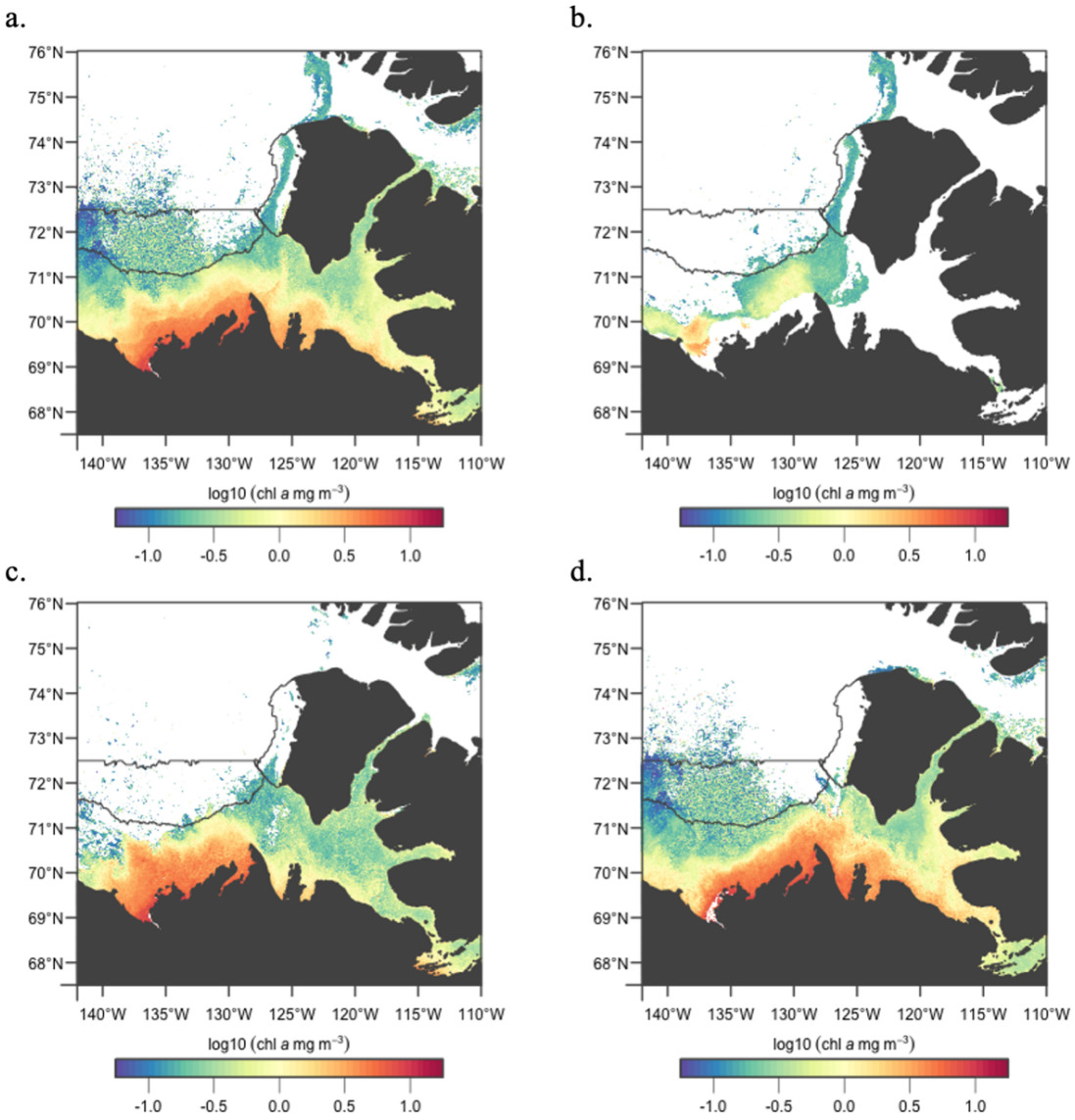

Figure A.5: Mean chlorophyll *a* concentration in **(a)** year-weeks 18 to 41, **(b)** year-weeks 18 to 25, **(c)** year-weeks 26 to 33, **(d)** year-weeks 34 to 41 in 2002.

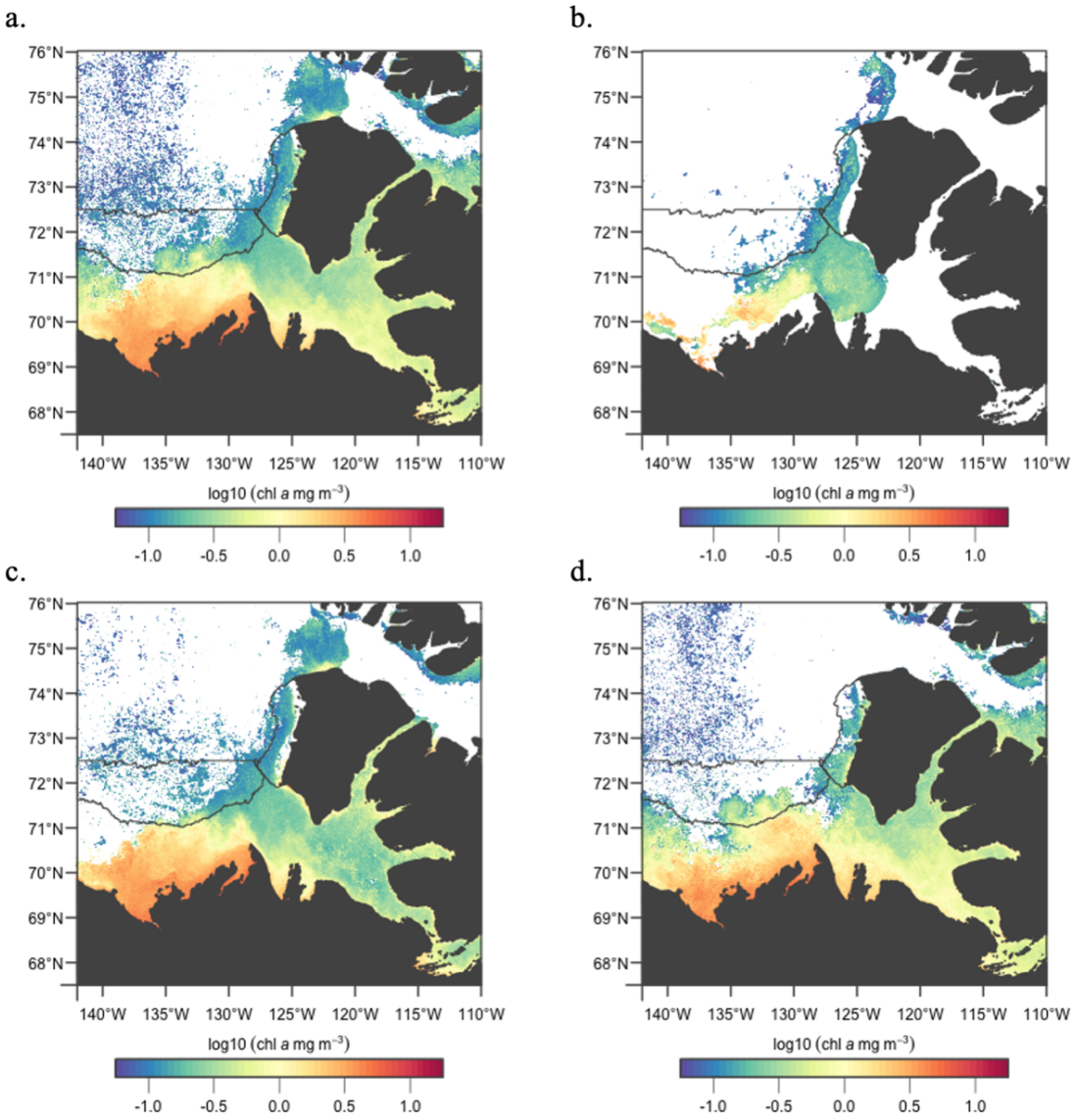

Figure A.6: Mean chlorophyll *a* concentration in **(a)** year-weeks 18 to 41, **(b)** year-weeks 18 to 25, **(c)** year-weeks 26 to 33, **(d)** year-weeks 34 to 41 in 2003.

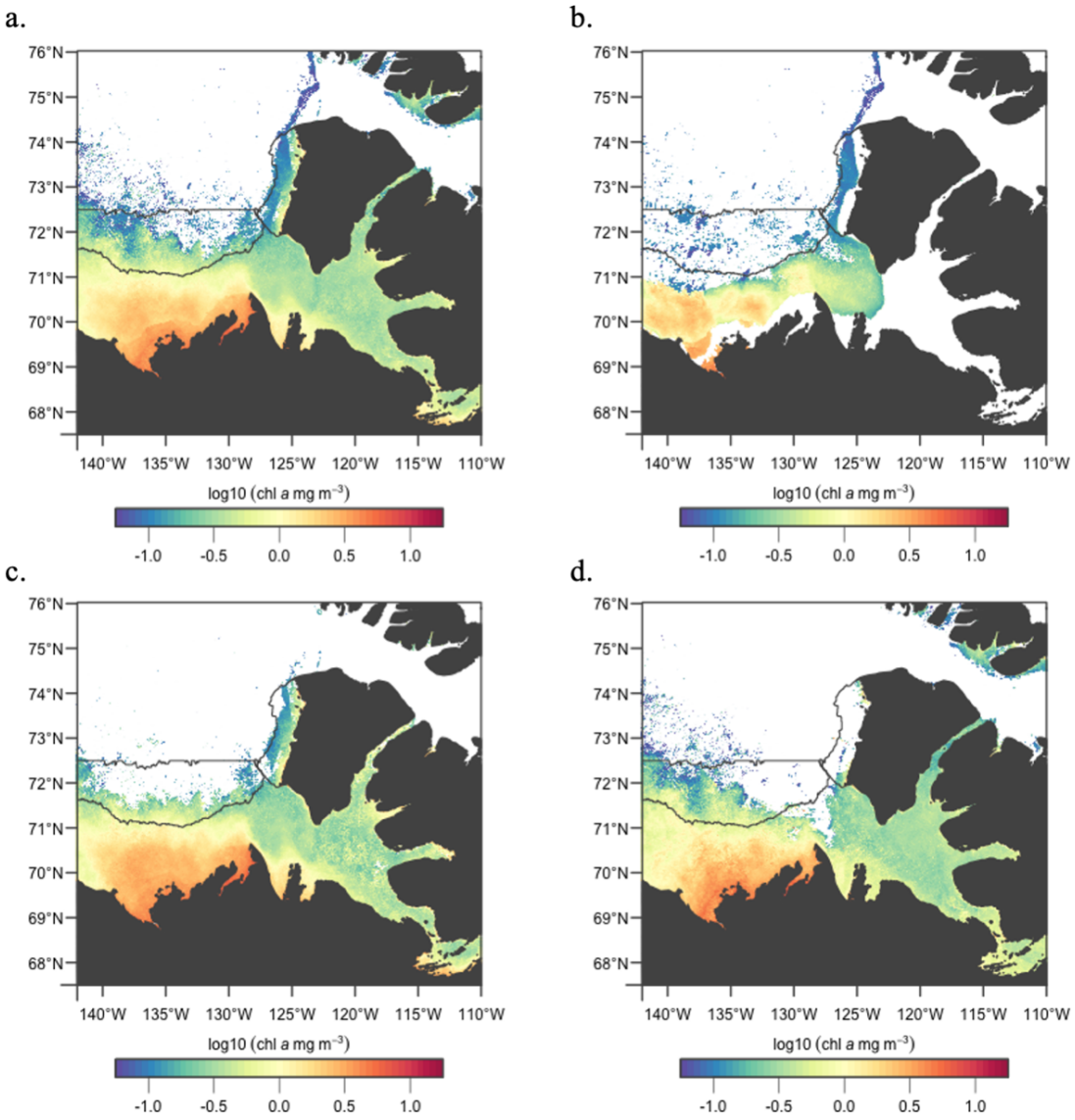

Figure A.7: Mean chlorophyll *a* concentration in **(a)** year-weeks 18 to 41, **(b)** year-weeks 18 to 25, **(c)** year-weeks 26 to 33, **(d)** year-weeks 34 to 41 in 2004.

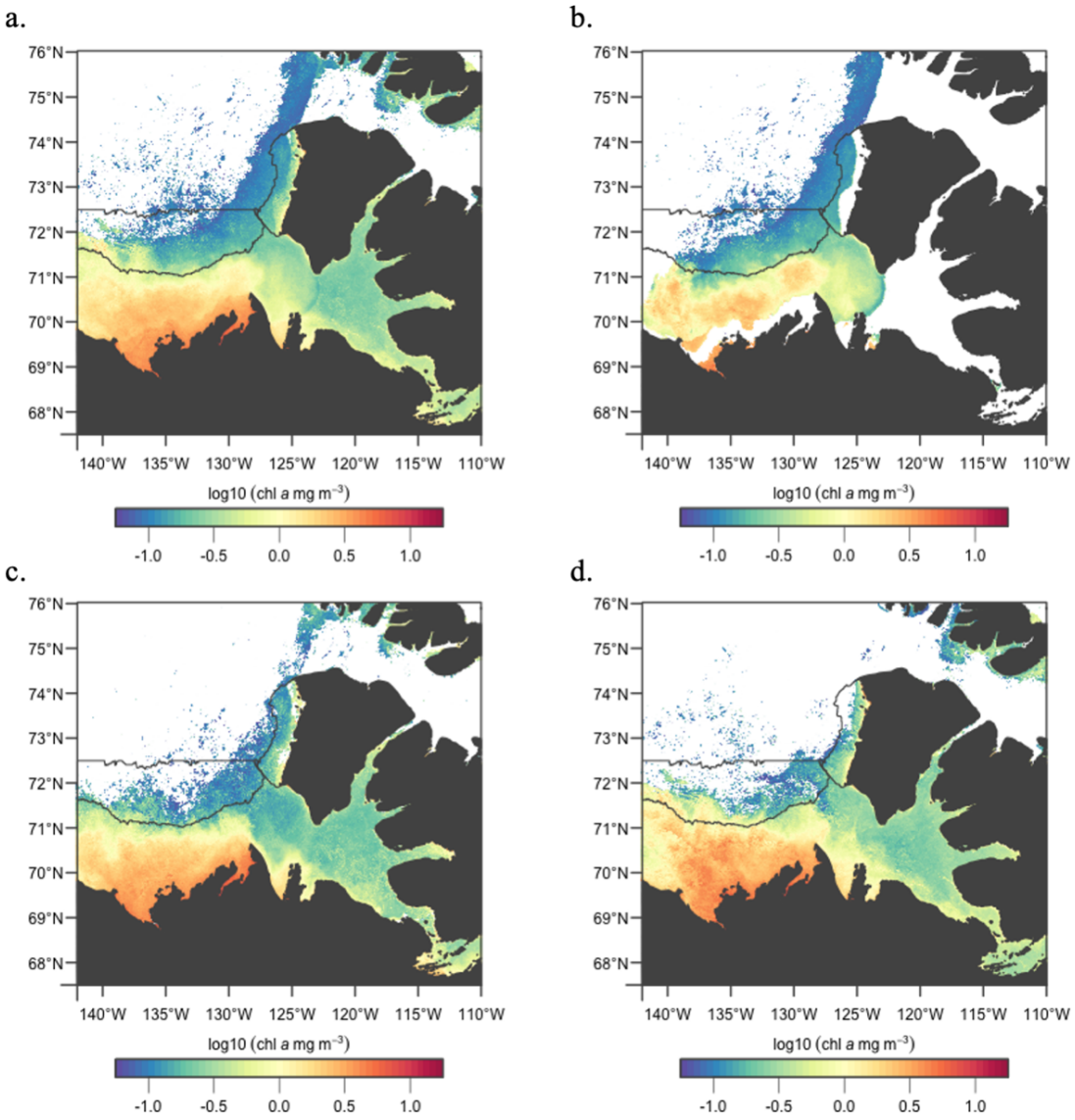

Figure A.8: Mean chlorophyll *a* concentration in **(a)** year-weeks 18 to 41, **(b)** year-weeks 18 to 25, **(c)** year-weeks 26 to 33, **(d)** year-weeks 34 to 41 in 2005.

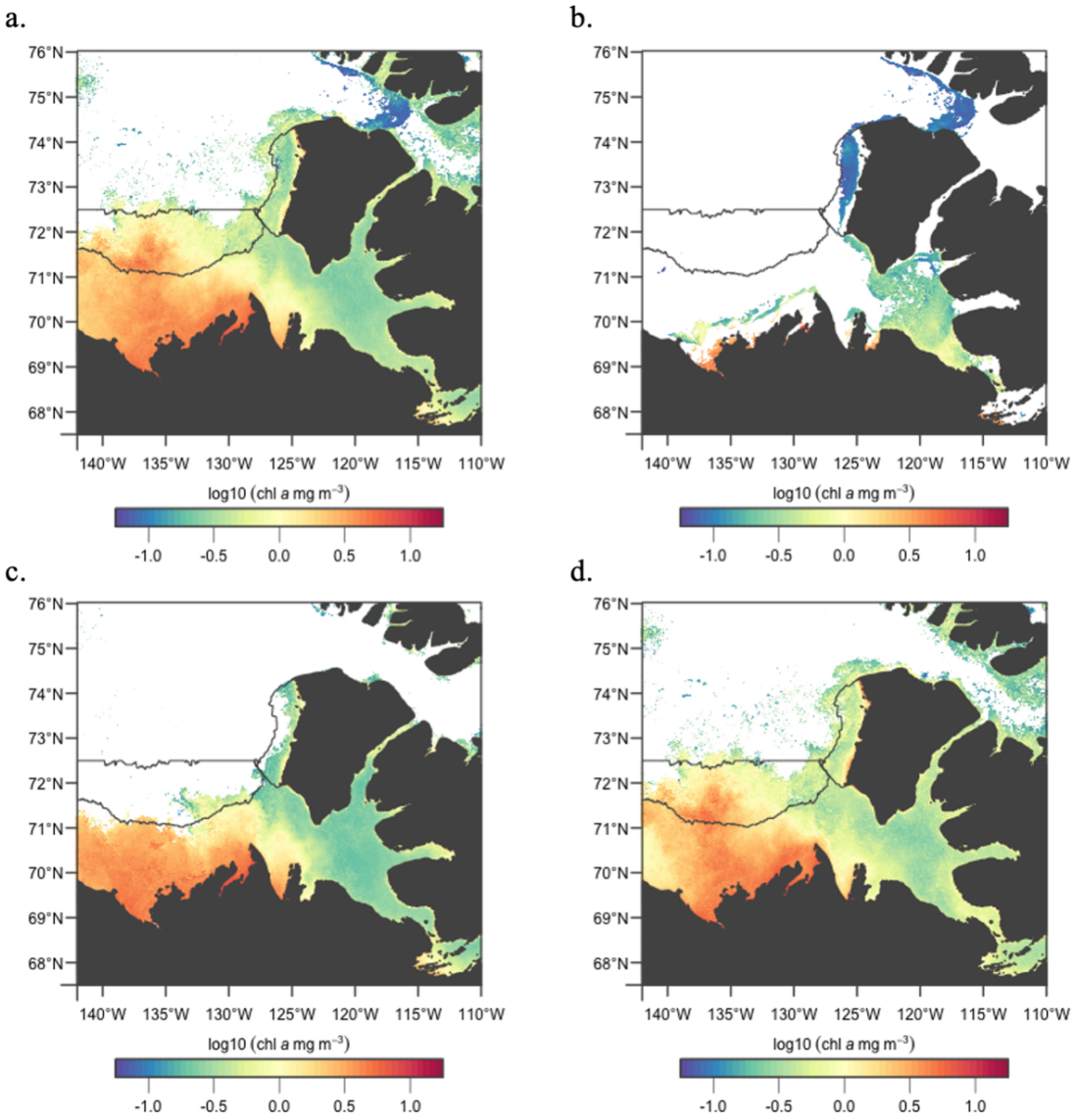

Figure A.9: Mean chlorophyll *a* concentration in **(a)** year-weeks 18 to 41, **(b)** year-weeks 18 to 25, **(c)** year-weeks 26 to 33, **(d)** year-weeks 34 to 41 in 2006.

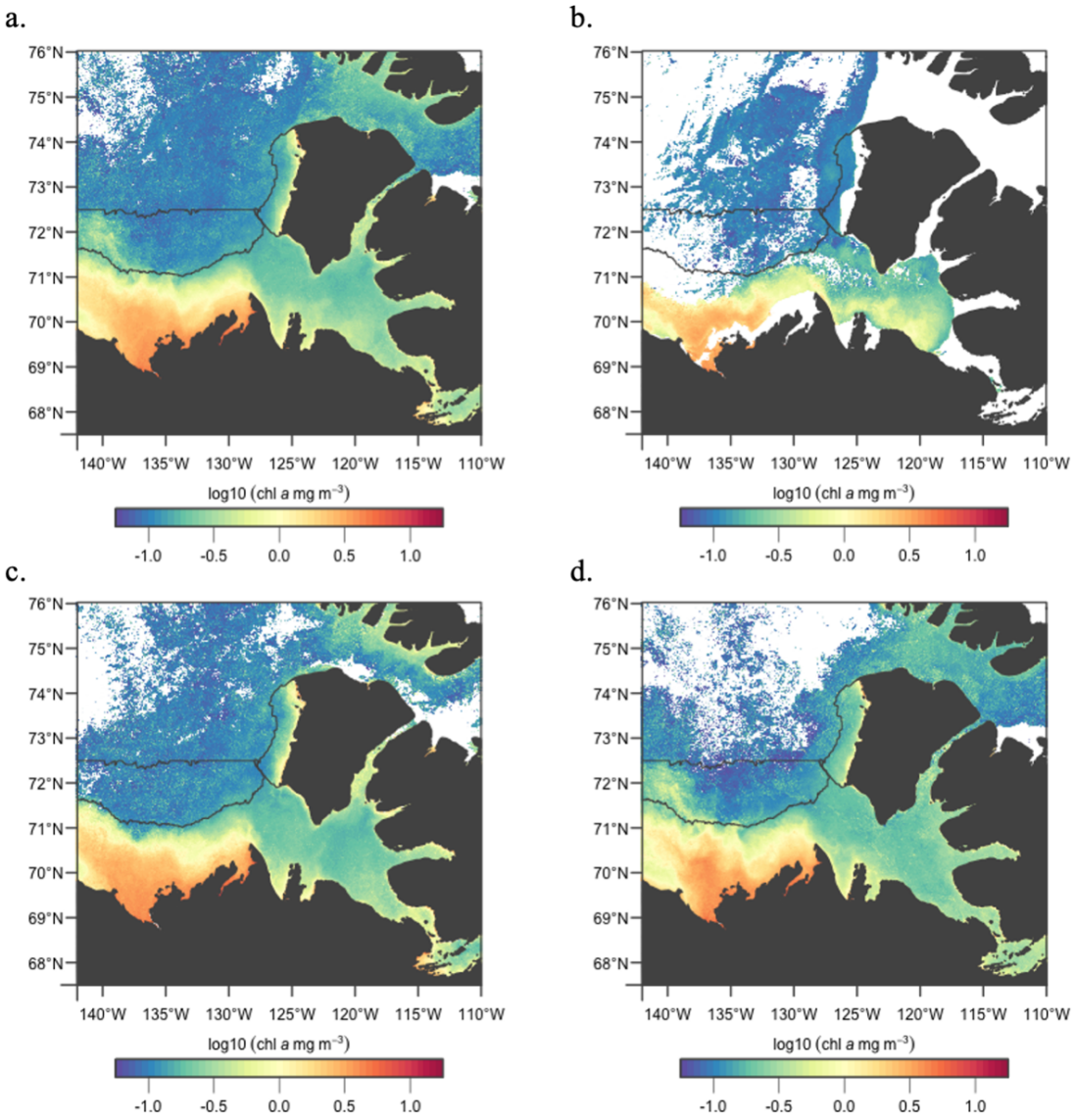

Figure A.10: Mean chlorophyll *a* concentration in **(a)** year-weeks 18 to 41, **(b)** year-weeks 18 to 25, **(c)** year-weeks 26 to 33, **(d)** year-weeks 34 to 41 in 2007.

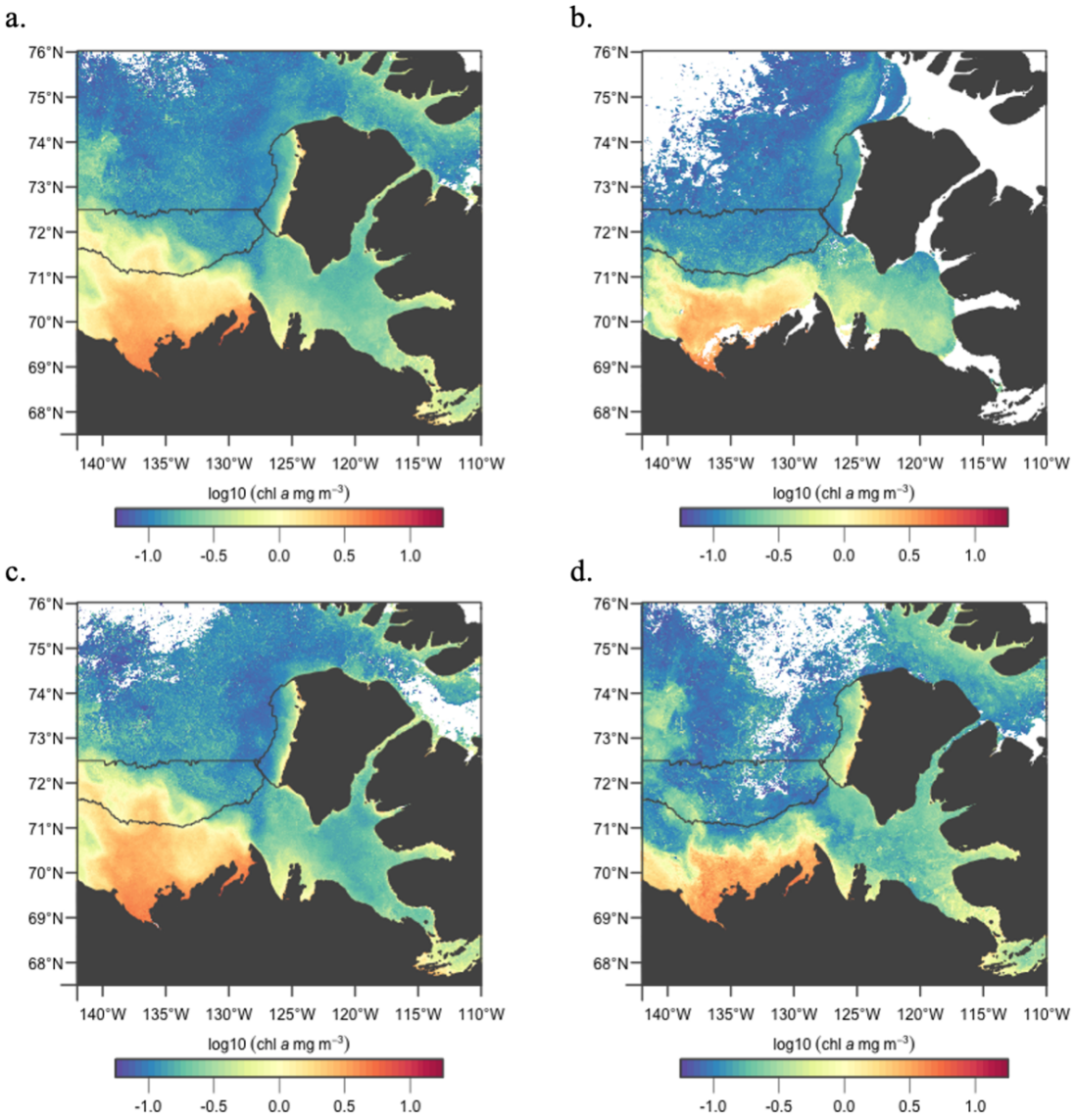

Figure A.11: Mean chlorophyll *a* concentration in **(a)** year-weeks 18 to 41, **(b)** year-weeks 18 to 25, **(c)** year-weeks 26 to 33, **(d)** year-weeks 34 to 41 in 2008.

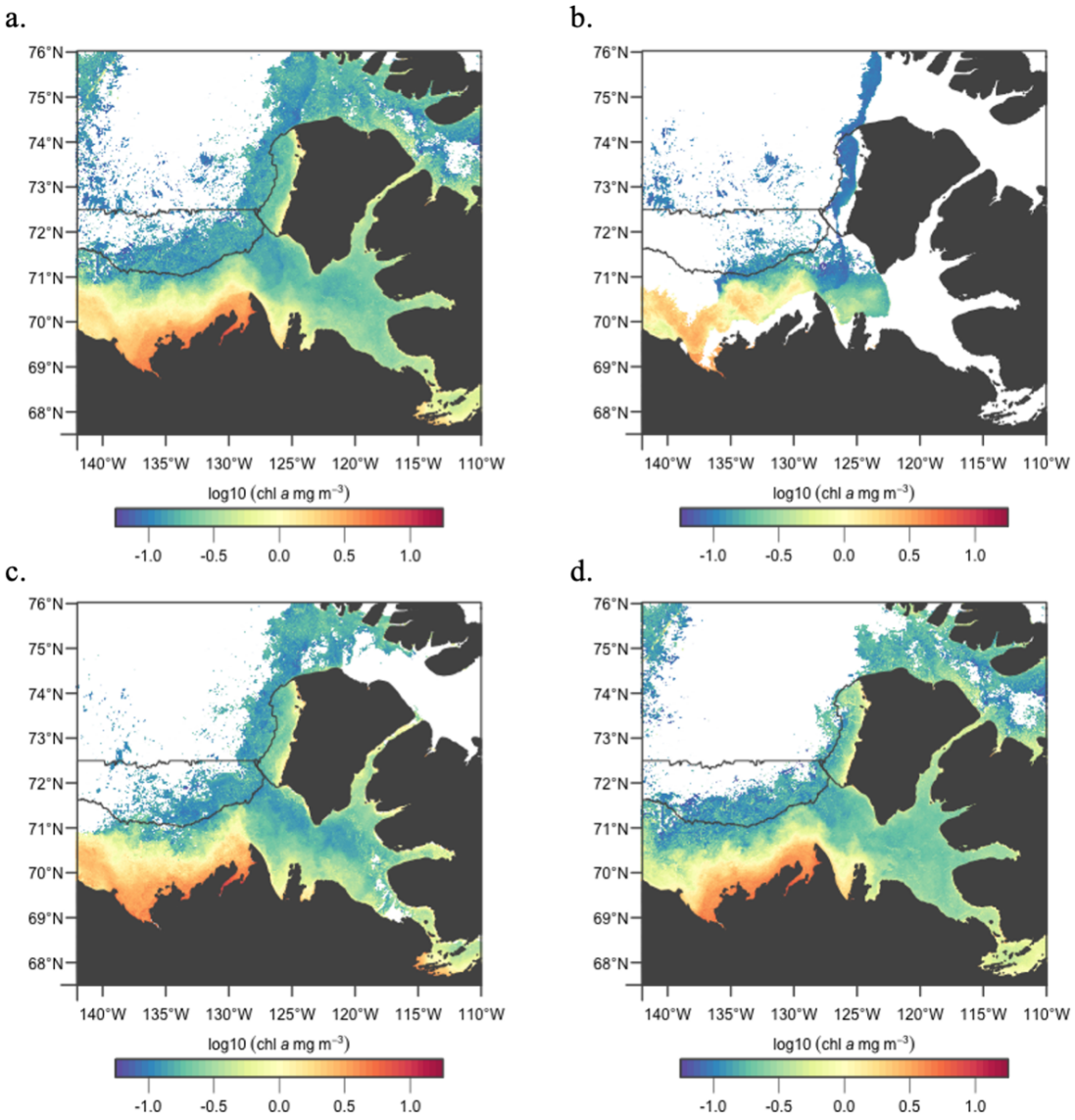

Figure A.12: Mean chlorophyll *a* concentration in **(a)** year-weeks 18 to 41, **(b)** year-weeks 18 to 25, **(c)** year-weeks 26 to 33, **(d)** year-weeks 34 to 41 in 2009.

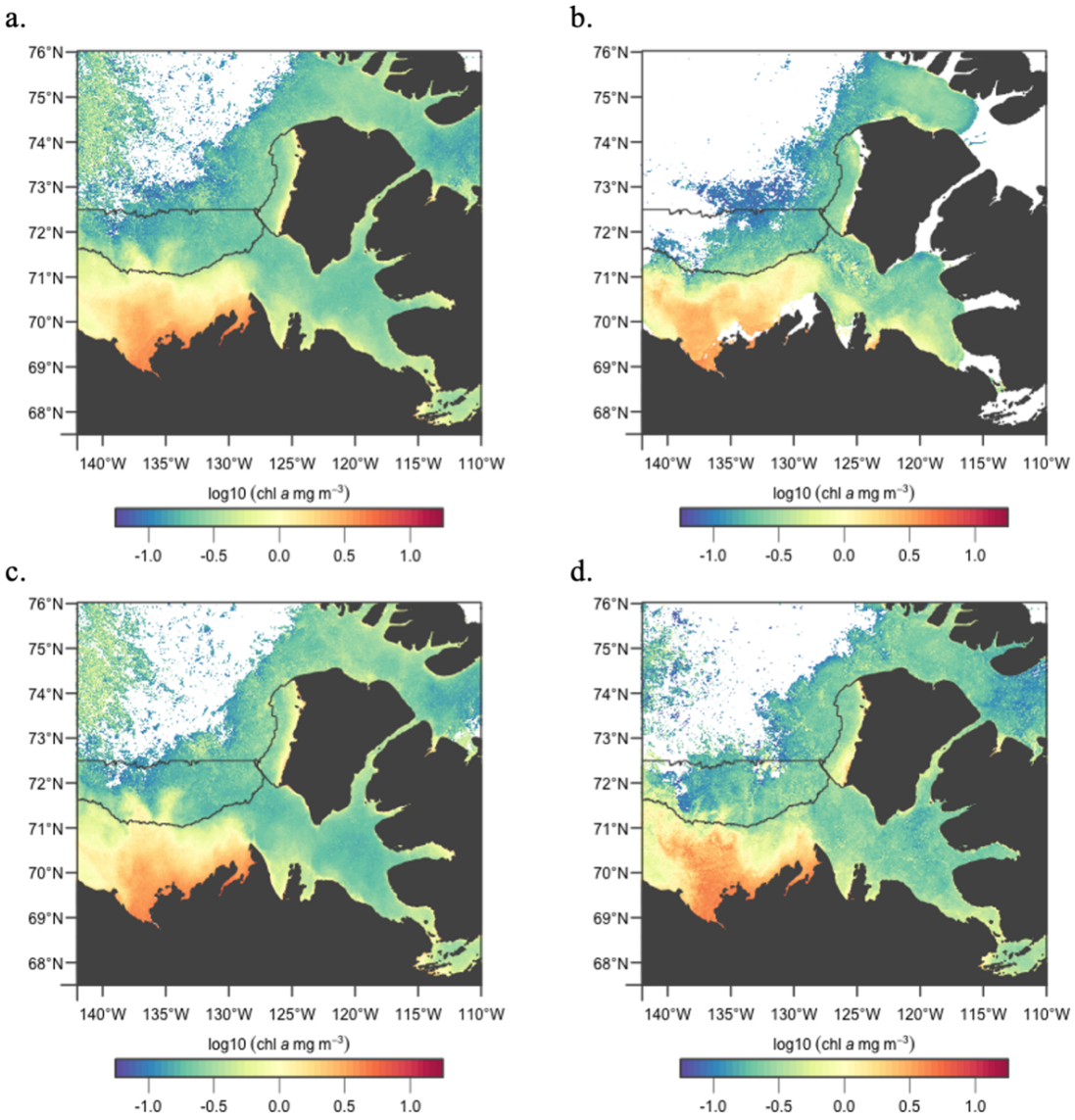

Figure A.13: Mean chlorophyll *a* concentration in **(a)** year-weeks 18 to 41, **(b)** year-weeks 18 to 25, **(c)** year-weeks 26 to 33, **(d)** year-weeks 34 to 41 in 2010.

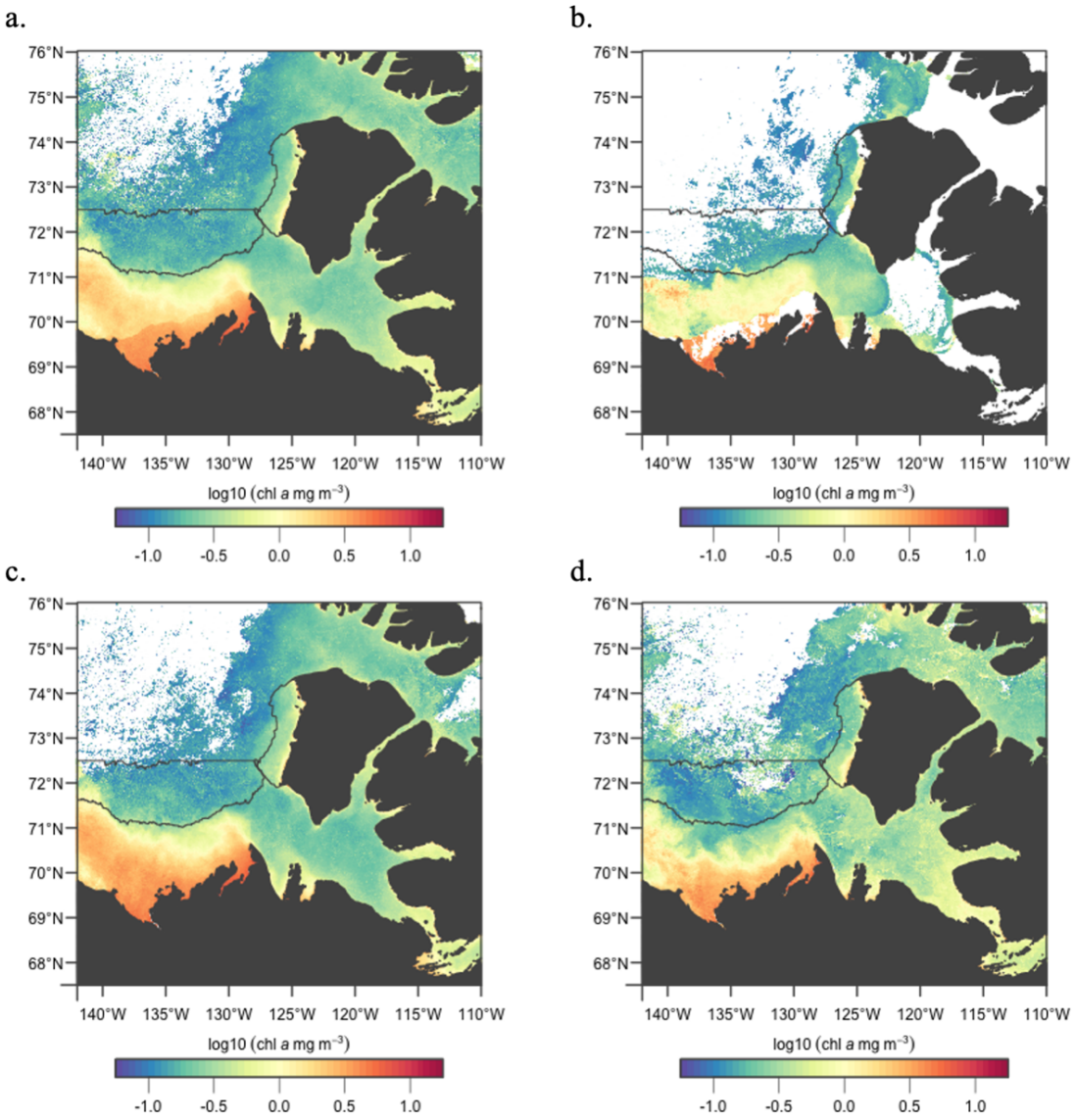

Figure A.14: Mean chlorophyll *a* concentration in **(a)** year-weeks 18 to 41, **(b)** year-weeks 18 to 25, **(c)** year-weeks 26 to 33, **(d)** year-weeks 34 to 41 in 2011.

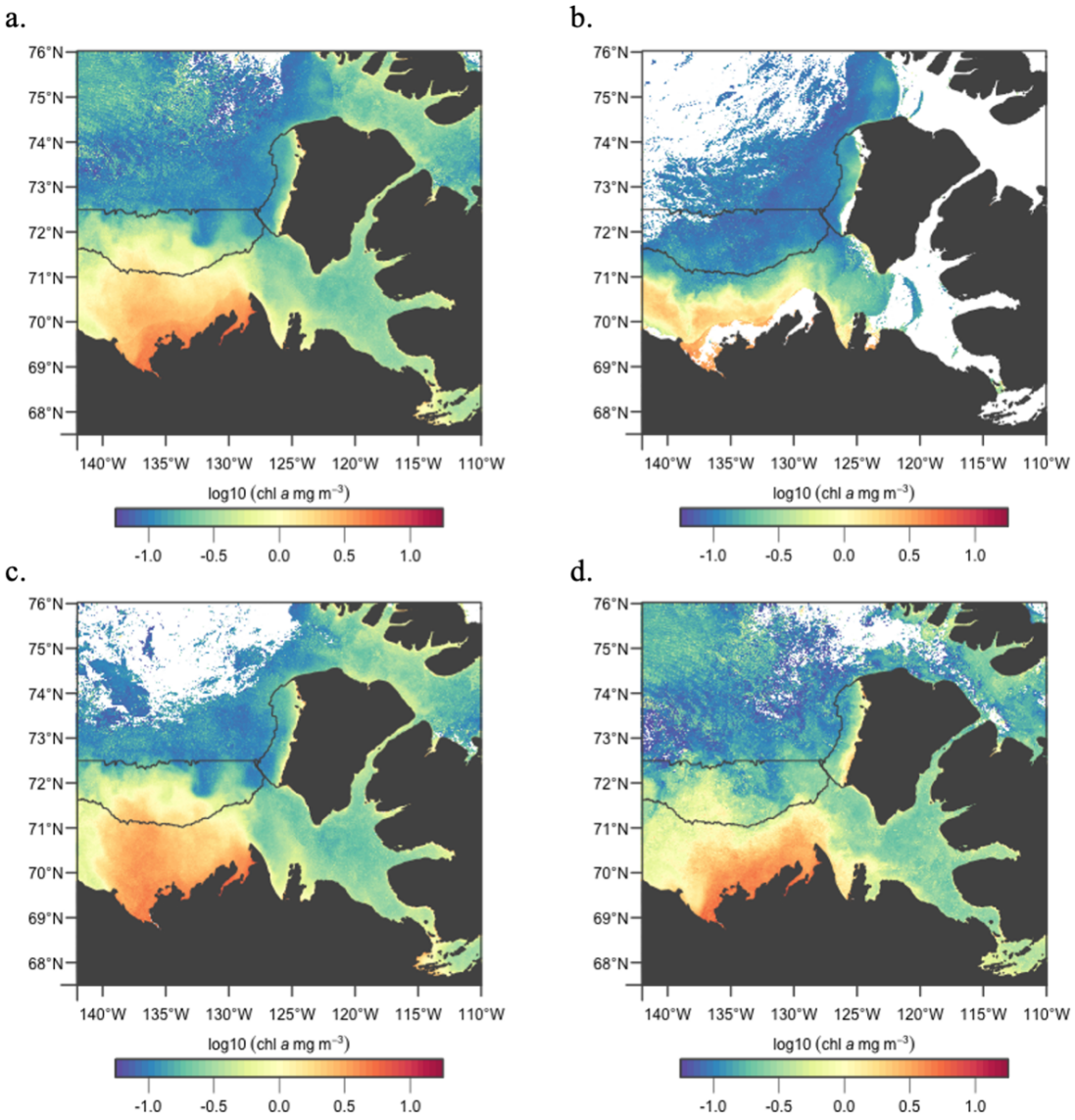

Figure A.15: Mean chlorophyll *a* concentration in **(a)** year-weeks 18 to 41, **(b)** year-weeks 18 to 25, **(c)** year-weeks 26 to 33, **(d)** year-weeks 34 to 41 in 2012.

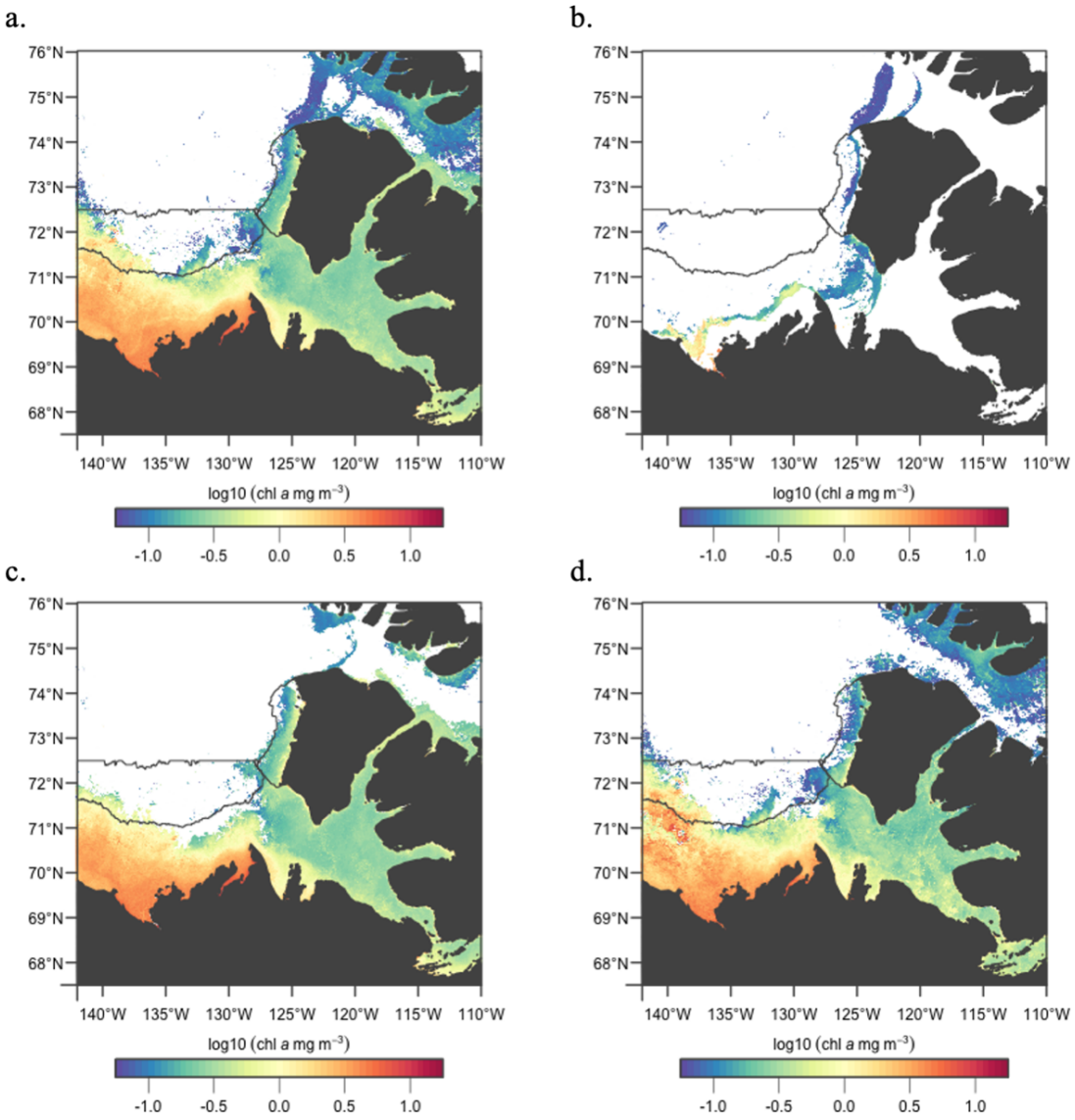

Figure A.16: Mean chlorophyll *a* concentration in **(a)** year-weeks 18 to 41, **(b)** year-weeks 18 to 25, **(c)** year-weeks 26 to 33, **(d)** year-weeks 34 to 41 in 2013.

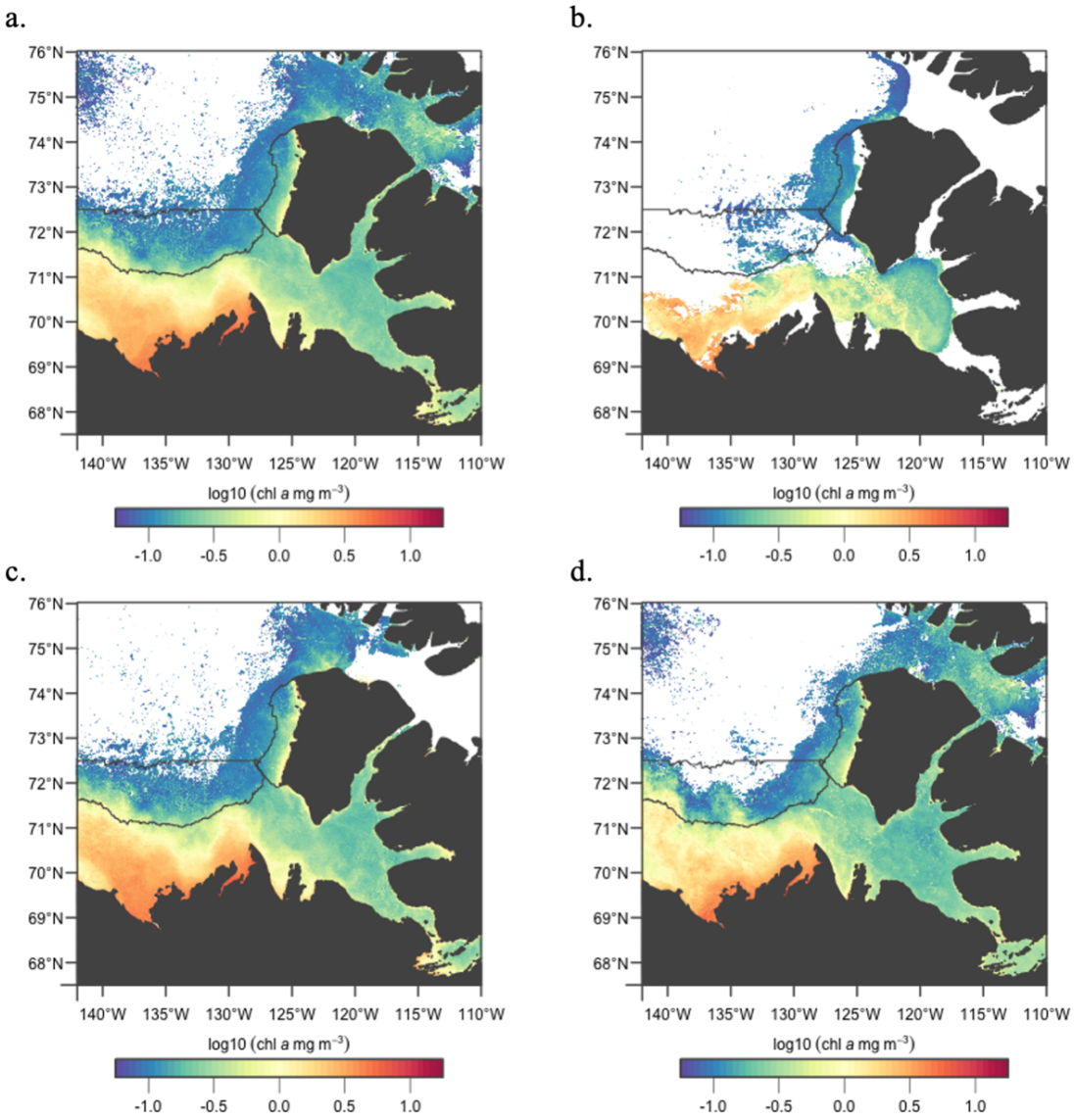

Figure A.17: Mean chlorophyll *a* concentration in **(a)** year-weeks 18 to 41, **(b)** year-weeks 18 to 25, **(c)** year-weeks 26 to 33, **(d)** year-weeks 34 to 41 in 2014.

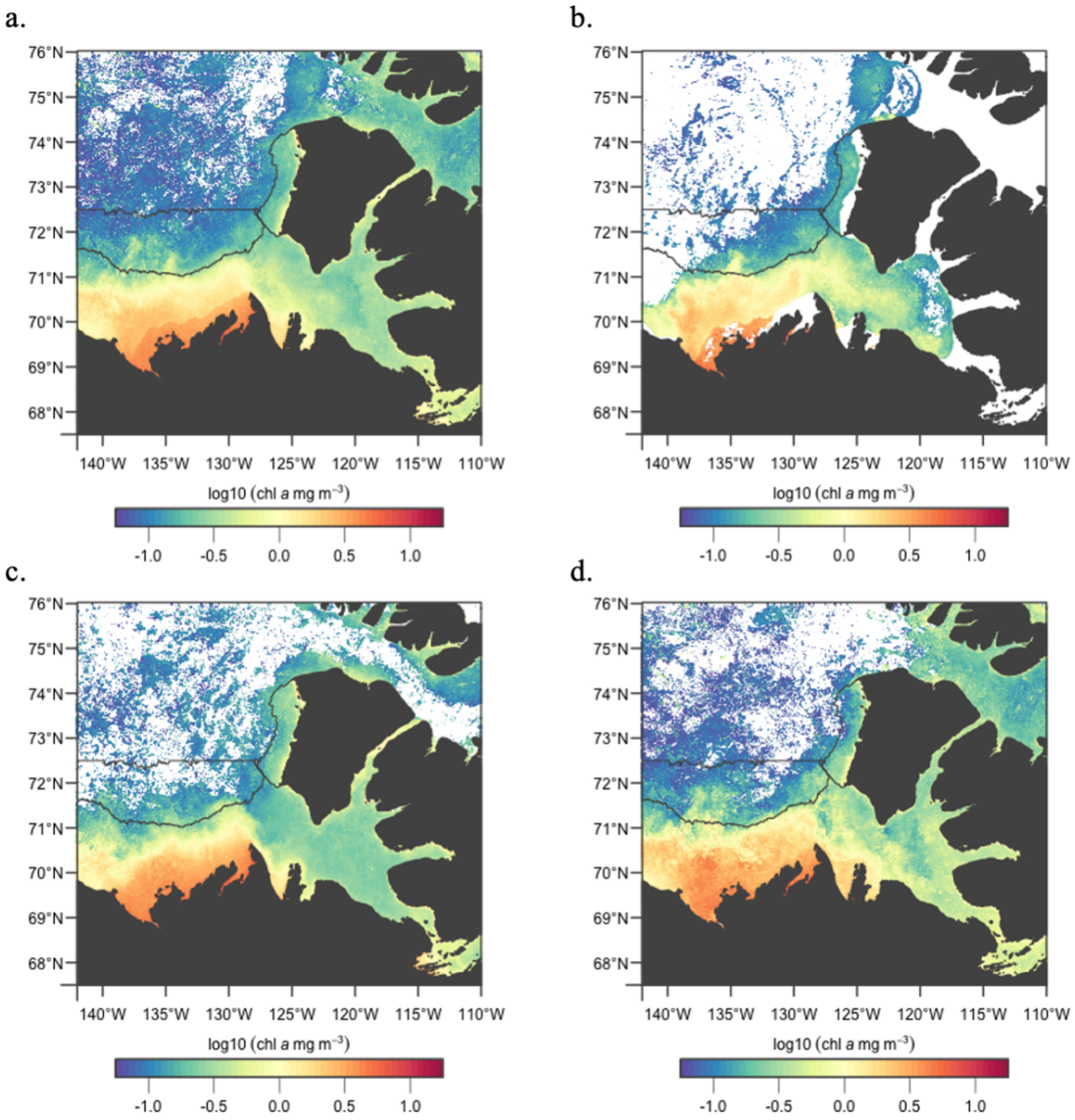

Figure A.18: Mean chlorophyll *a* concentration in **(a)** year-weeks 18 to 41, **(b)** year-weeks 18 to 25, **(c)** year-weeks 26 to 33, **(d)** year-weeks 34 to 41 in 2015.

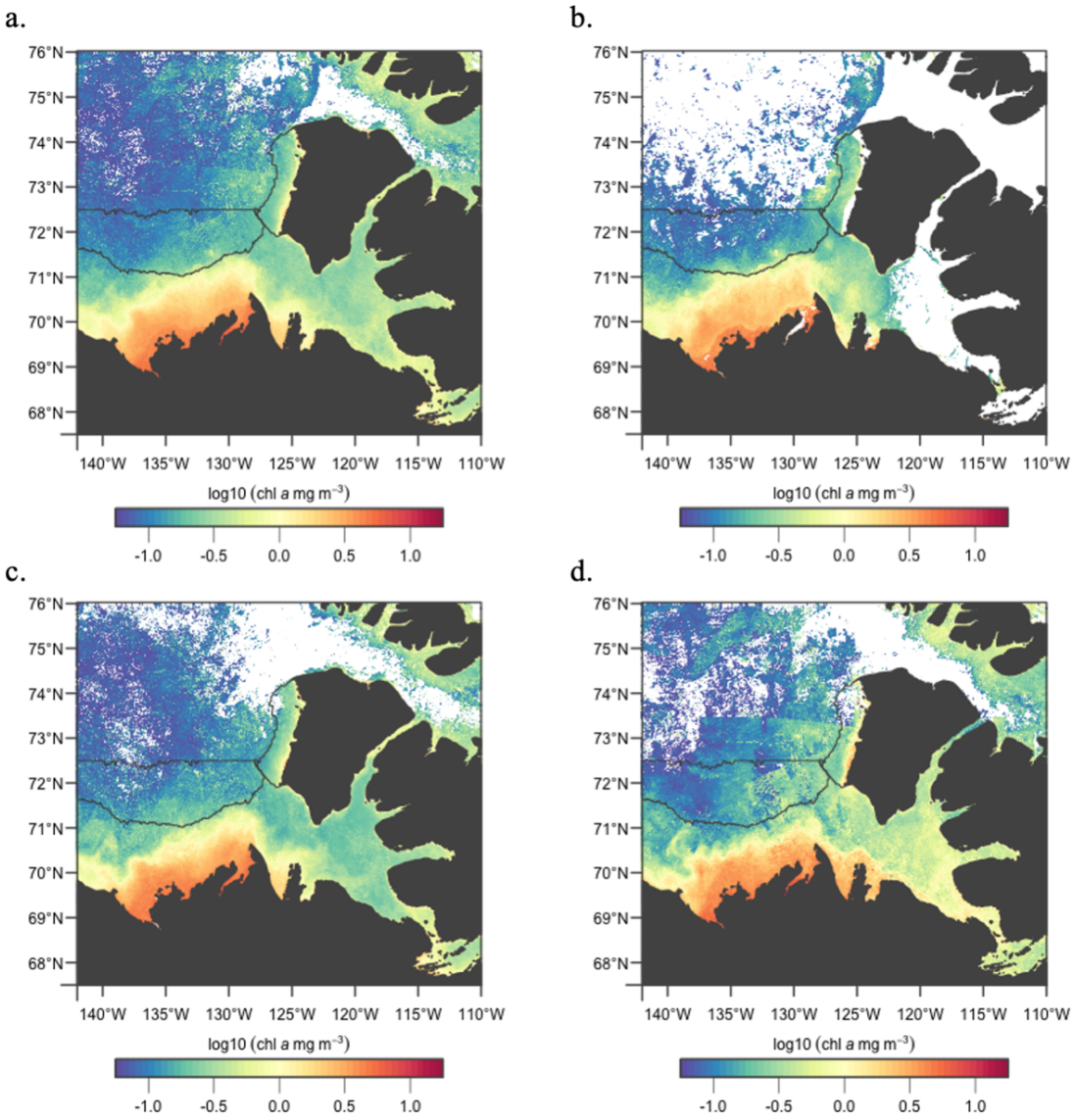

Figure A.19: Mean chlorophyll *a* concentration in **(a)** year-weeks 18 to 41, **(b)** year-weeks 18 to 25, **(c)** year-weeks 26 to 33, **(d)** year-weeks 34 to 41 in 2016.

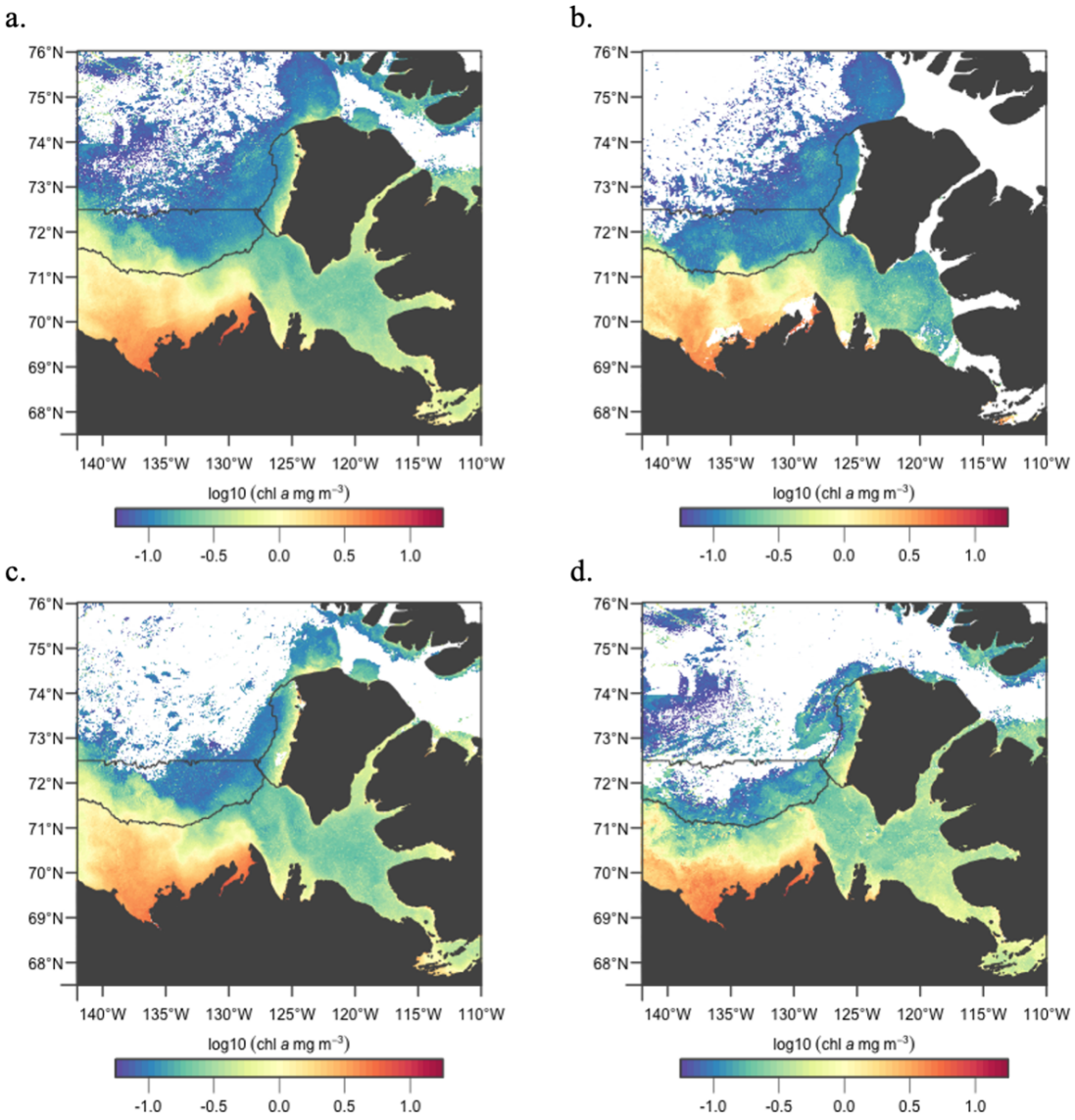

Figure A.20: Mean chlorophyll *a* concentration in **(a)** year-weeks 18 to 41, **(b)** year-weeks 18 to 25, **(c)** year-weeks 26 to 33, **(d)** year-weeks 34 to 41 in 2017.

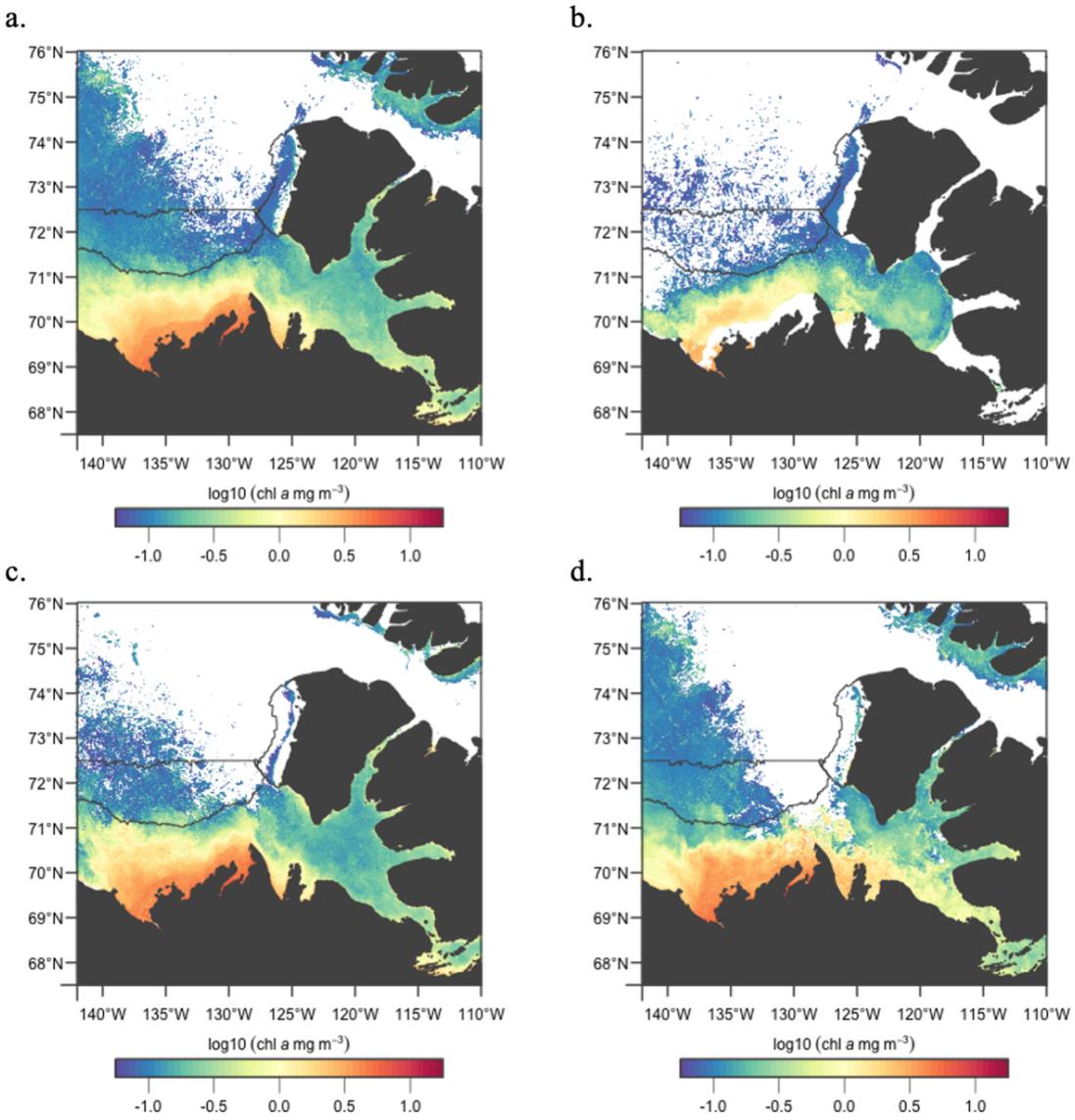

Figure A.21: Mean chlorophyll *a* concentration in **(a)** year-weeks 18 to 41, **(b)** year-weeks 18 to 25, **(c)** year-weeks 26 to 33, **(d)** year-weeks 34 to 41 in 2018.

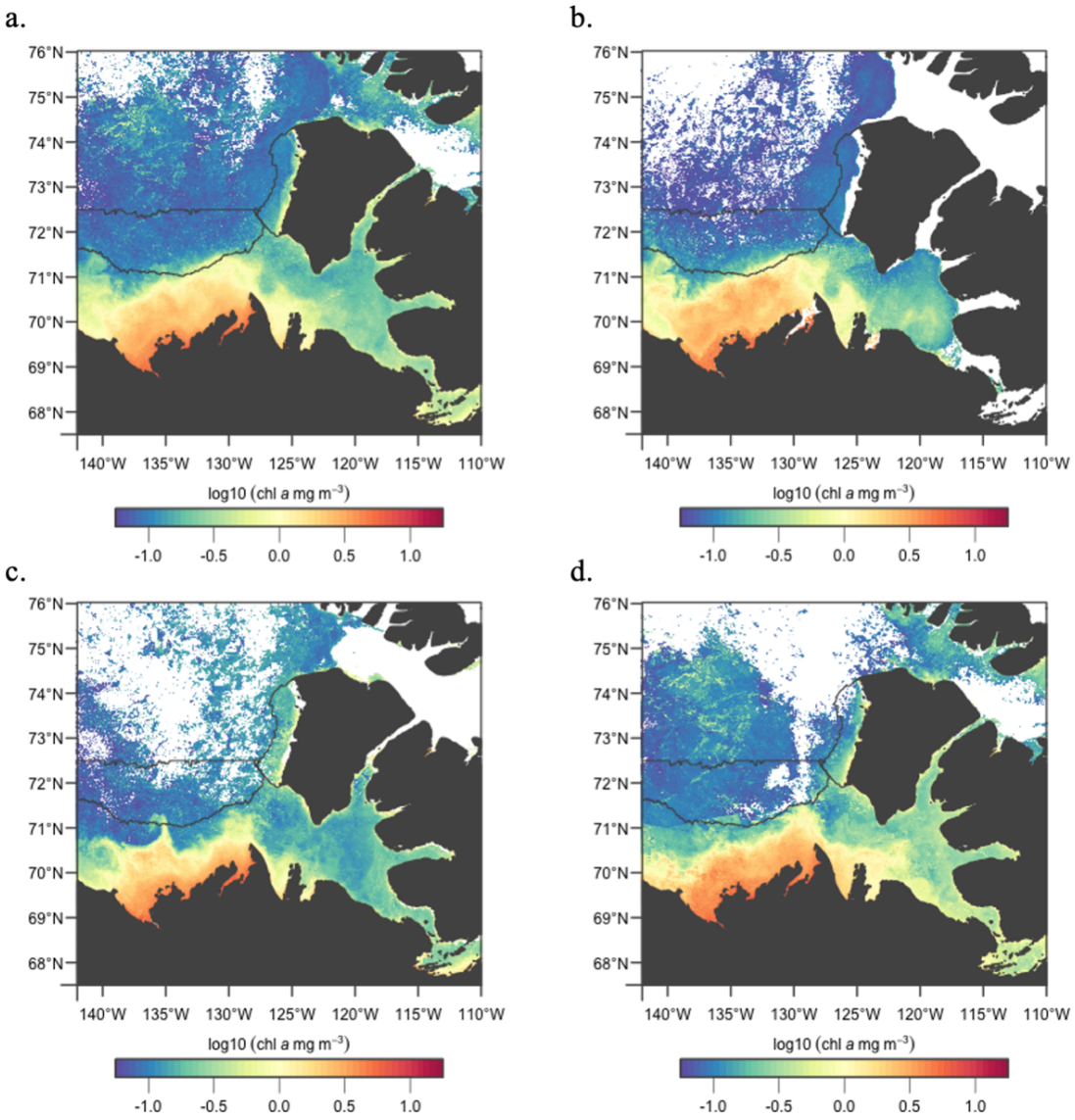

Figure A.22: Mean chlorophyll *a* concentration in **(a)** year-weeks 18 to 41, **(b)** year-weeks 18 to 25, **(c)** year-weeks 26 to 33, **(d)** year-weeks 34 to 41 in 2019.

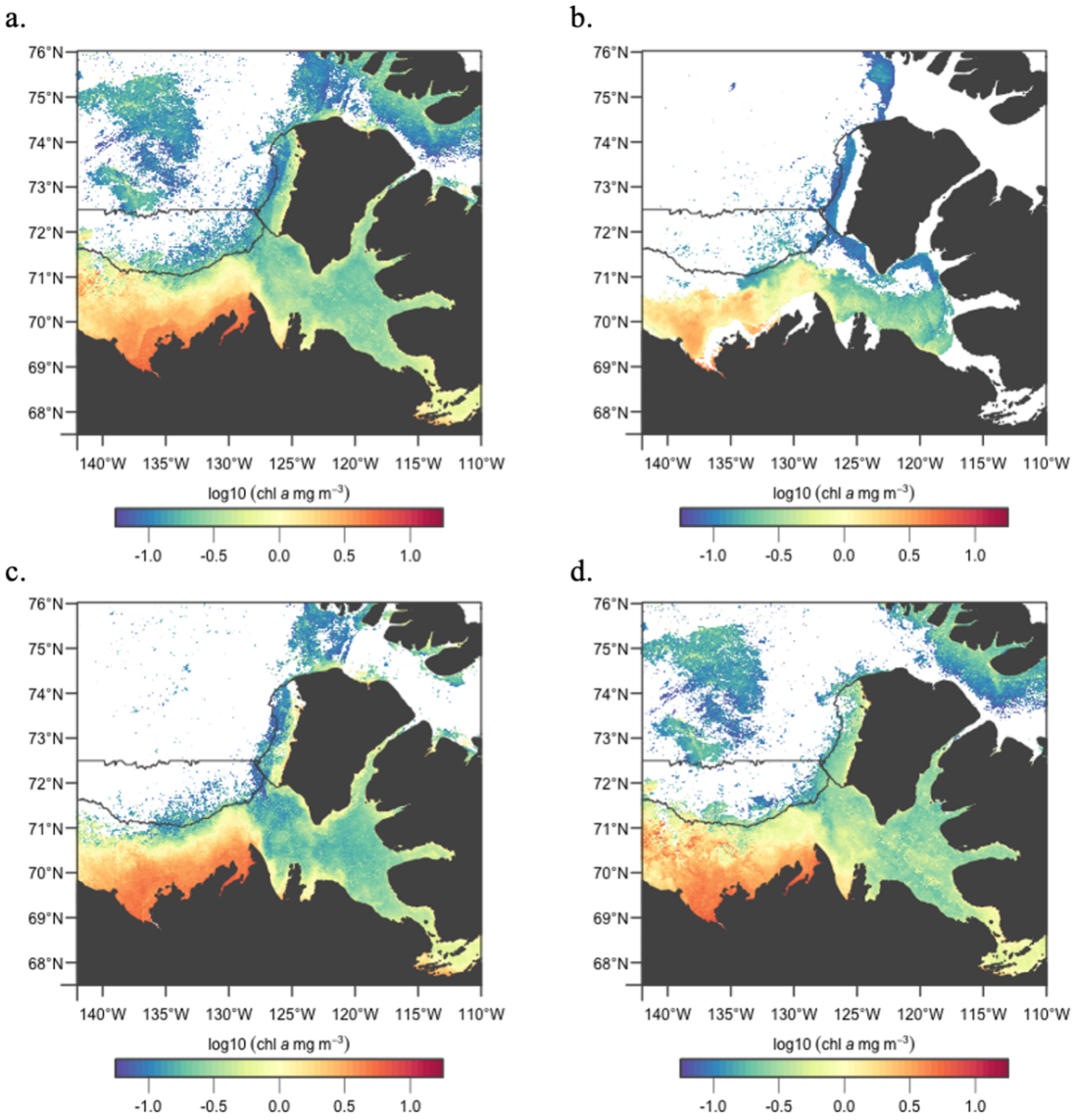

Figure A.23: Mean chlorophyll *a* concentration in **(a)** year-weeks 18 to 41, **(b)** year-weeks 18 to 25, **(c)** year-weeks 26 to 33, **(d)** year-weeks 34 to 41 in 2020.

B Chlorophyll *a* concentration standard deviation in the study region by year

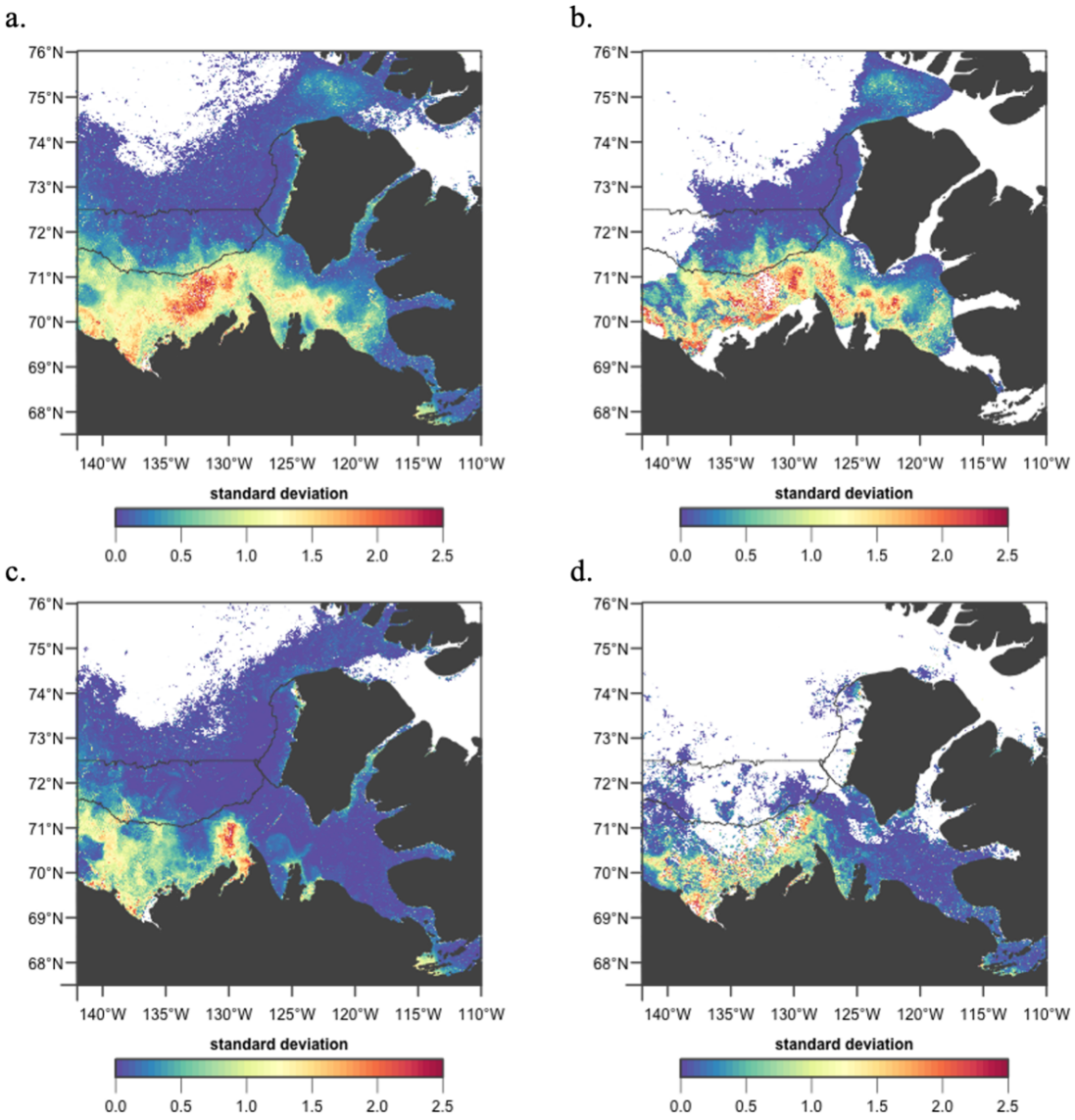

Figure B.1: Chlorophyll *a* standard deviation in **(a)** year-weeks 18 to 41, **(b)** year-weeks 18 to 25, **(c)** year-weeks 26 to 33, **(d)** year-weeks 34 to 41 in 1998.

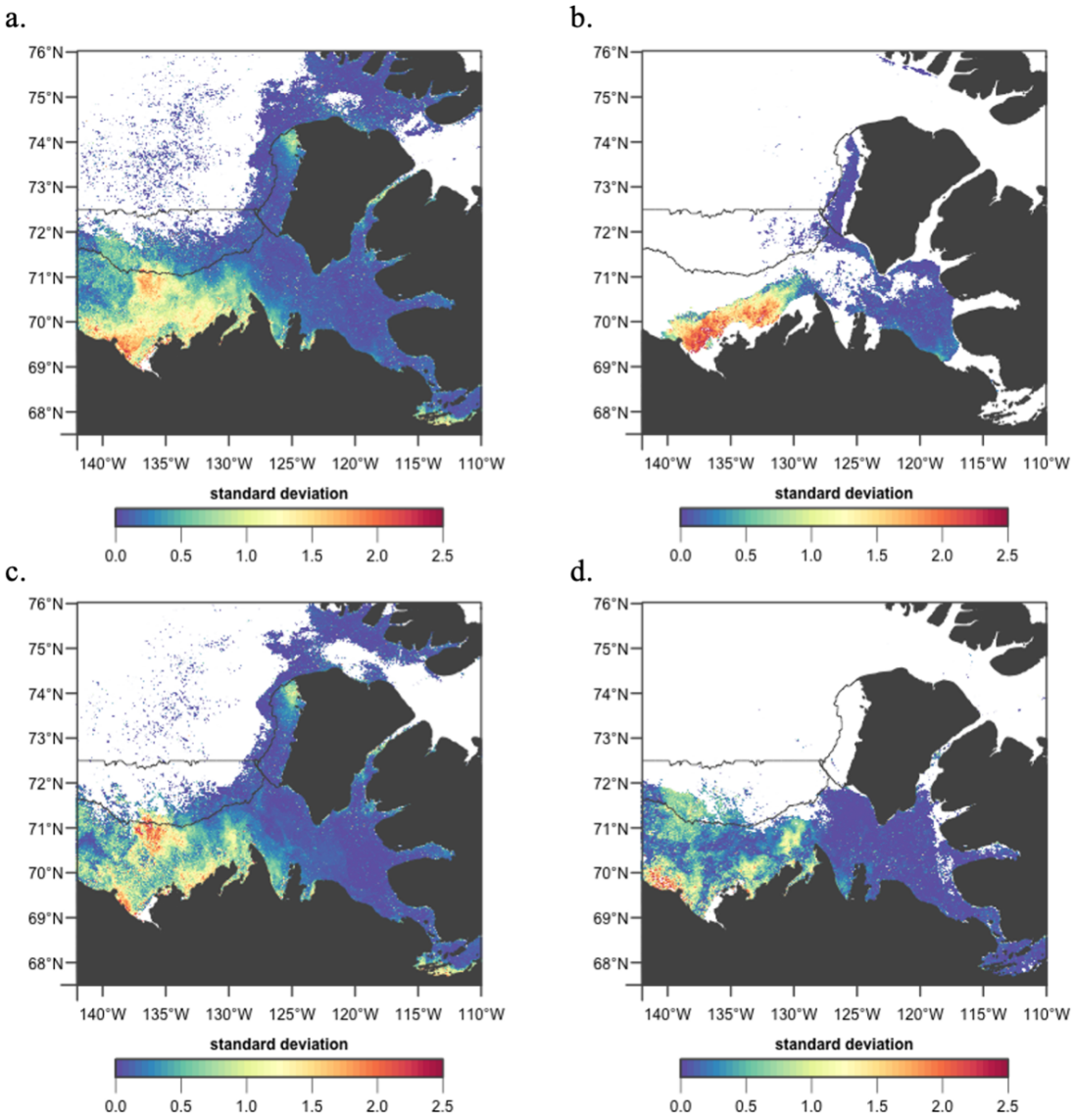

Figure B.2: Chlorophyll *a* standard deviation in **(a)** year-weeks 18 to 41, **(b)** year-weeks 18 to 25, **(c)** year-weeks 26 to 33, **(d)** year-weeks 34 to 41 in 1999.

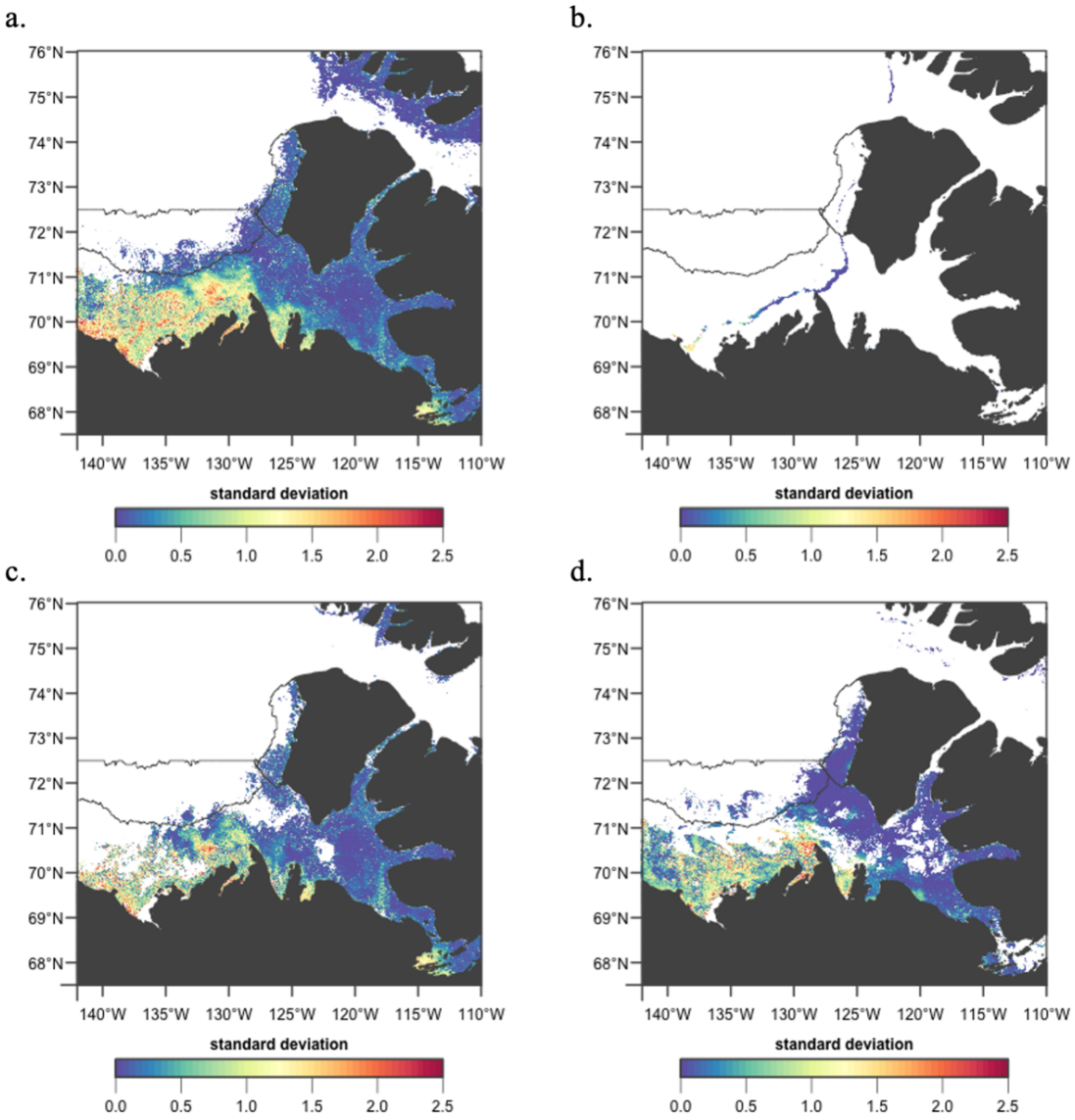

Figure B.3: Chlorophyll *a* standard deviation in **(a)** year-weeks 18 to 41, **(b)** year-weeks 18 to 25, **(c)** year-weeks 26 to 33, **(d)** year-weeks 34 to 41 in 2000.

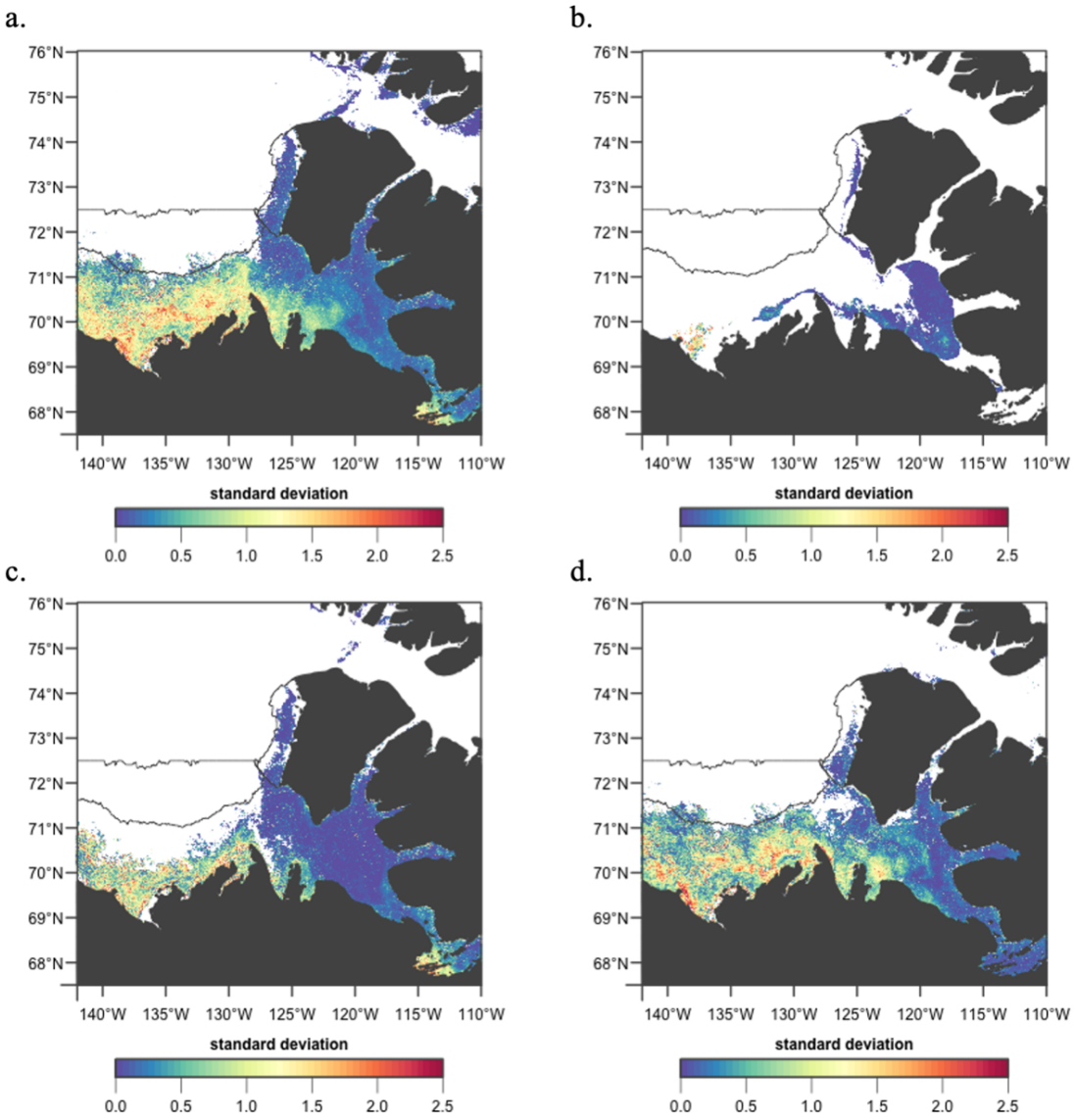

Figure B.4: Chlorophyll *a* standard deviation in **(a)** year-weeks 18 to 41, **(b)** year-weeks 18 to 25, **(c)** year-weeks 26 to 33, **(d)** year-weeks 34 to 41 in 2001.

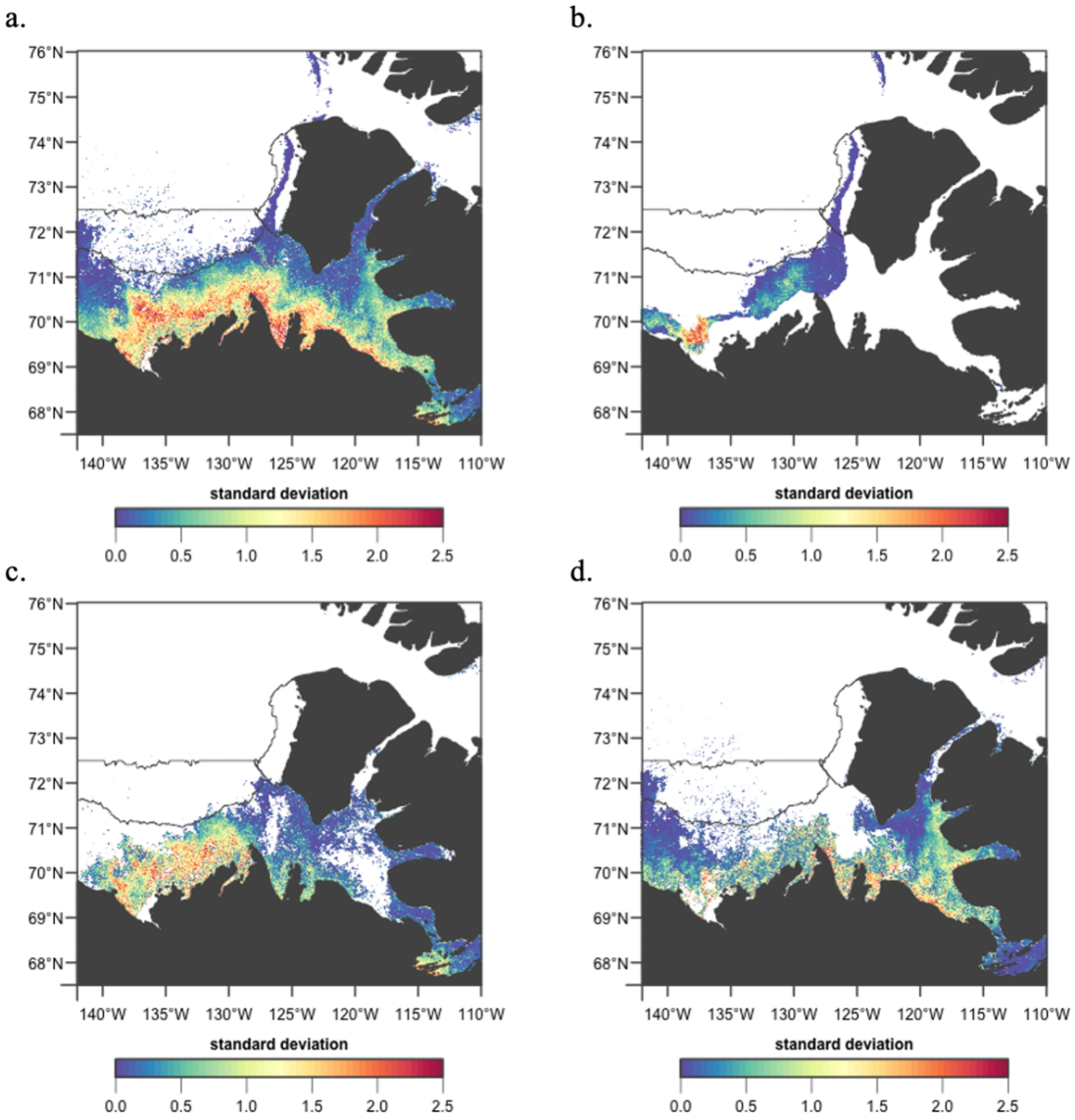

Figure B.5: Chlorophyll *a* standard deviation in **(a)** year-weeks 18 to 41, **(b)** year-weeks 18 to 25, **(c)** year-weeks 26 to 33, **(d)** year-weeks 34 to 41 in 2002.

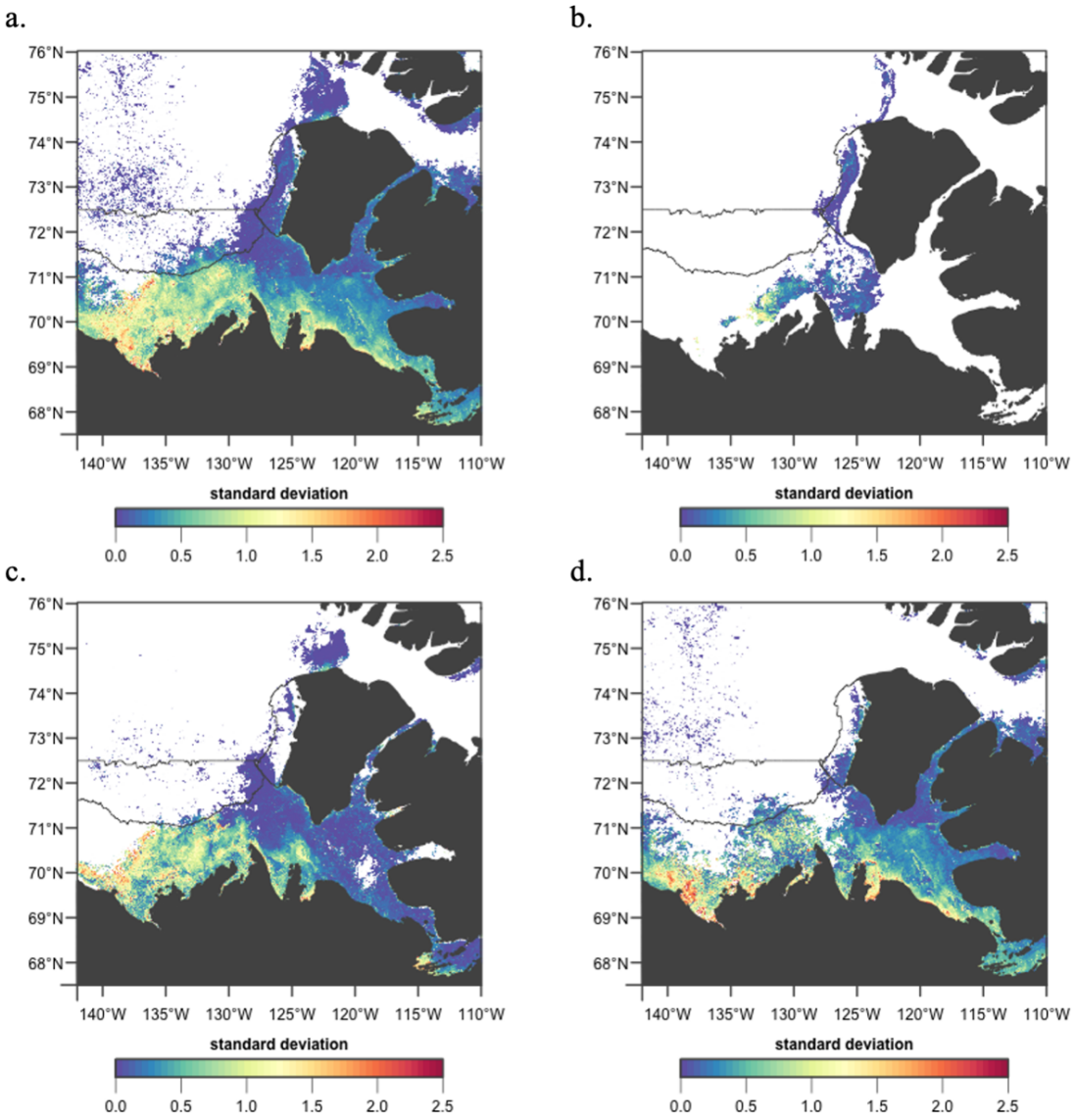

Figure B.6: Chlorophyll *a* standard deviation in **(a)** year-weeks 18 to 41, **(b)** year-weeks 18 to 25, **(c)** year-weeks 26 to 33, **(d)** year-weeks 34 to 41 in 2003.

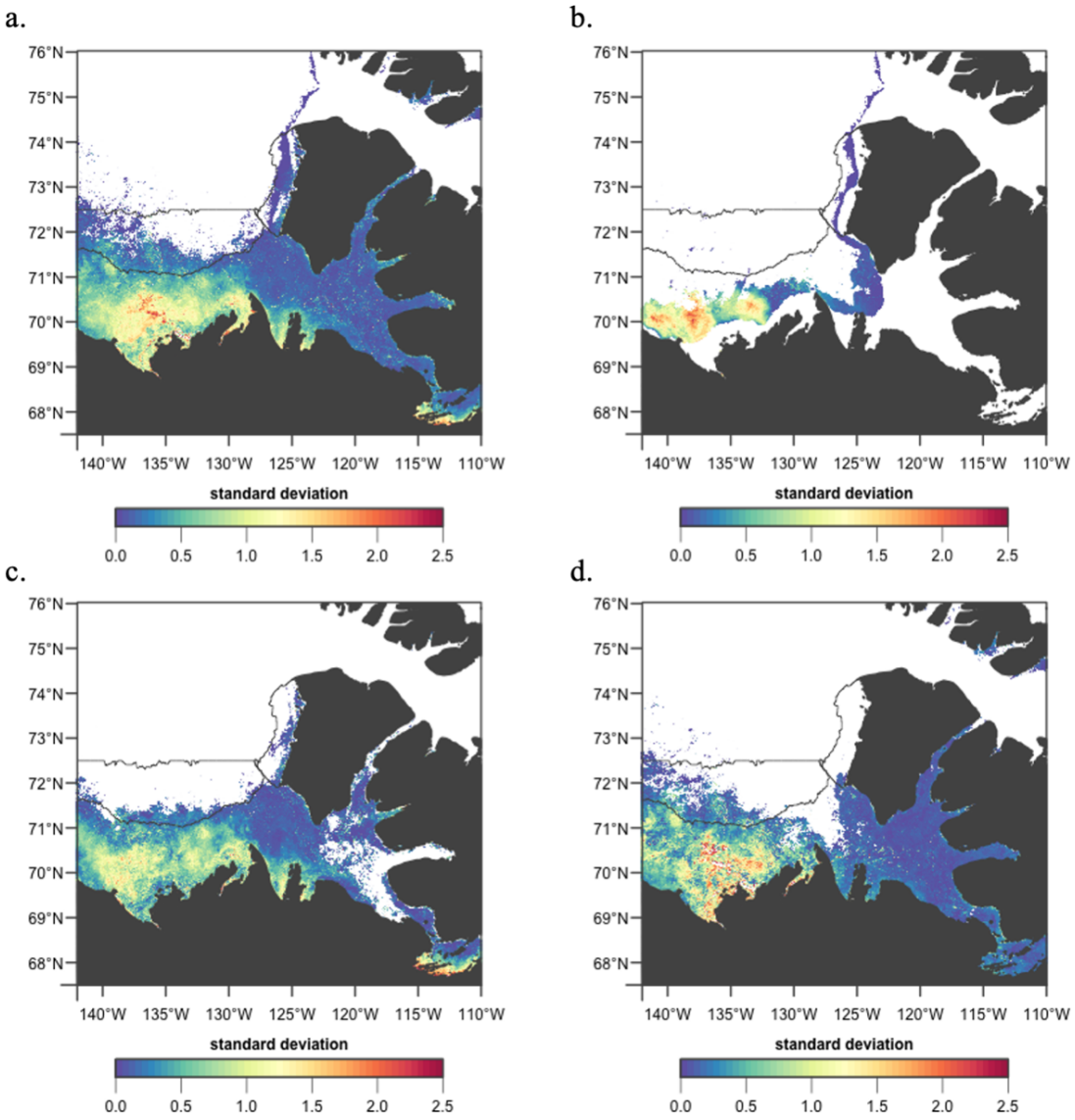

Figure B.7: Chlorophyll *a* standard deviation in **(a)** year-weeks 18 to 41, **(b)** year-weeks 18 to 25, **(c)** year-weeks 26 to 33, **(d)** year-weeks 34 to 41 in 2004.

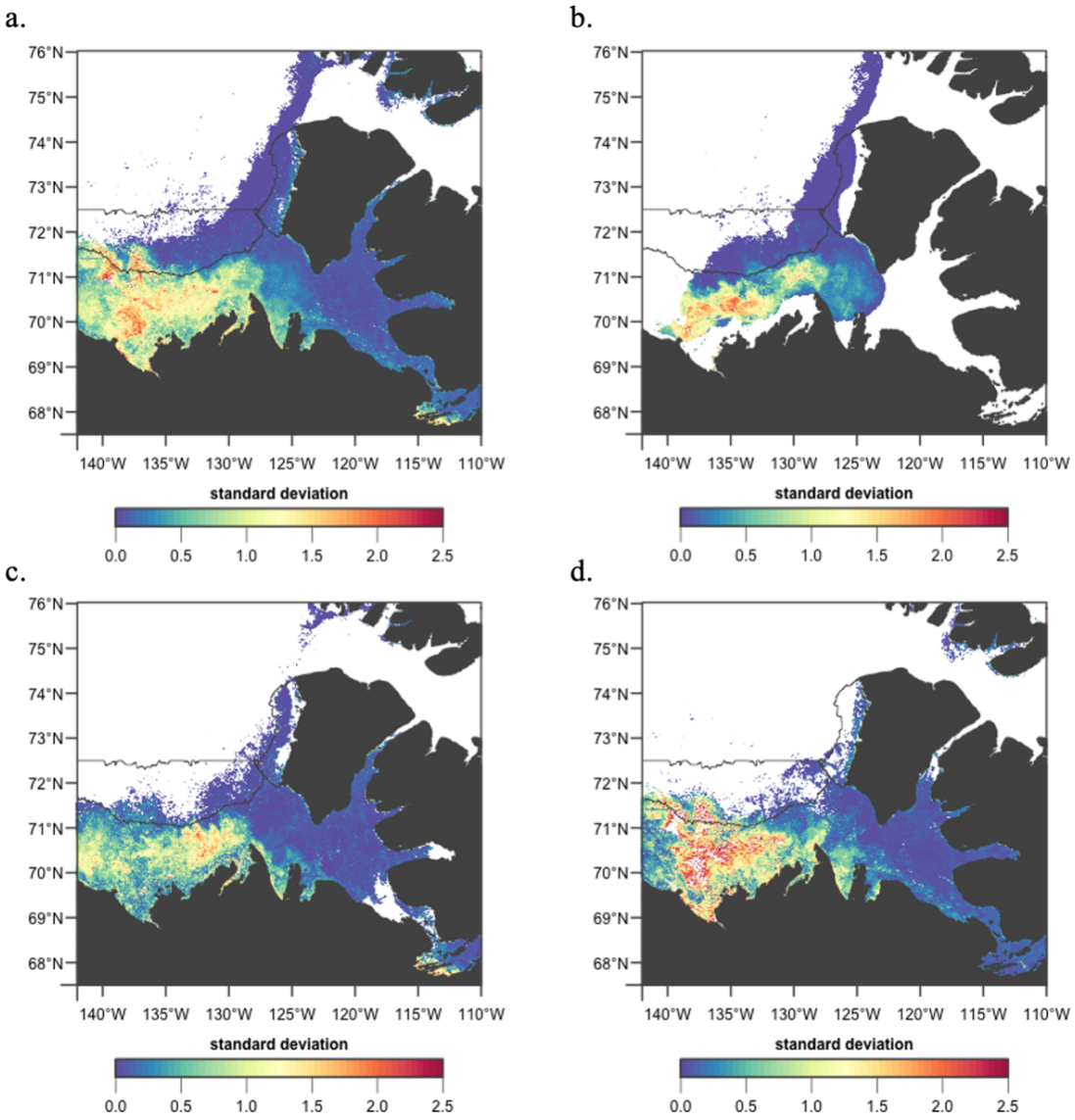

Figure B.8: Chlorophyll *a* standard deviation in **(a)** year-weeks 18 to 41, **(b)** year-weeks 18 to 25, **(c)** year-weeks 26 to 33, **(d)** year-weeks 34 to 41 in 2005.

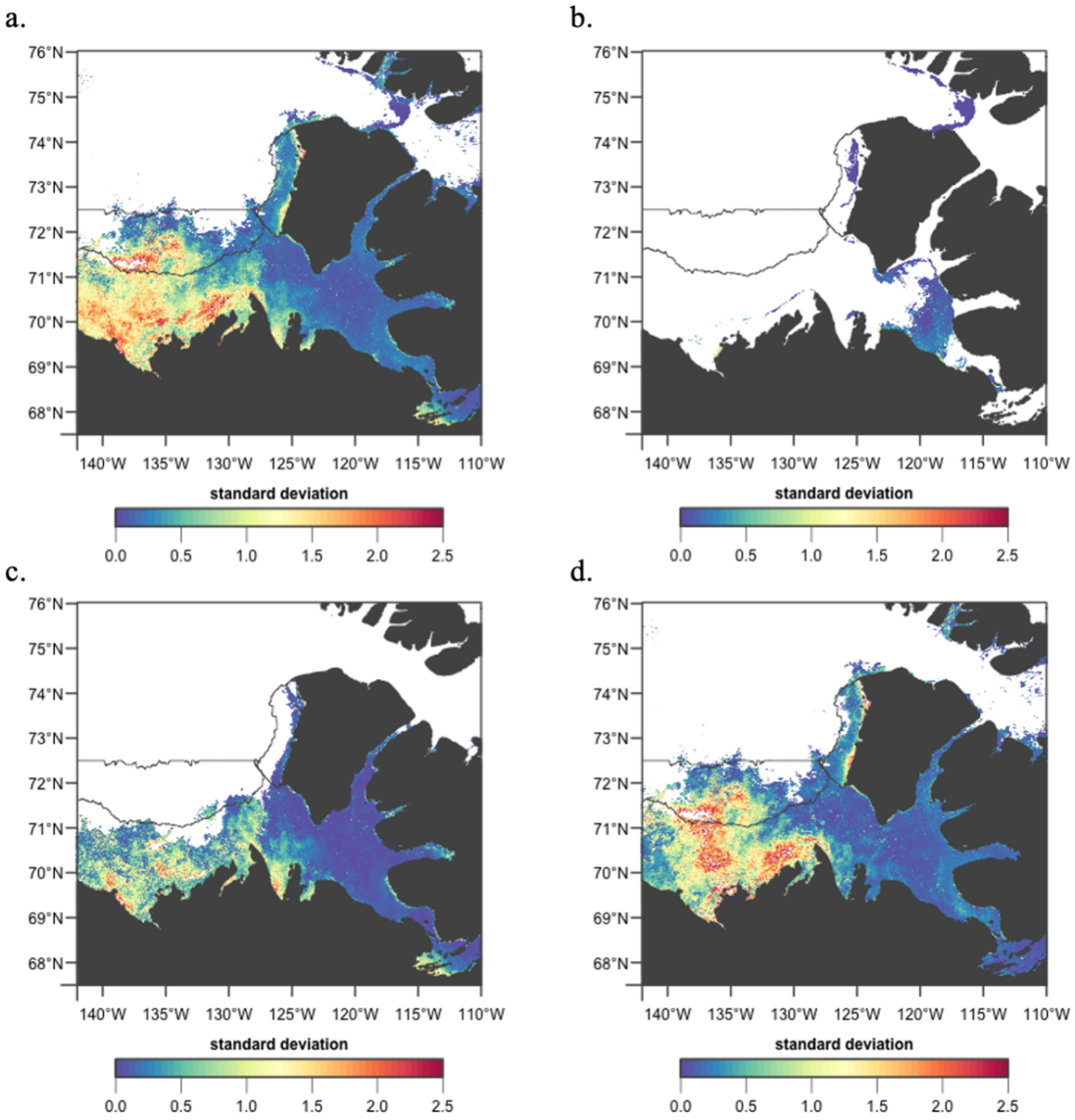

Figure B.9: Chlorophyll *a* standard deviation in **(a)** year-weeks 18 to 41, **(b)** year-weeks 18 to 25, **(c)** year-weeks 26 to 33, **(d)** year-weeks 34 to 41 in 2006.

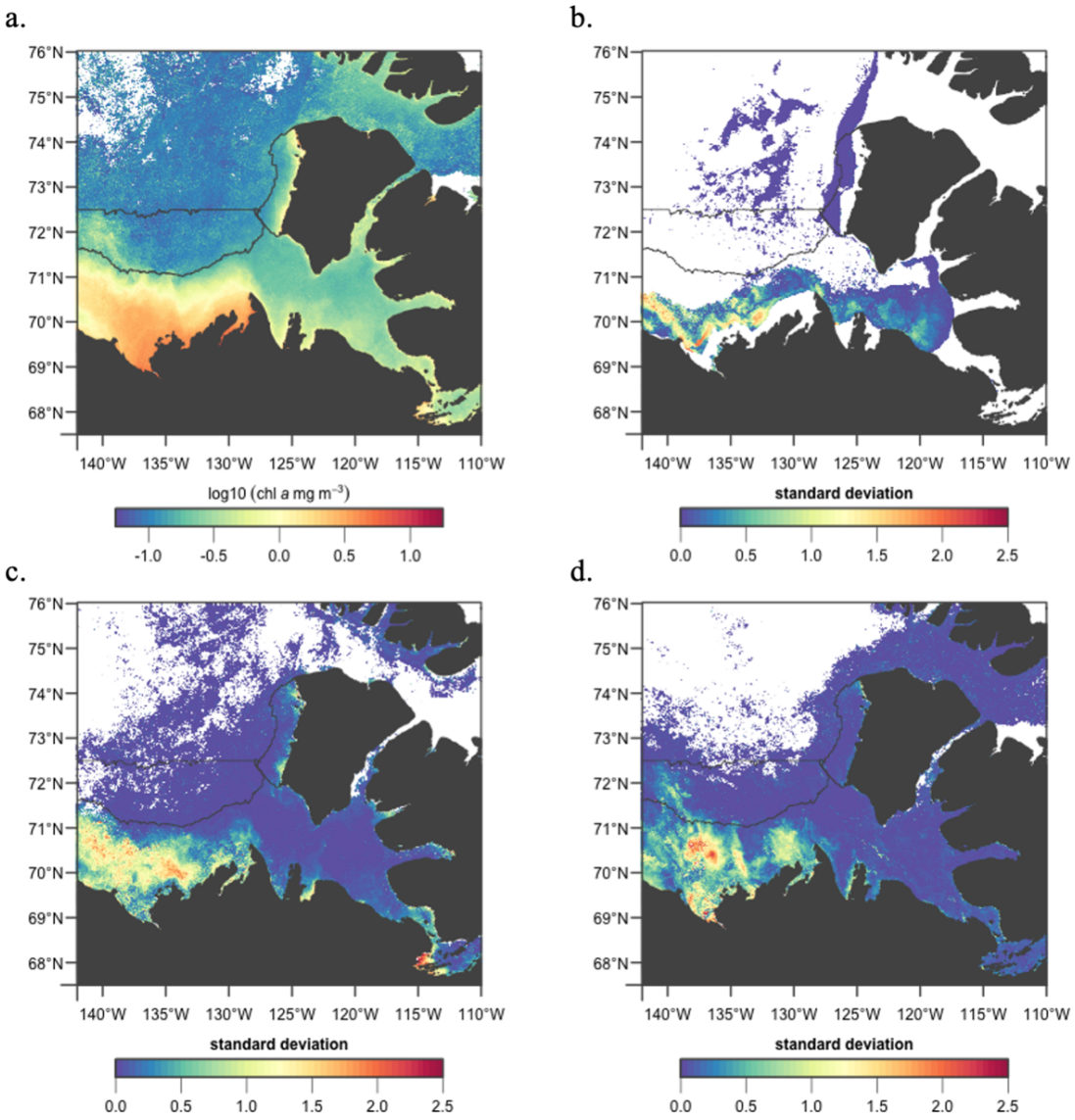

Figure B.10: Chlorophyll *a* standard deviation in **(a)** year-weeks 18 to 41, **(b)** year-weeks 18 to 25, **(c)** year-weeks 26 to 33, **(d)** year-weeks 34 to 41 in 2007.

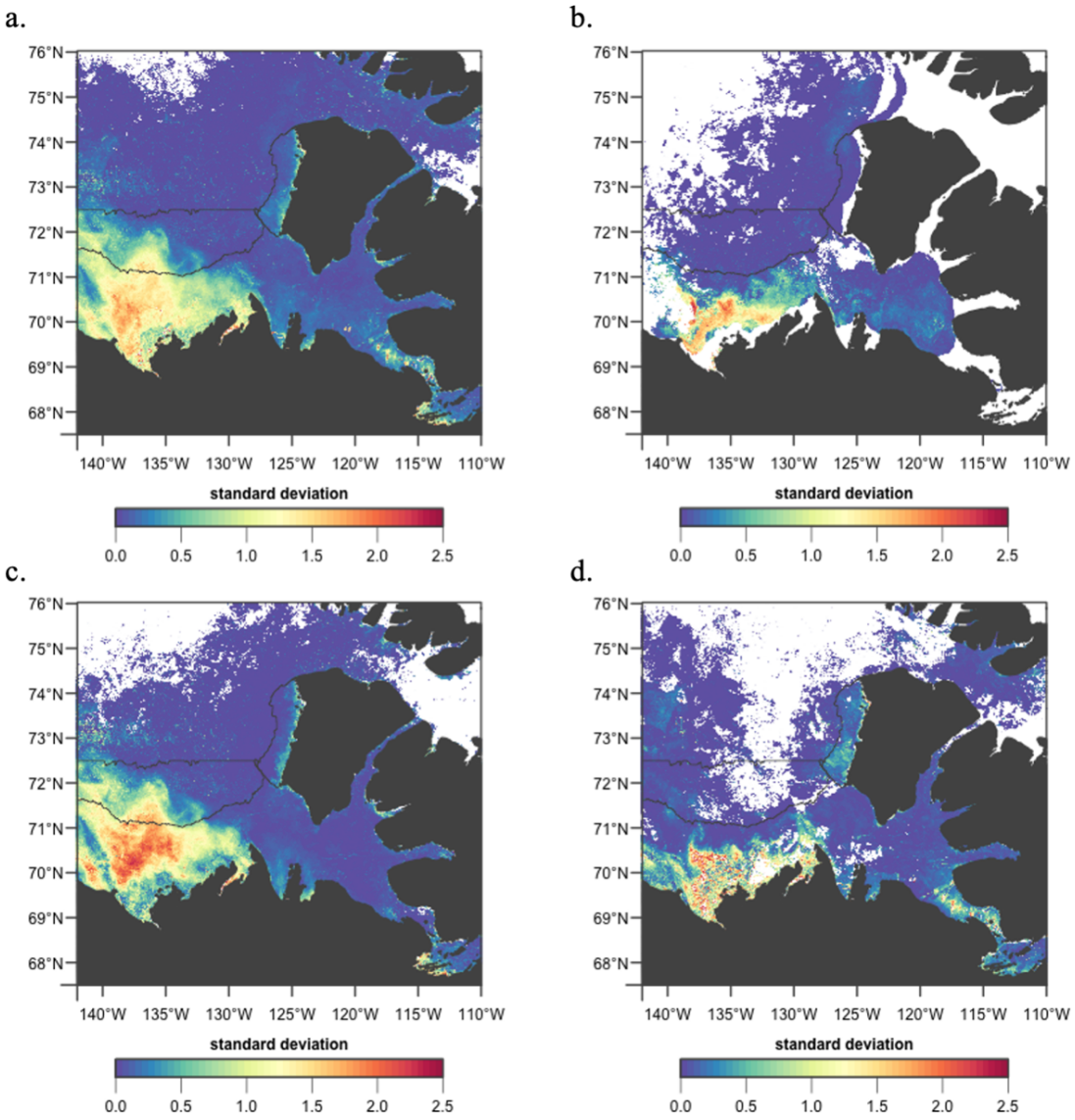

Figure B.11: Chlorophyll *a* standard deviation in **(a)** year-weeks 18 to 41, **(b)** year-weeks 18 to 25, **(c)** year-weeks 26 to 33, **(d)** year-weeks 34 to 41 in 2008.

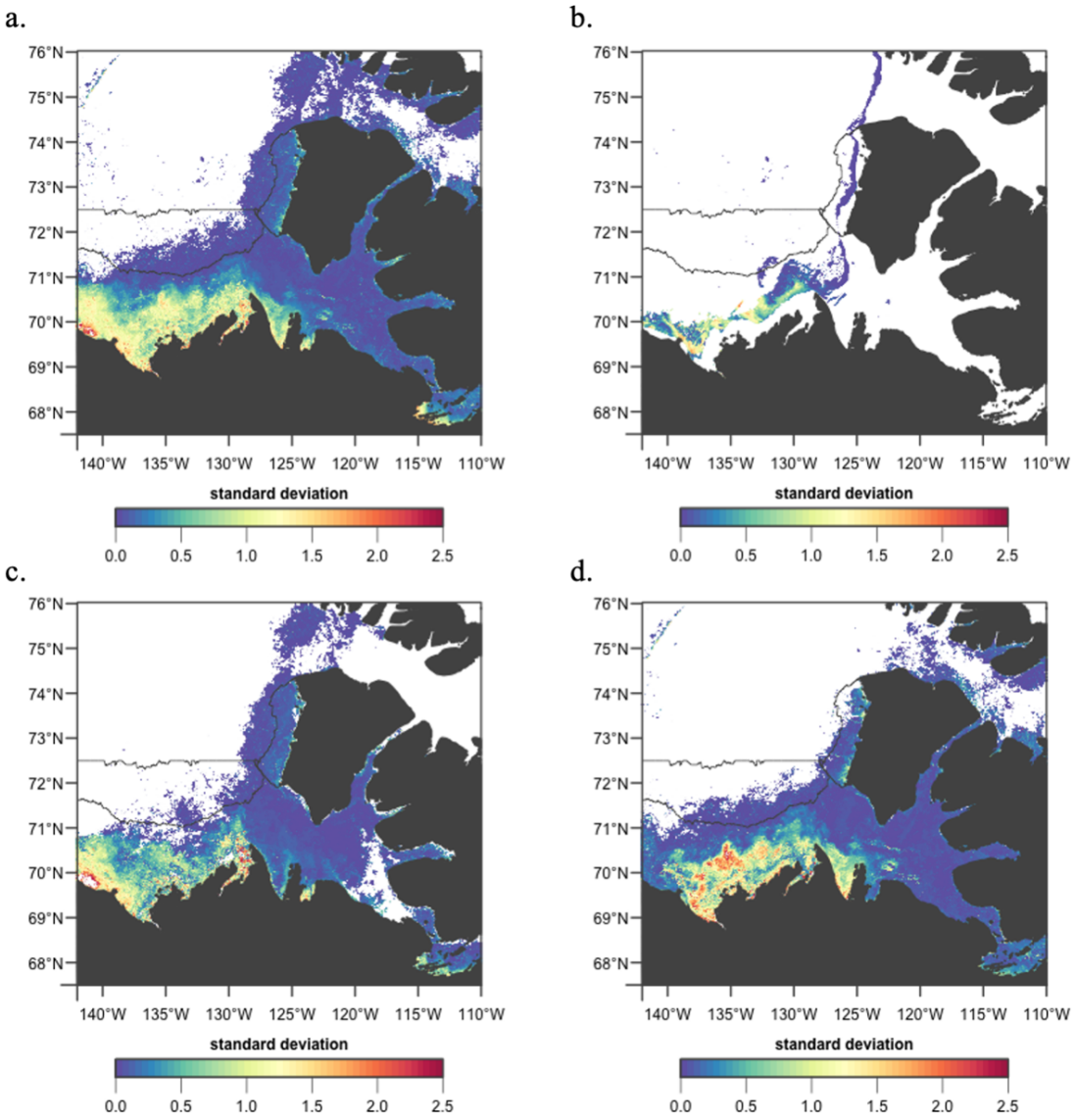

Figure B.12: Chlorophyll *a* standard deviation in **(a)** year-weeks 18 to 41, **(b)** year-weeks 18 to 25, **(c)** year-weeks 26 to 33, **(d)** year-weeks 34 to 41 in 2009.

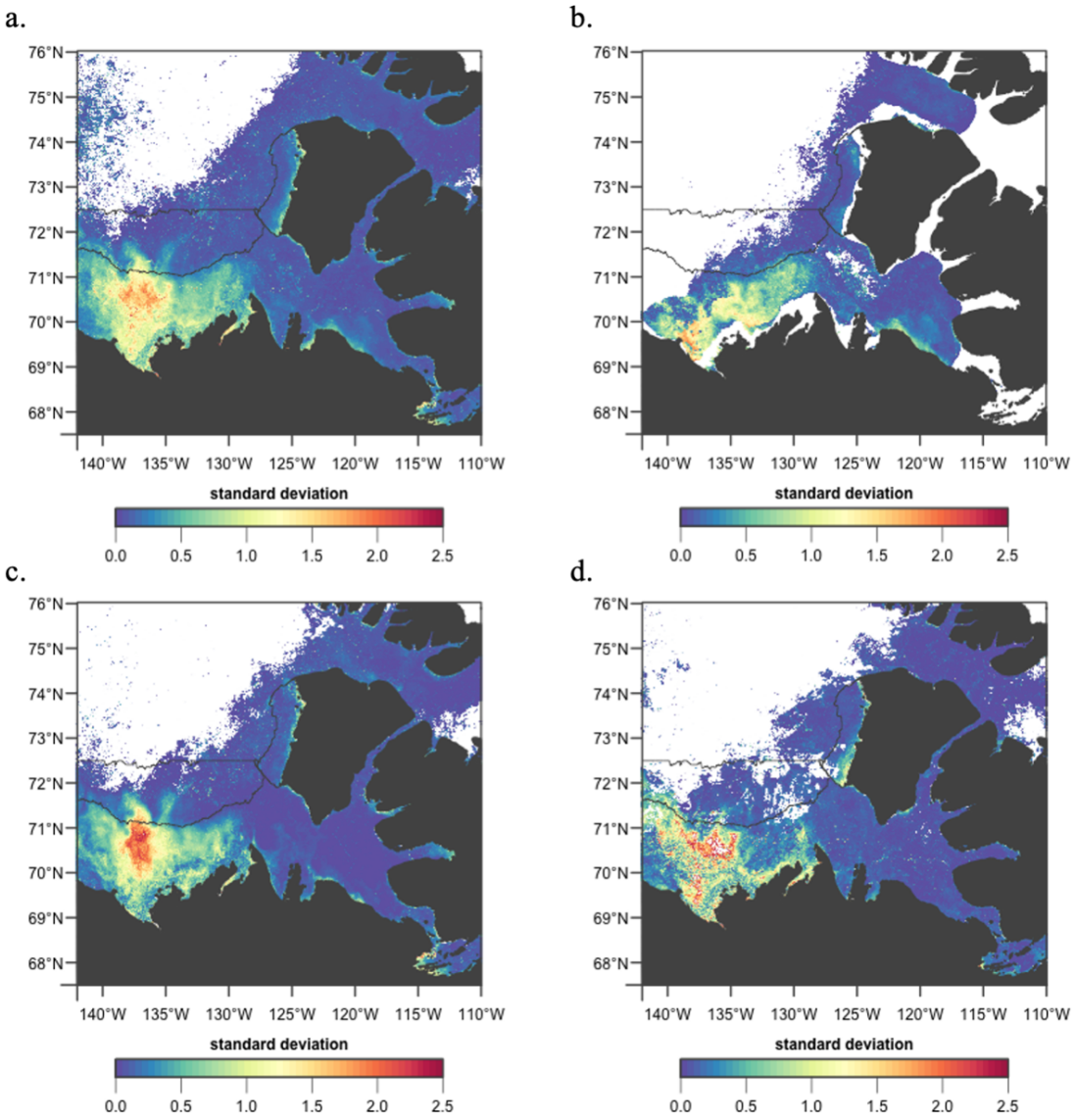

Figure B.13: Chlorophyll *a* standard deviation in **(a)** year-weeks 18 to 41, **(b)** year-weeks 18 to 25, **(c)** year-weeks 26 to 33, **(d)** year-weeks 34 to 41 in 2010.

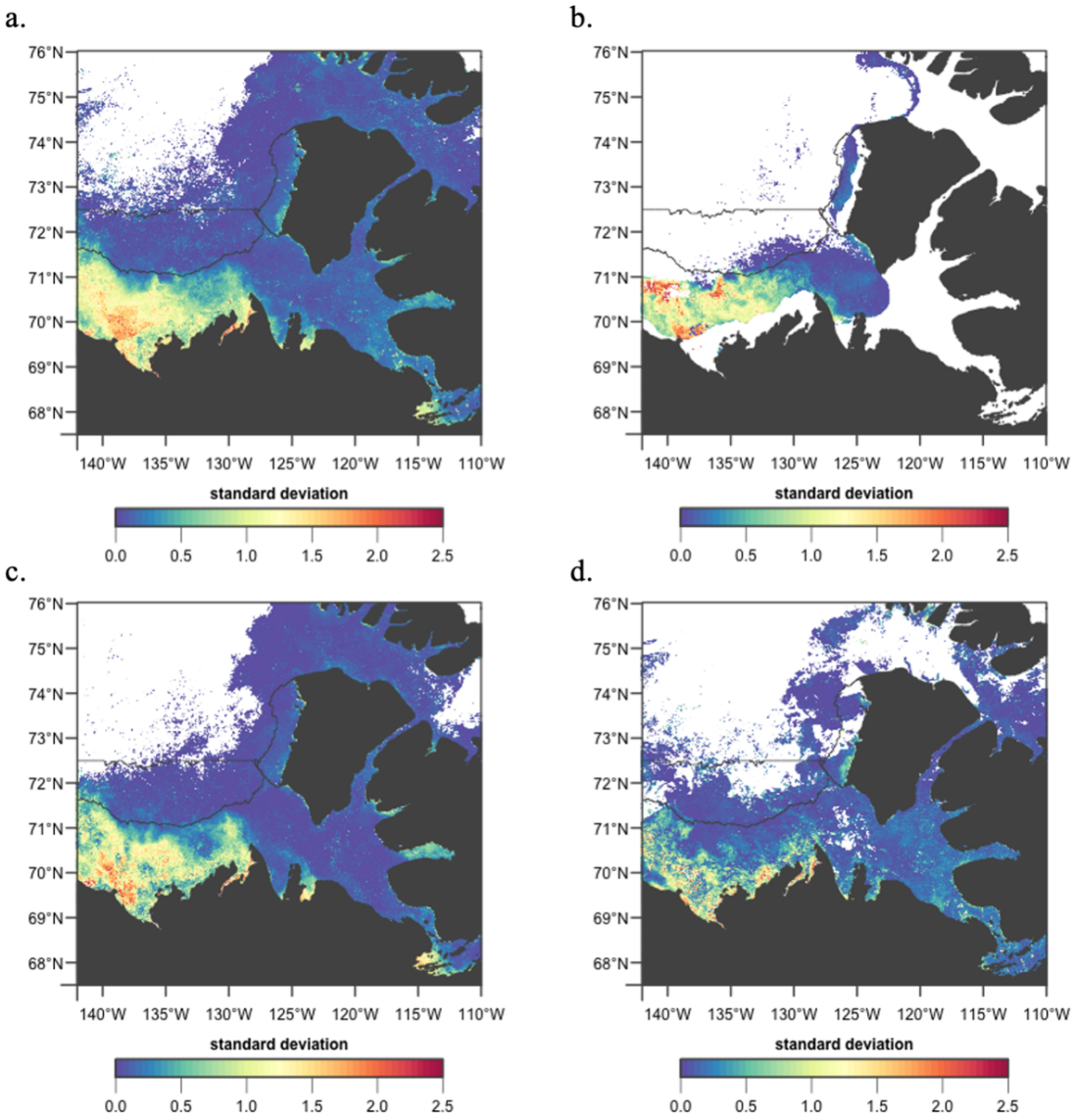

Figure B.14: Chlorophyll *a* standard deviation in **(a)** year-weeks 18 to 41, **(b)** year-weeks 18 to 25, **(c)** year-weeks 26 to 33, **(d)** year-weeks 34 to 41 in 2011.

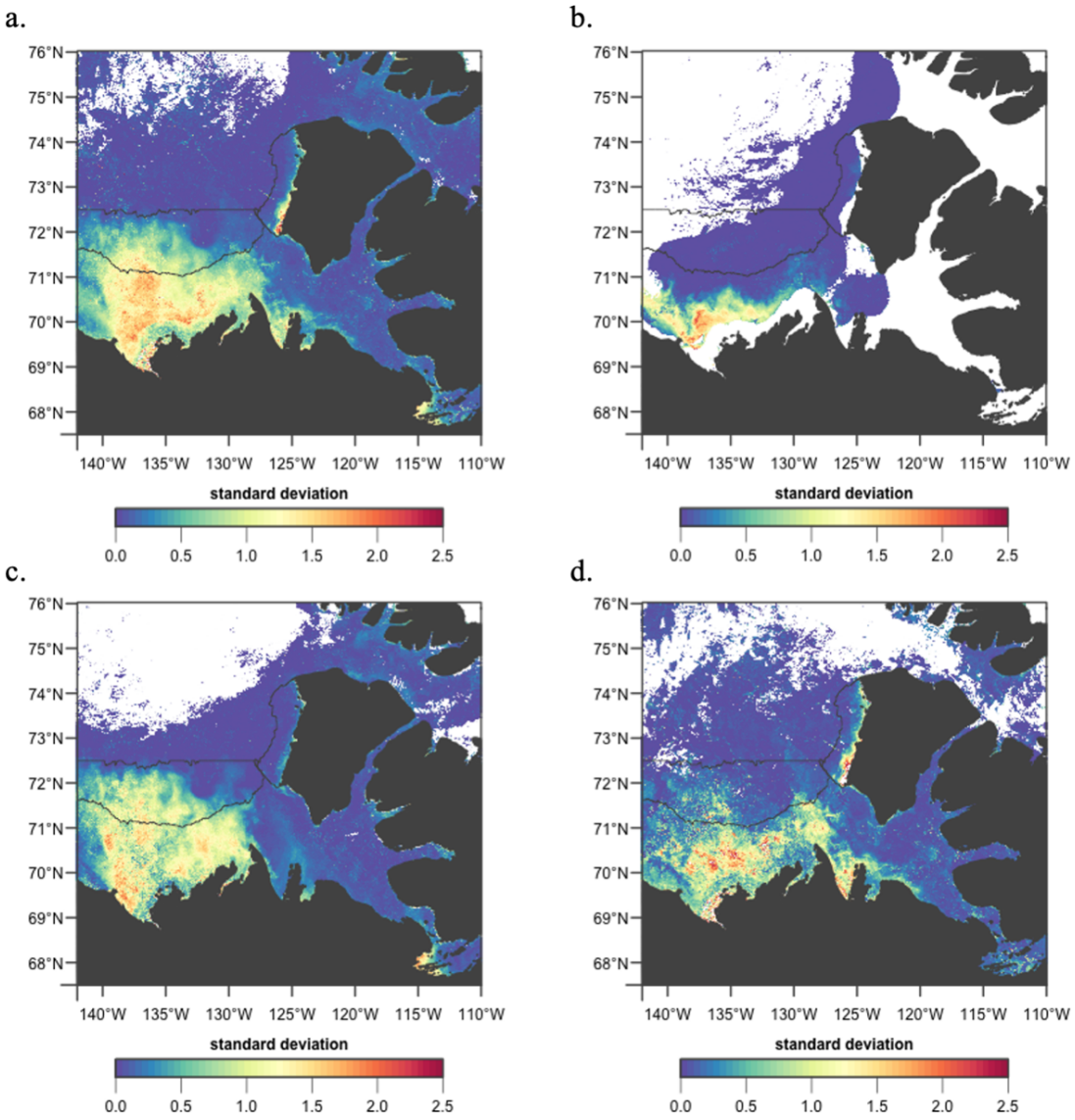

Figure B.15: Chlorophyll *a* standard deviation in **(a)** year-weeks 18 to 41, **(b)** year-weeks 18 to 25, **(c)** year-weeks 26 to 33, **(d)** year-weeks 34 to 41 in 2012.

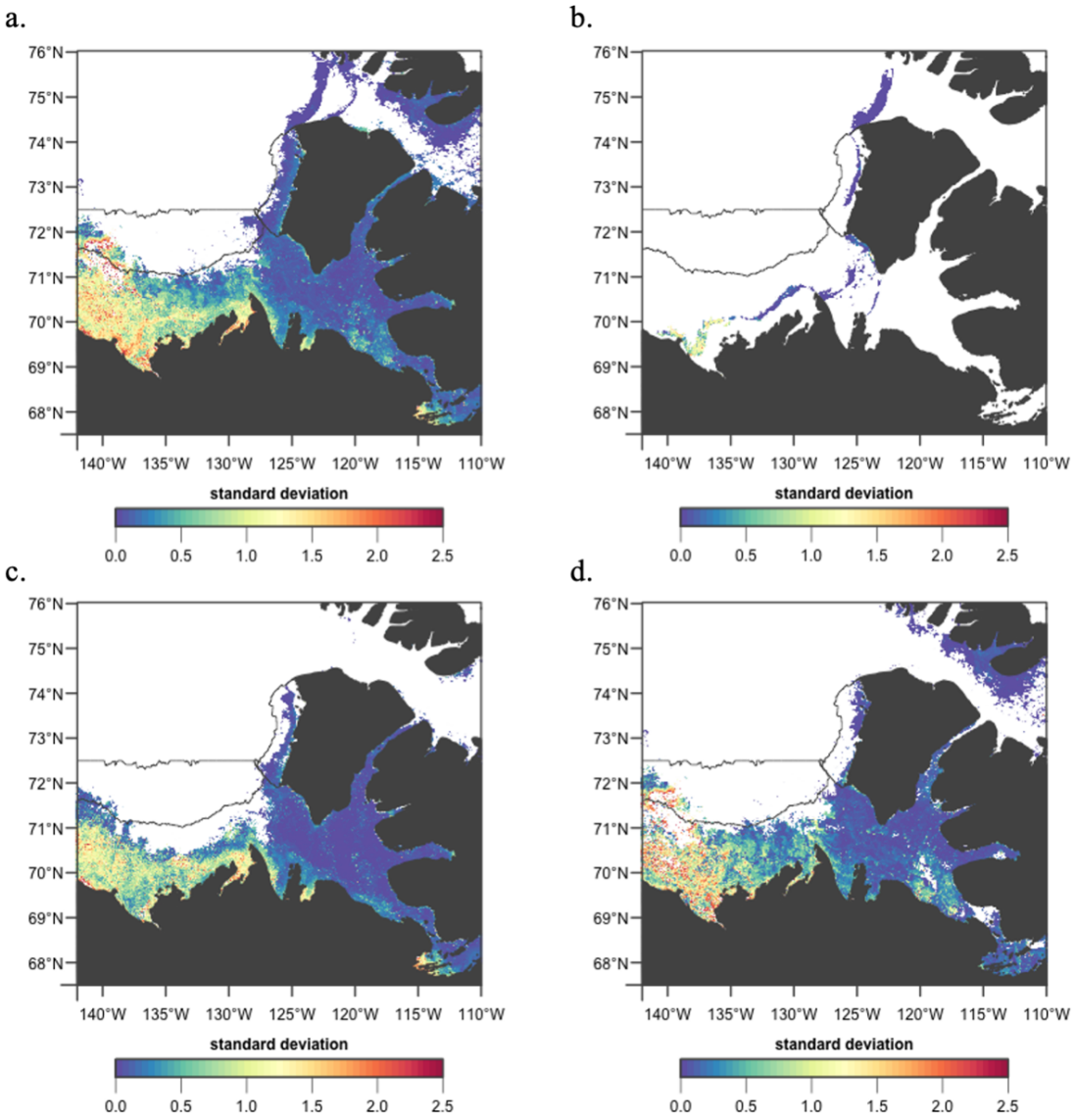

Figure B.16: Chlorophyll *a* standard deviation in **(a)** year-weeks 18 to 41, **(b)** year-weeks 18 to 25, **(c)** year-weeks 26 to 33, **(d)** year-weeks 34 to 41 in 2013.

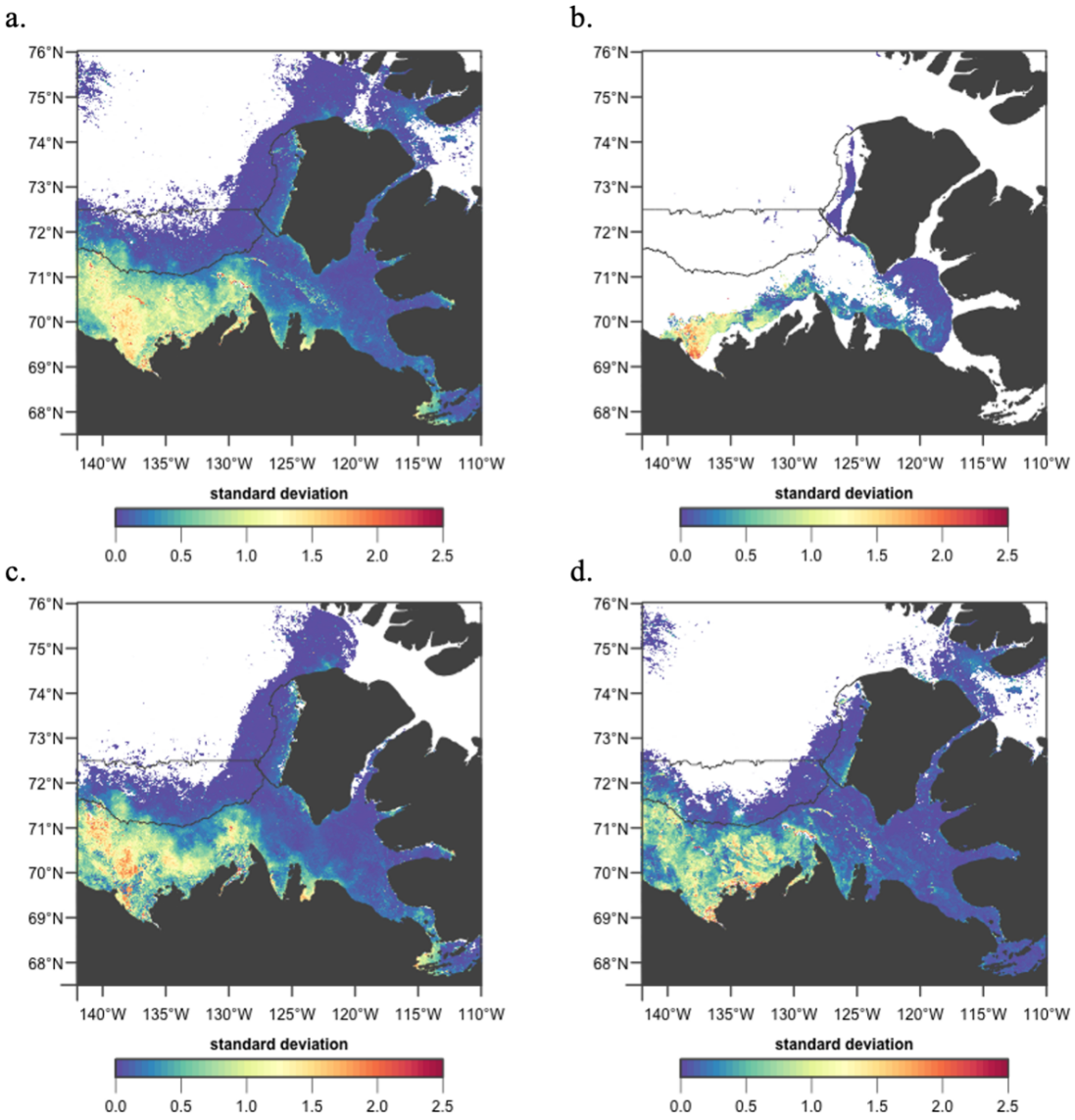

Figure B.17: Chlorophyll *a* standard deviation in **(a)** year-weeks 18 to 41, **(b)** year-weeks 18 to 25, **(c)** year-weeks 26 to 33, **(d)** year-weeks 34 to 41 in 2014.

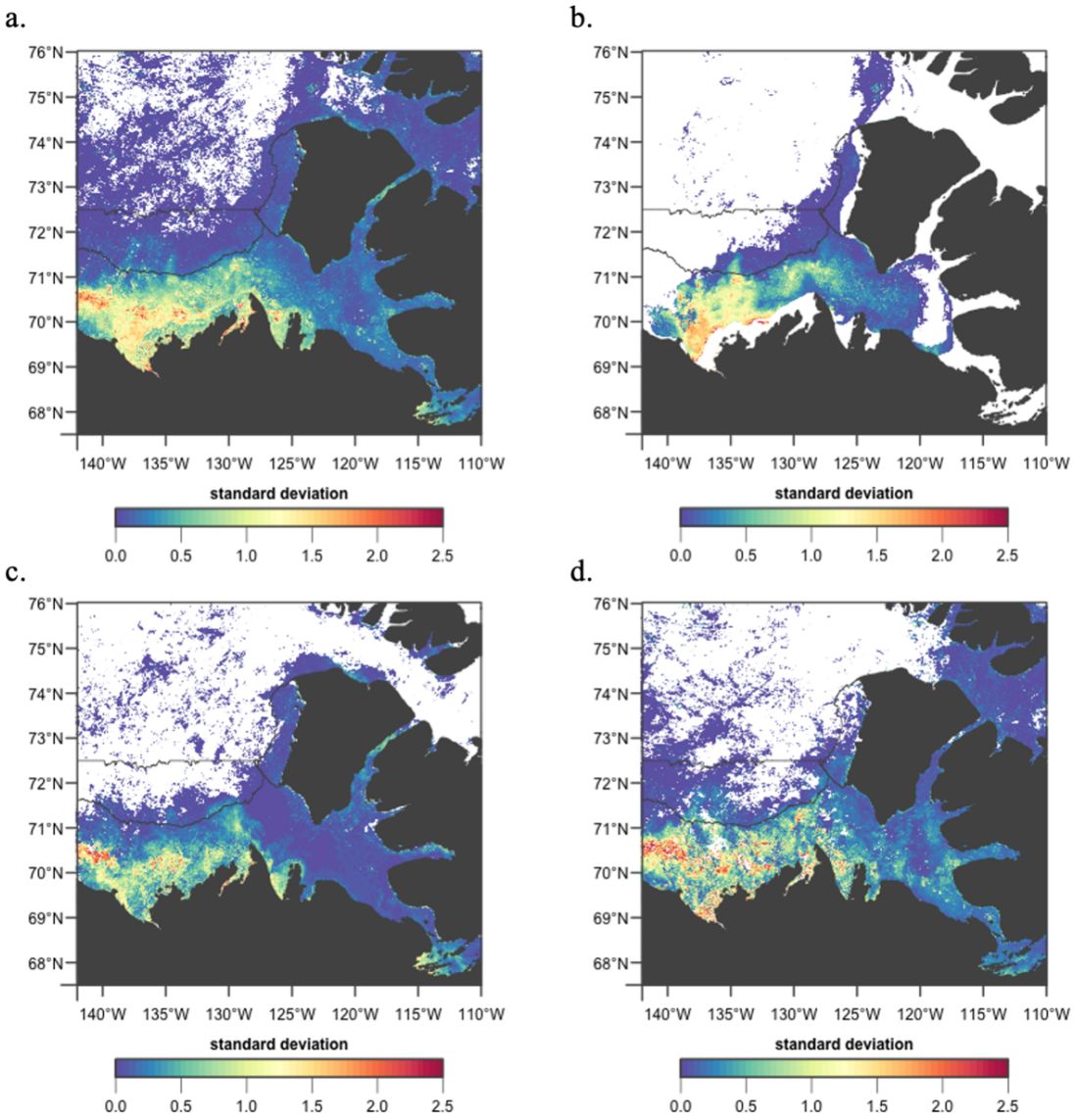

Figure B.18: Chlorophyll *a* standard deviation in **(a)** year-weeks 18 to 41, **(b)** year-weeks 18 to 25, **(c)** year-weeks 26 to 33, **(d)** year-weeks 34 to 41 in 2015.

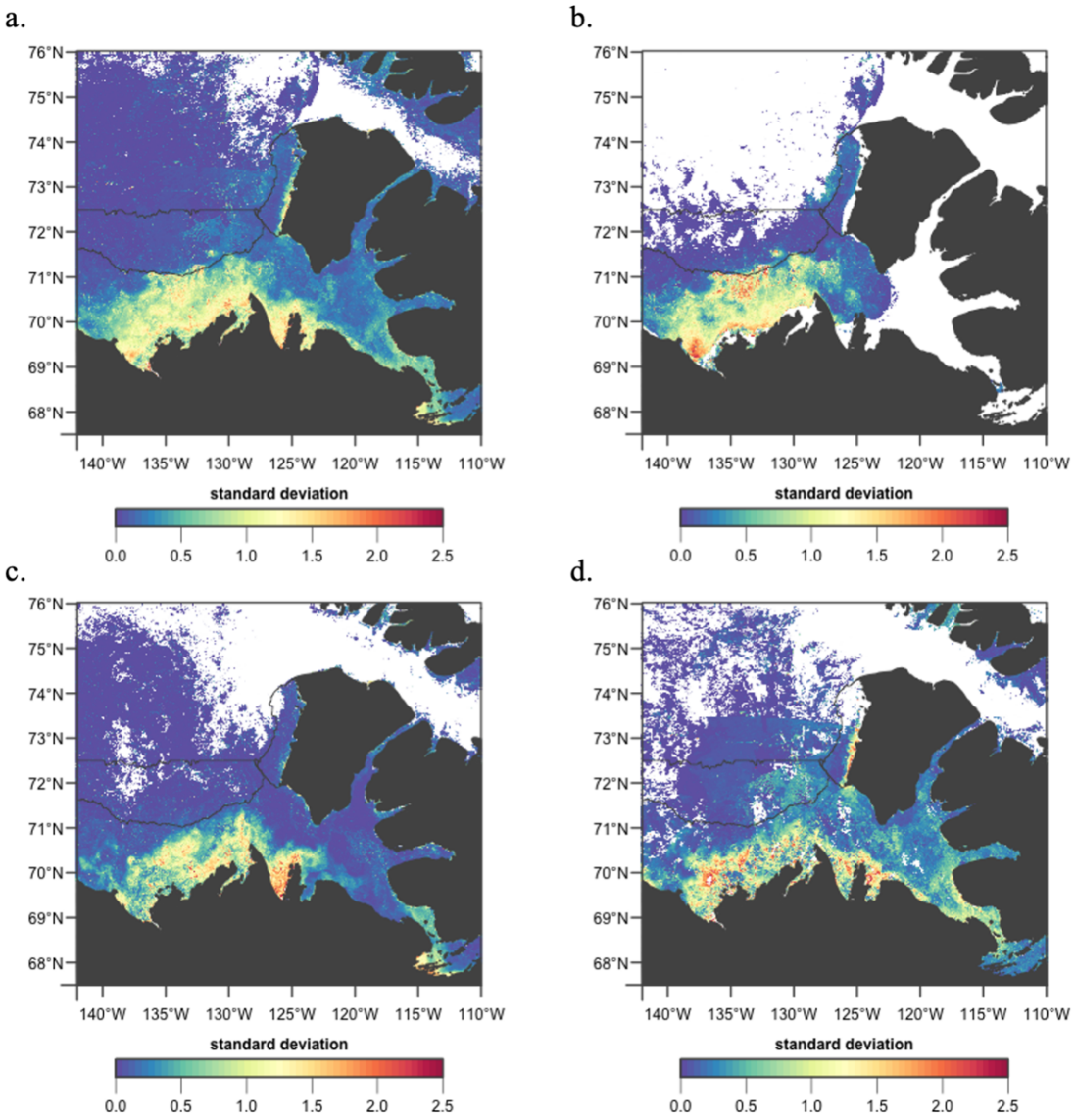

Figure B.19: Chlorophyll *a* standard deviation in **(a)** year-weeks 18 to 41, **(b)** year-weeks 18 to 25, **(c)** year-weeks 26 to 33, **(d)** year-weeks 34 to 41 in 2016.

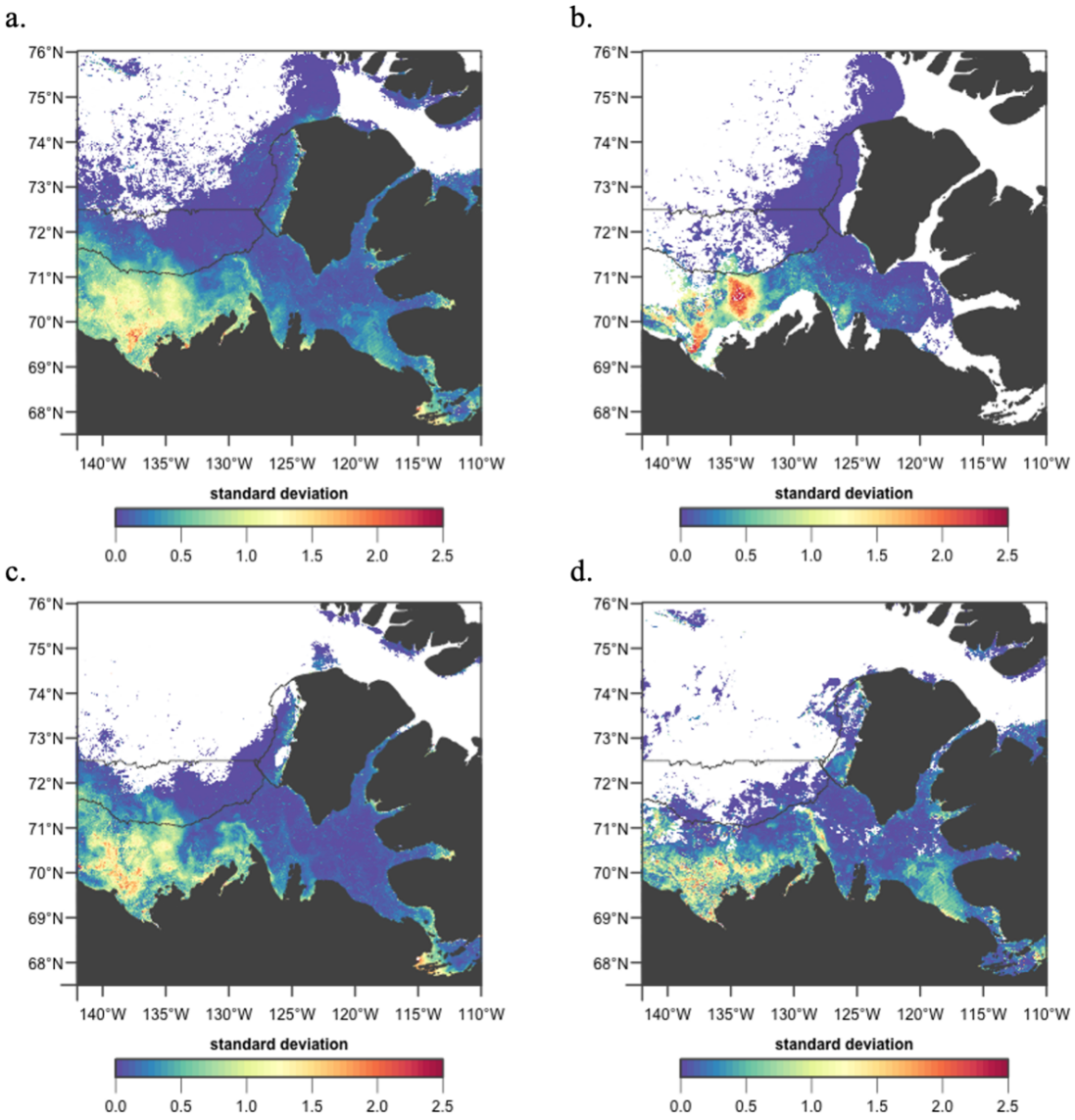

Figure B.20: Chlorophyll *a* standard deviation in **(a)** year-weeks 18 to 41, **(b)** year-weeks 18 to 25, **(c)** year-weeks 26 to 33, **(d)** year-weeks 34 to 41 in 2017.

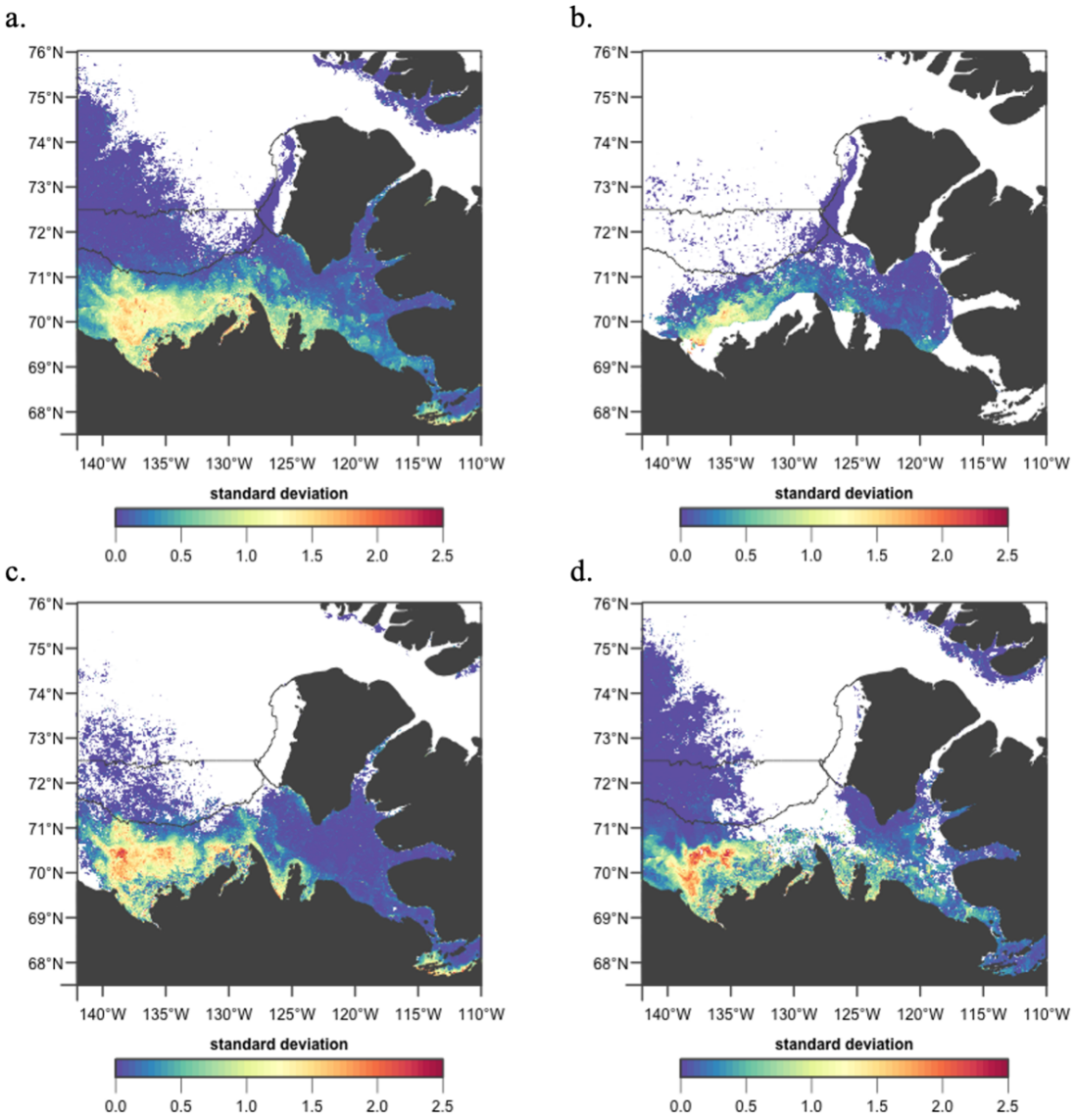

Figure B.21: Chlorophyll *a* standard deviation in **(a)** year-weeks 18 to 41, **(b)** year-weeks 18 to 25, **(c)** year-weeks 26 to 33, **(d)** year-weeks 34 to 41 in 2018.

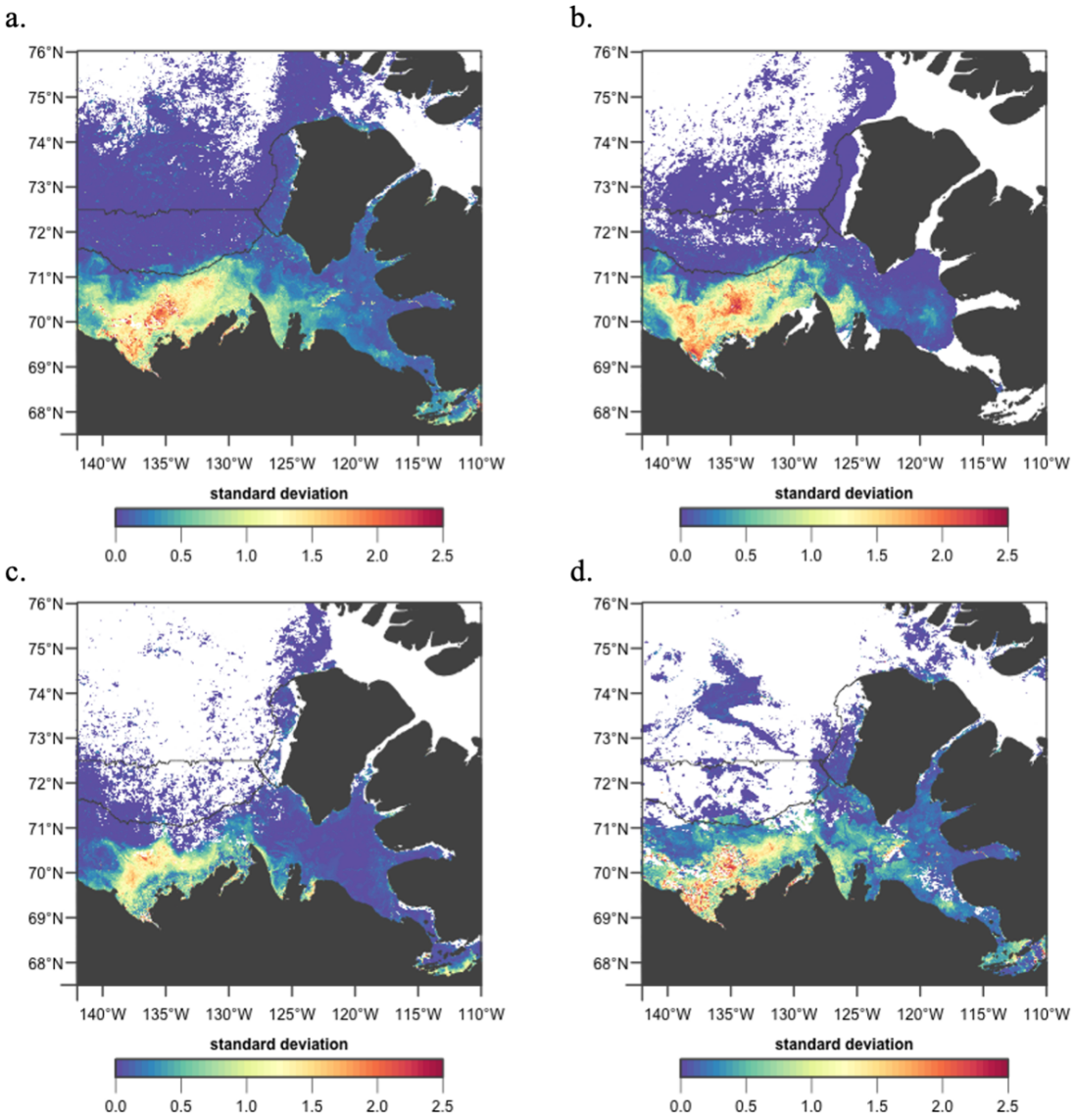

Figure B.22: Chlorophyll *a* standard deviation in **(a)** year-weeks 18 to 41, **(b)** year-weeks 18 to 25, **(c)** year-weeks 26 to 33, **(d)** year-weeks 34 to 41 in 2019.

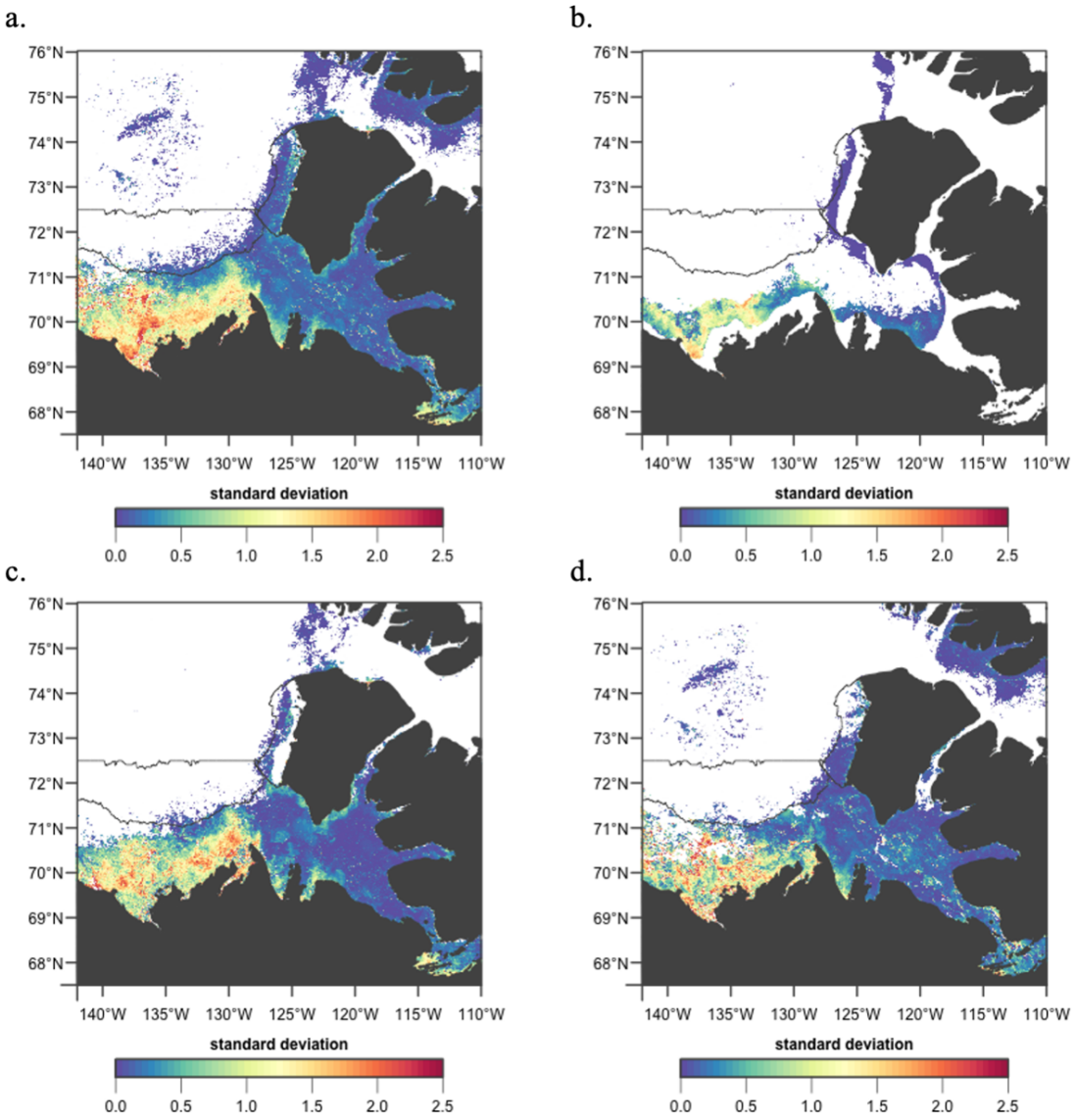

Figure B.23: Chlorophyll *a* standard deviation in **(a)** year-weeks 18 to 41, **(b)** year-weeks 18 to 25, **(c)** year-weeks 26 to 33, **(d)** year-weeks 34 to 41 in 2020.

C Annual sea-ice concentration in the study region

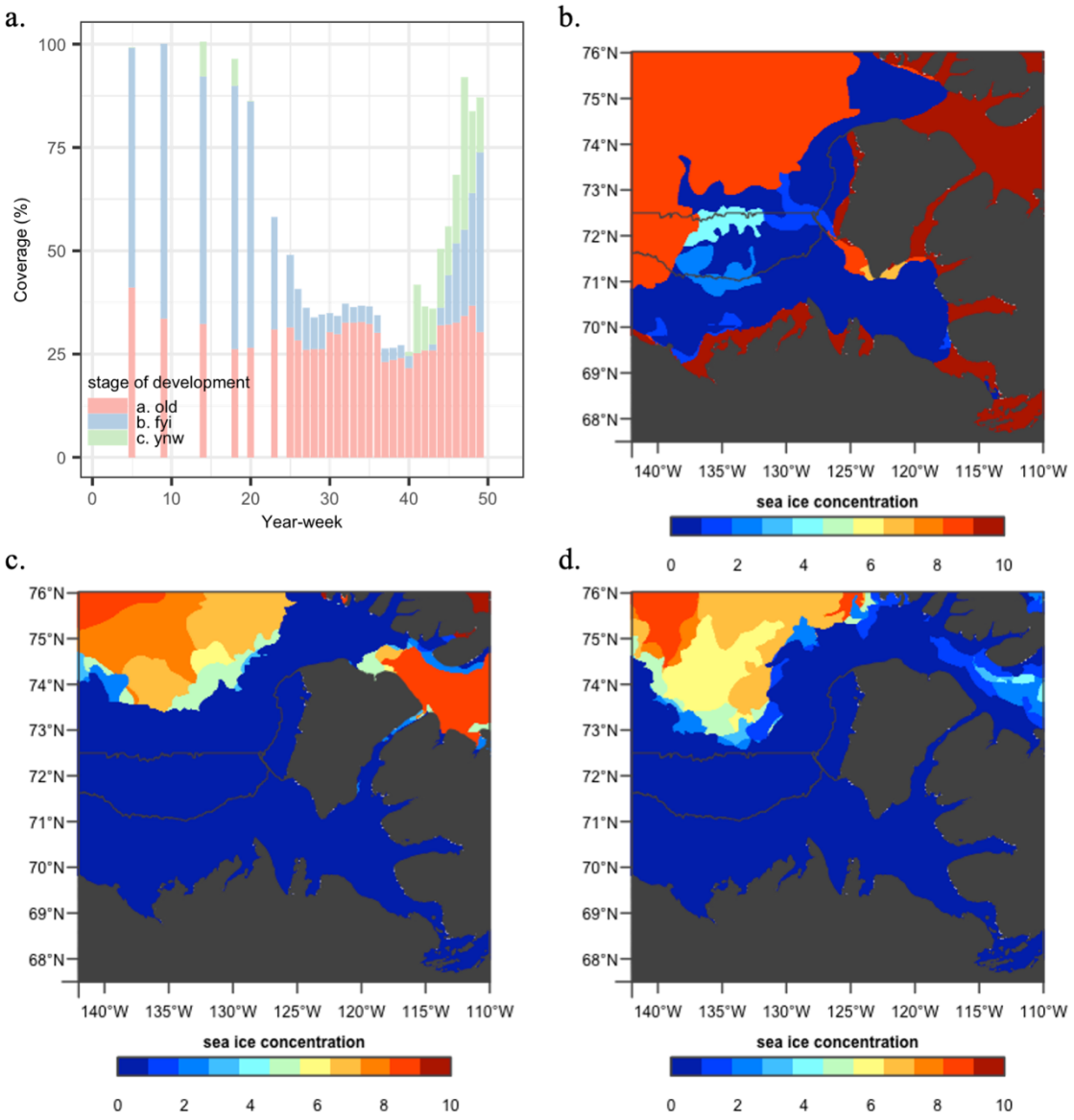

Figure C.1: **(a)** Annual evolution of percent sea-ice coverage by stage of development in 1998, **(b)** minimum sea-ice concentration in year-weeks 18 to 25, **(c)** minimum sea-ice concentration in year-weeks 26 to 33, and **(d)** minimum sea-ice concentration in year-weeks 34 to 41 in 1998.

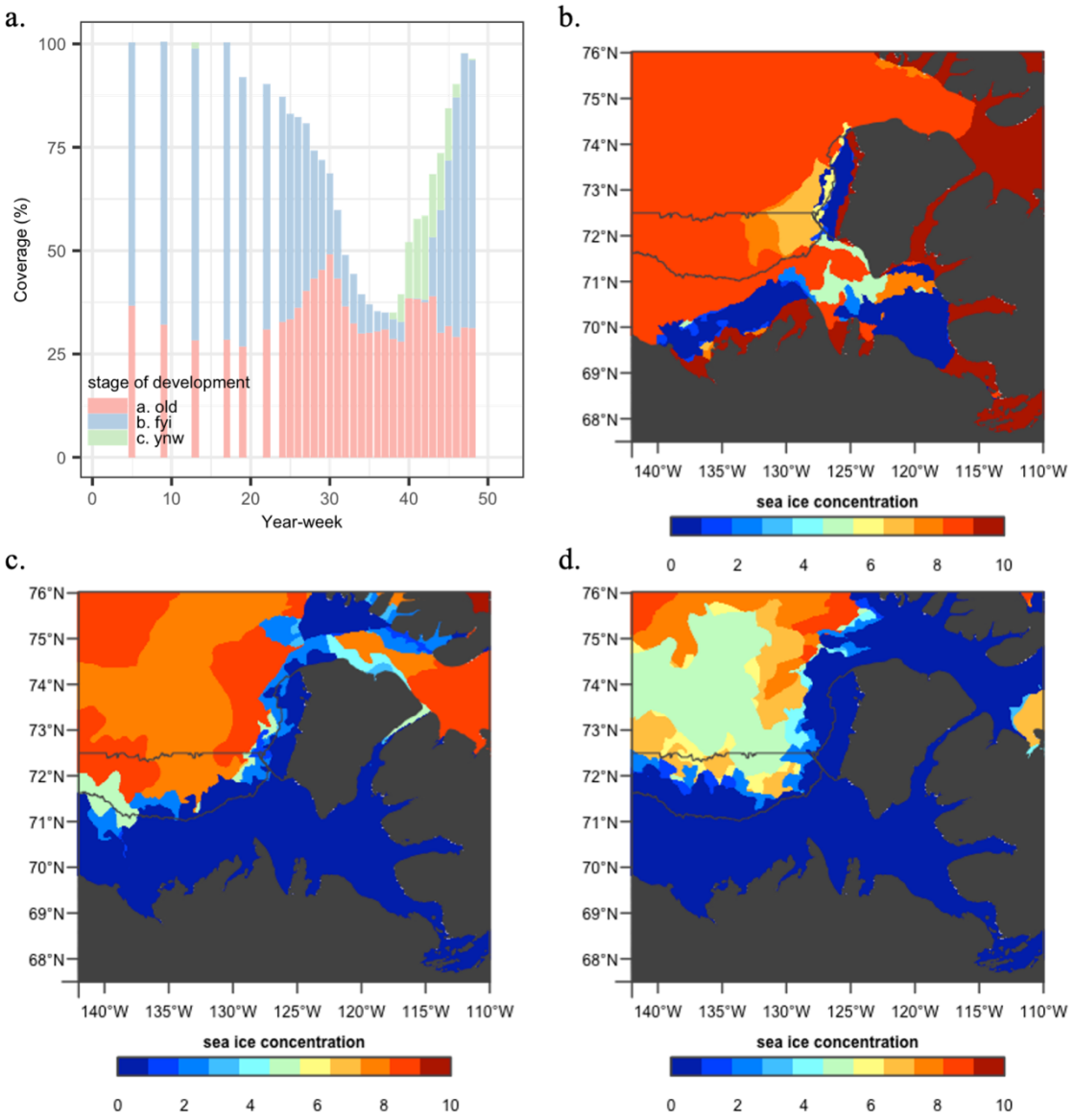

Figure C.2: **(a)** Annual evolution of percent sea-ice coverage by stage of development in 1999, **(b)** minimum sea-ice concentration in year-weeks 18 to 25, **(c)** minimum sea-ice concentration in year-weeks 26 to 33, and **(d)** minimum sea-ice concentration in year-weeks 34 to 41 in 1999.

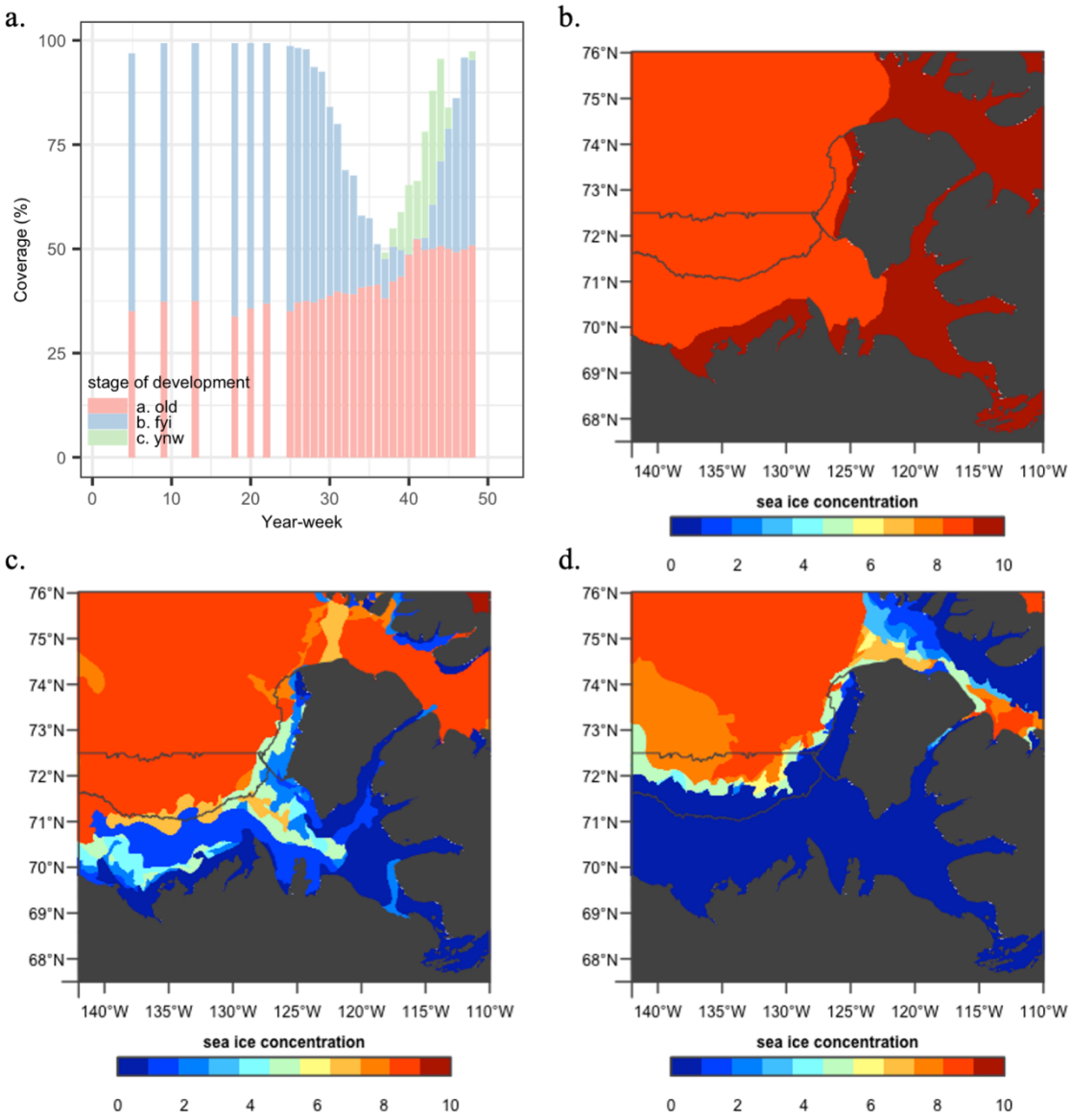

Figure C.3: **(a)** Annual evolution of percent sea-ice coverage by stage of development in 2000, **(b)** minimum sea-ice concentration in year-weeks 18 to 25, **(c)** minimum sea-ice concentration in year-weeks 26 to 33, and **(d)** minimum sea-ice concentration in year-weeks 34 to 41 in 2000.

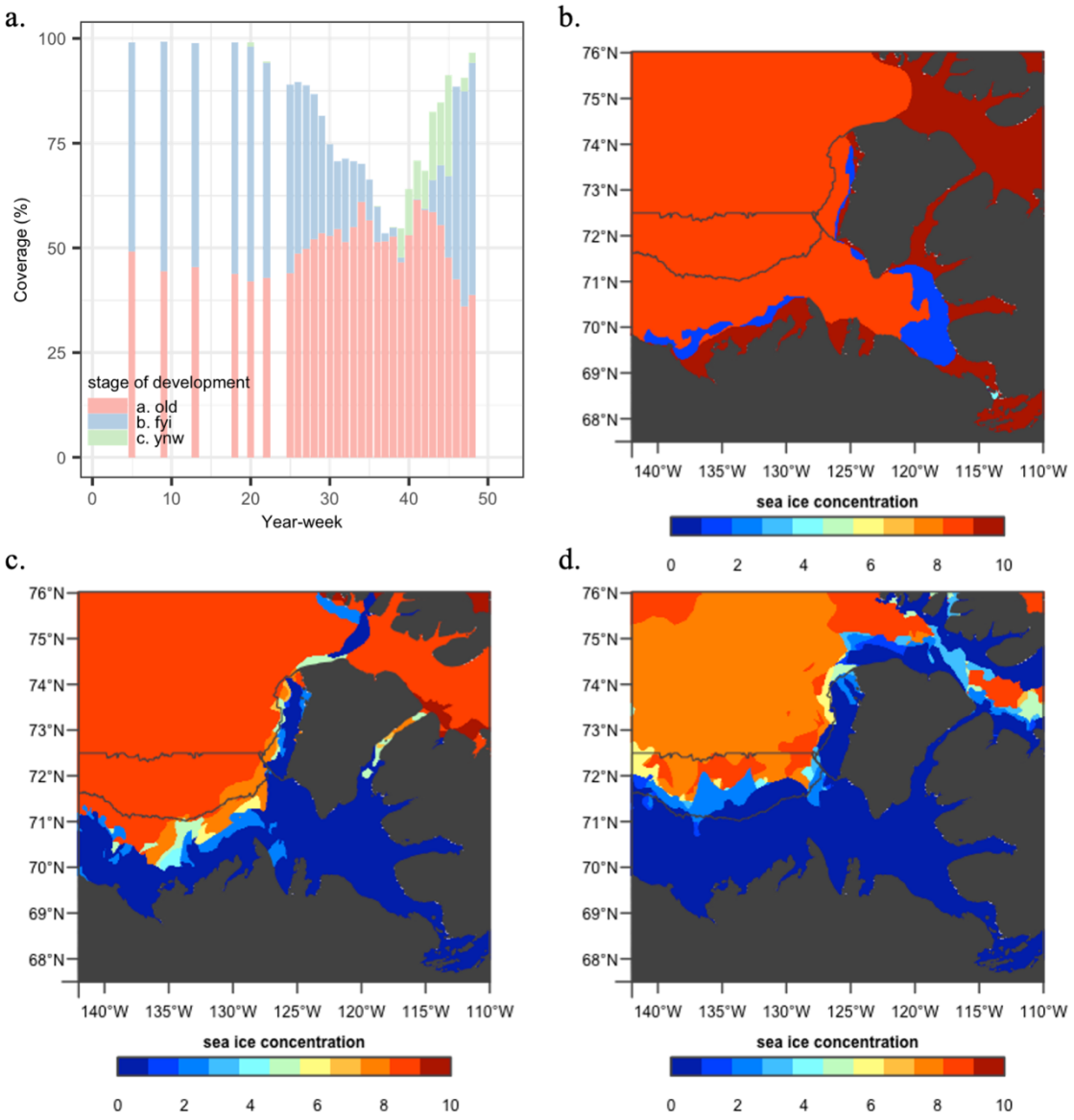

Figure C.4: **(a)** Annual evolution of percent sea-ice coverage by stage of development in 2001, **(b)** minimum sea ice concentration in year-weeks 18 to 25, **(c)** minimum sea-ice concentration in year-weeks 26 to 33, and **(d)** minimum sea-ice concentration in year-weeks 34 to 41 in 2001.

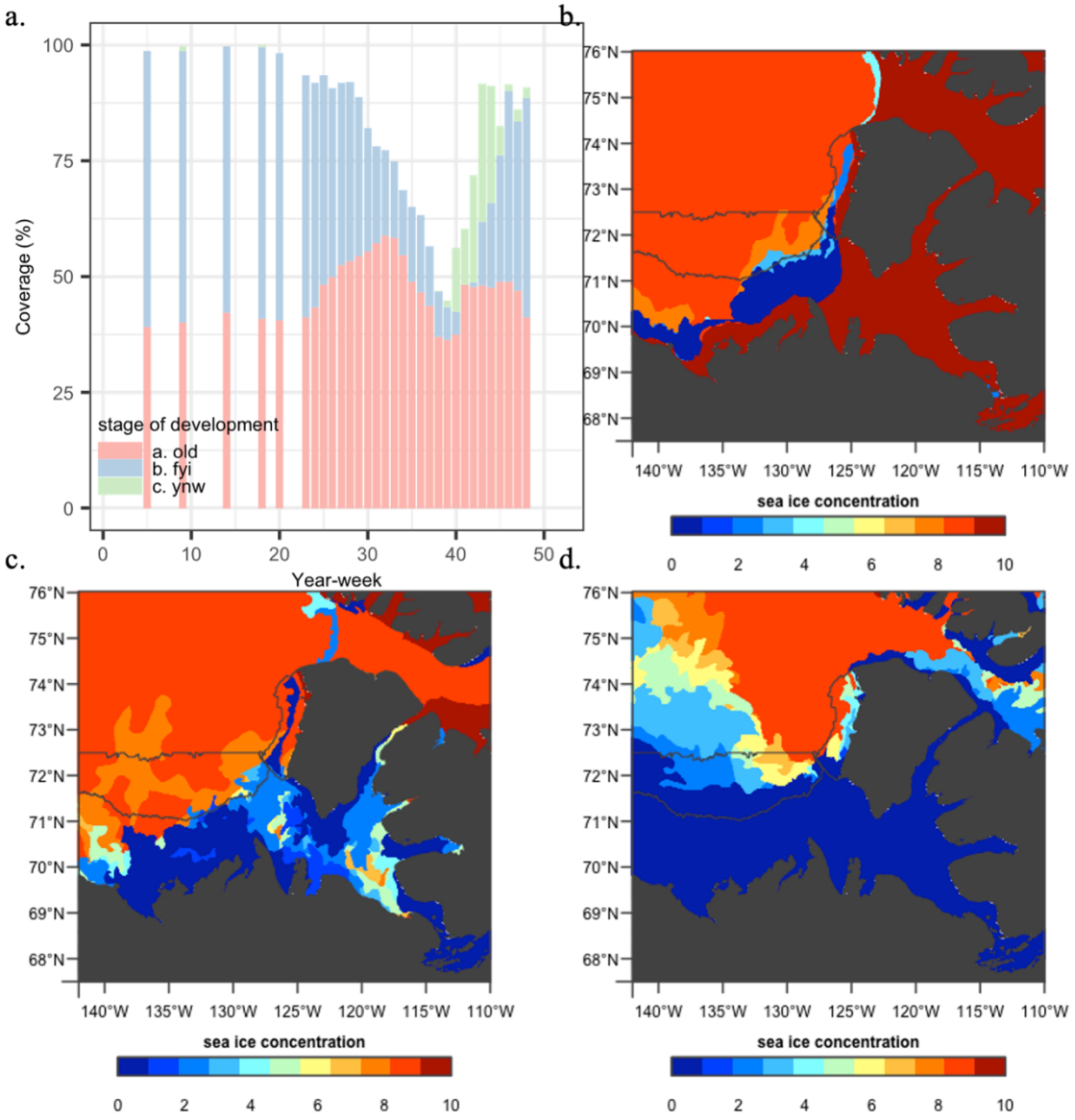

Figure C.5: **(a)** Annual evolution of percent sea-ice coverage by stage of development in 2002, **(b)** minimum sea-ice concentration in year-weeks 18 to 25, **(c)** minimum sea-ice concentration in year-weeks 26 to 33, and **(d)** minimum sea-ice concentration in year-weeks 34 to 41 in 2002.

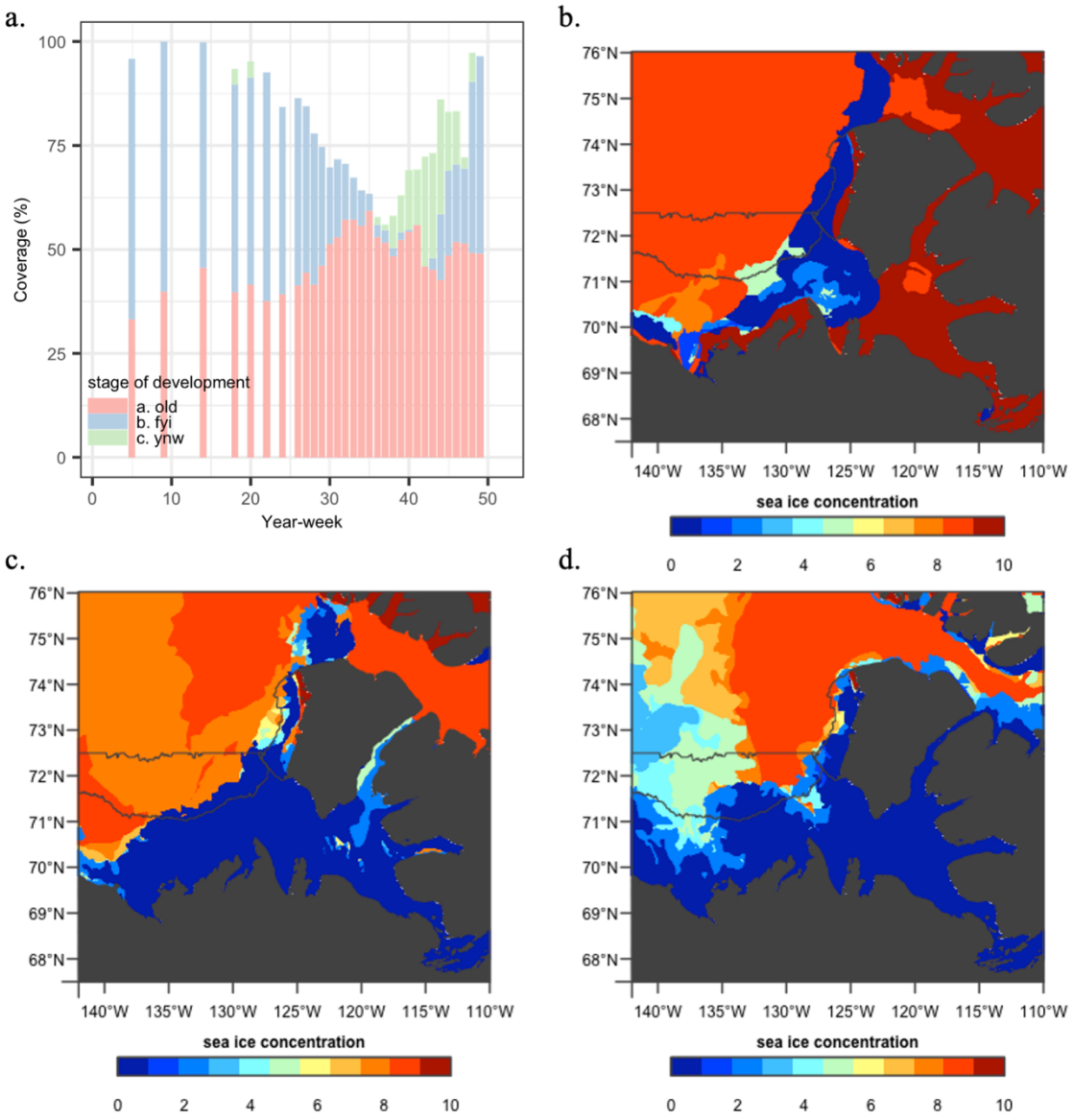

Figure C.6: **(a)** Annual evolution of percent sea-ice coverage by stage of development in 2003, **(b)** minimum sea-ice concentration in year-weeks 18 to 25, **(c)** minimum sea-ice concentration in year-weeks 26 to 33, and **(d)** minimum sea-ice concentration in year-weeks 34 to 41 in 2003.

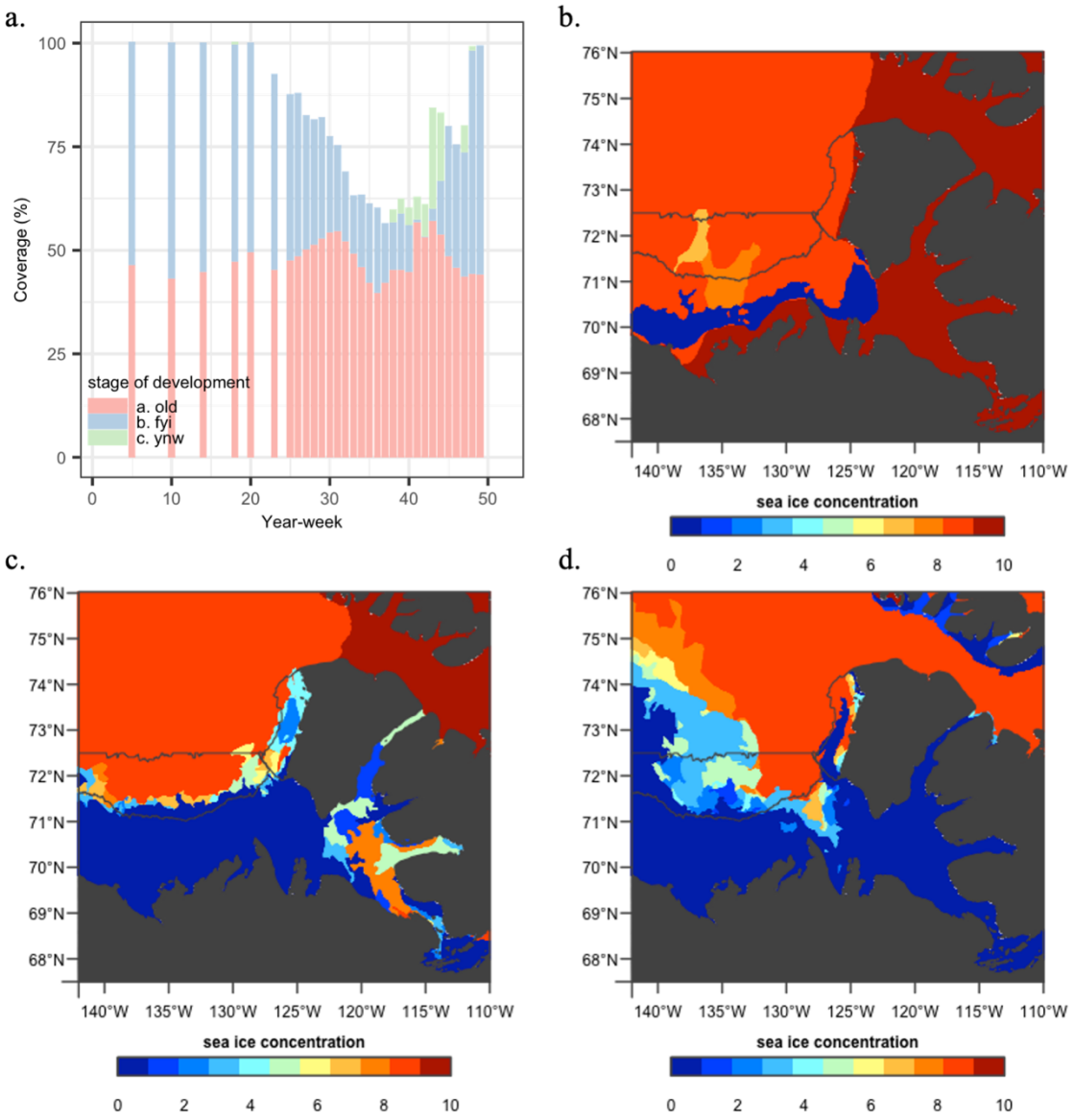

Figure C.7: **(a)** Annual evolution of percent sea-ice coverage by stage of development in 2004, **(b)** minimum sea-ice concentration in year-weeks 18 to 25, **(c)** minimum sea-ice concentration in year-weeks 26 to 33, and **(d)** minimum sea-ice concentration in year-weeks 34 to 41 in 2004.

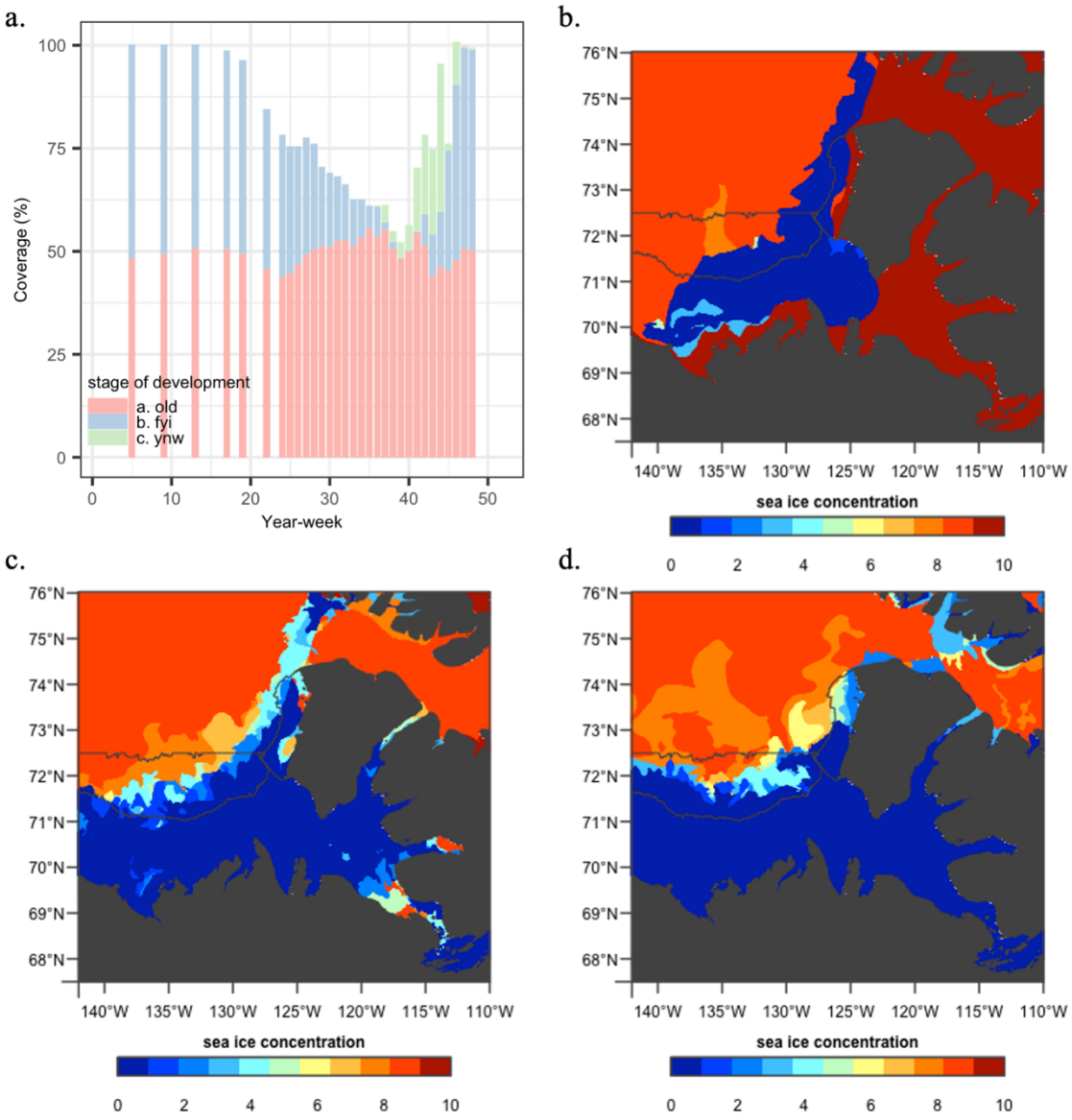

Figure C.8: **(a)** Annual evolution of percent sea-ice coverage by stage of development in 2005, **(b)** minimum sea-ice concentration in year-weeks 18 to 25, **(c)** minimum sea-ice concentration in year-weeks 26 to 33, and **(d)** minimum sea-ice concentration in year-weeks 34 to 41 in 2005.

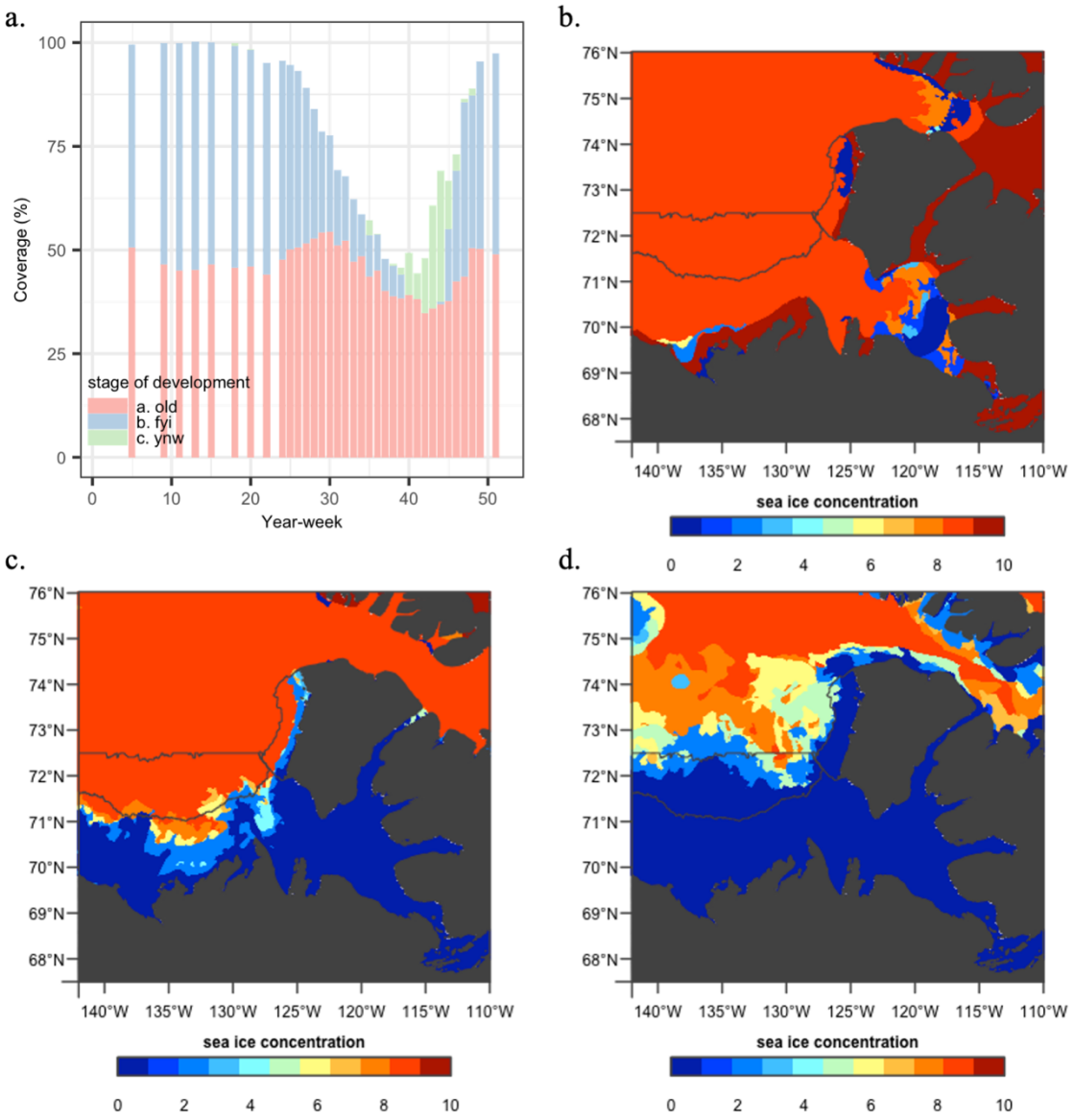

Figure C.9: **(a)** Annual evolution of percent sea-ice coverage by stage of development in 2006, **(b)** minimum sea-ice concentration in year-weeks 18 to 25, **(c)** minimum sea-ice concentration in year-weeks 26 to 33, and **(d)** minimum sea-ice concentration in year-weeks 34 to 41 in 2006.

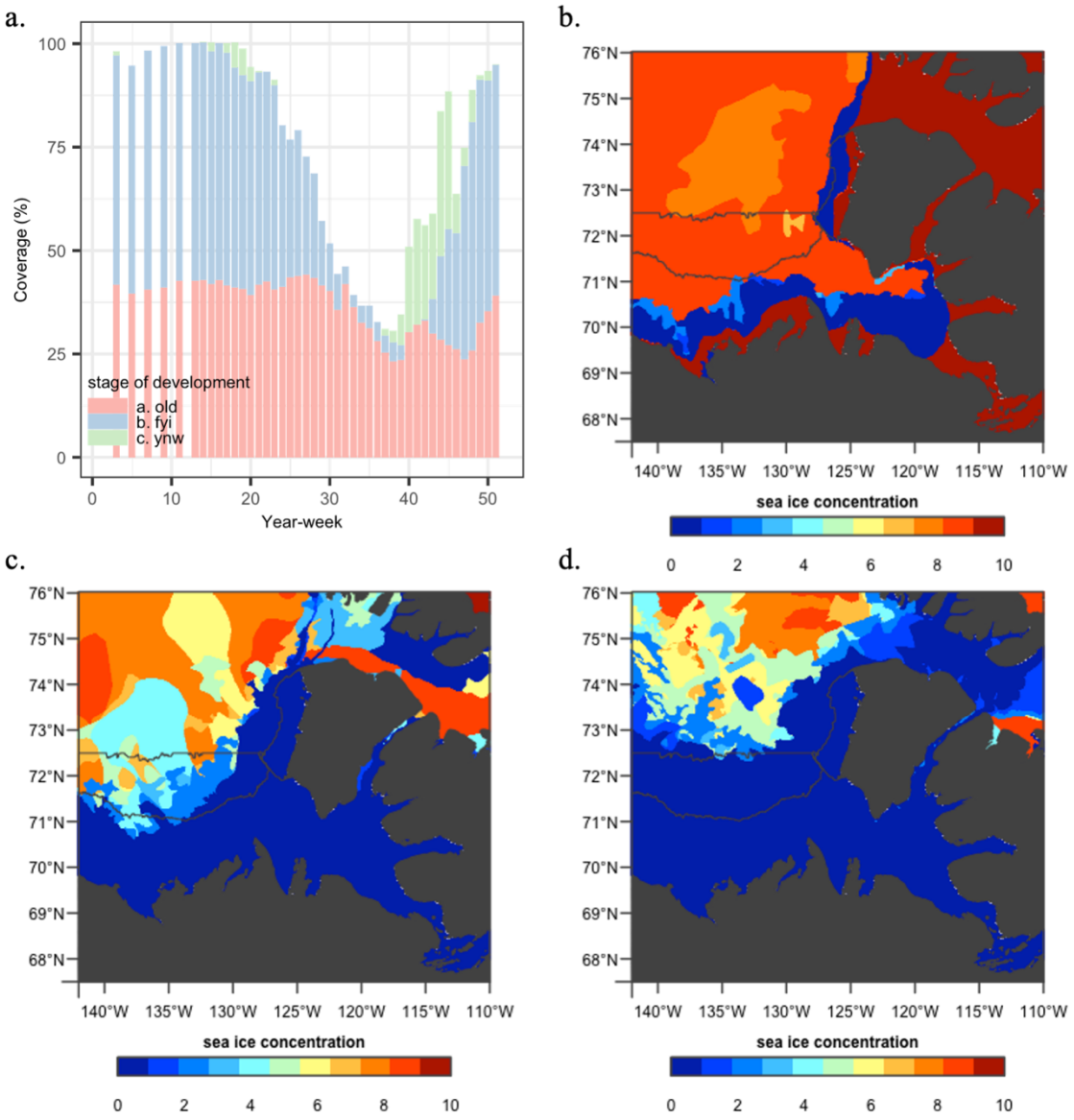

Figure C.10: **(a)** Annual evolution of percent sea-ice coverage by stage of development in 2007, **(b)** minimum sea-ice concentration in year-weeks 18 to 25, **(c)** minimum sea-ice concentration in year-weeks 26 to 33, and **(d)** minimum sea-ice concentration in year-weeks 34 to 41 in 2007.

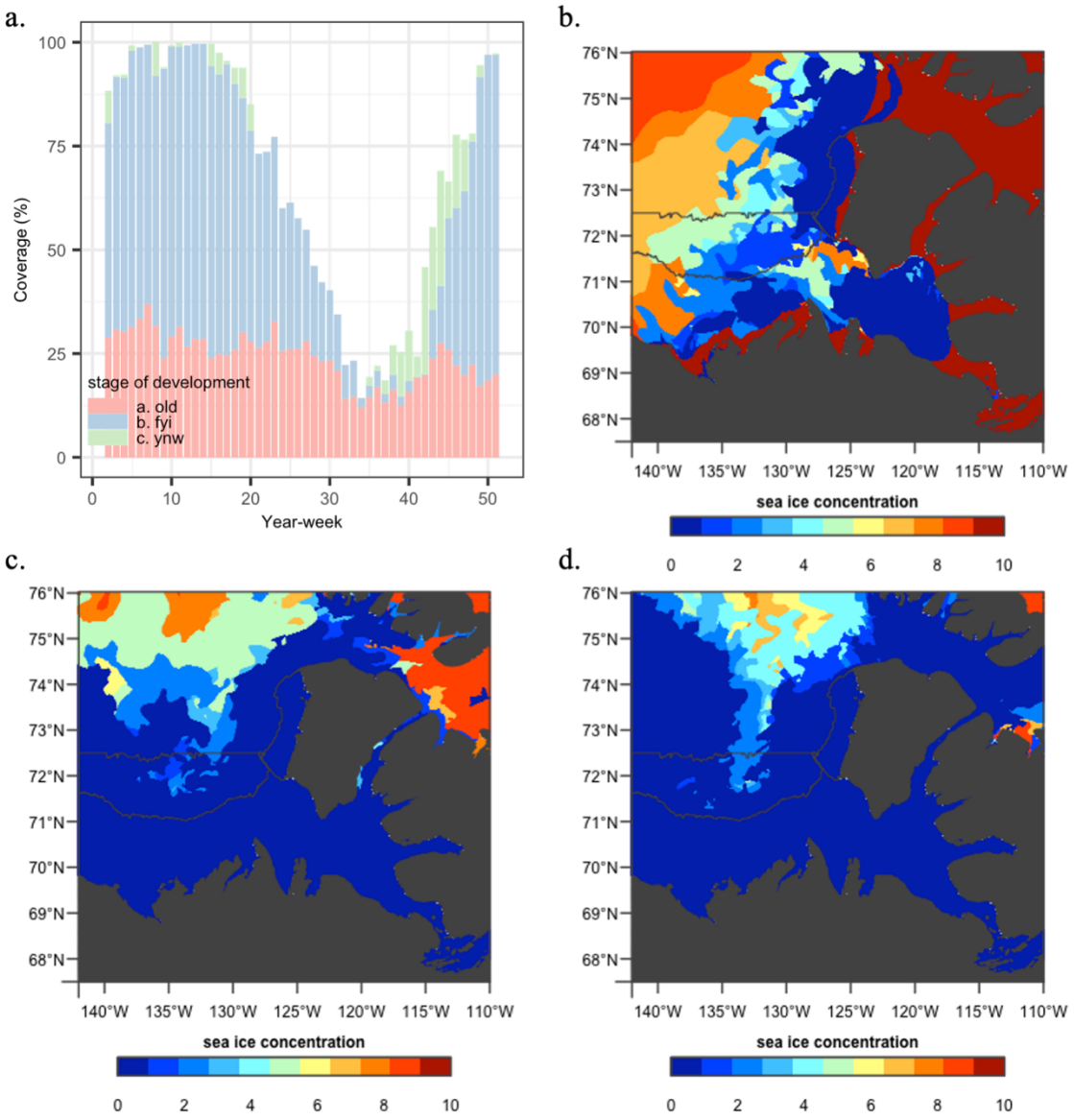

Figure C.11: **(a)** Annual evolution of percent sea-ice coverage by stage of development in 2008, **(b)** minimum sea-ice concentration in year-weeks 18 to 25, **(c)** minimum sea-ice concentration in year-weeks 26 to 33, and **(d)** minimum sea-ice concentration in year-weeks 34 to 41 in 2008.

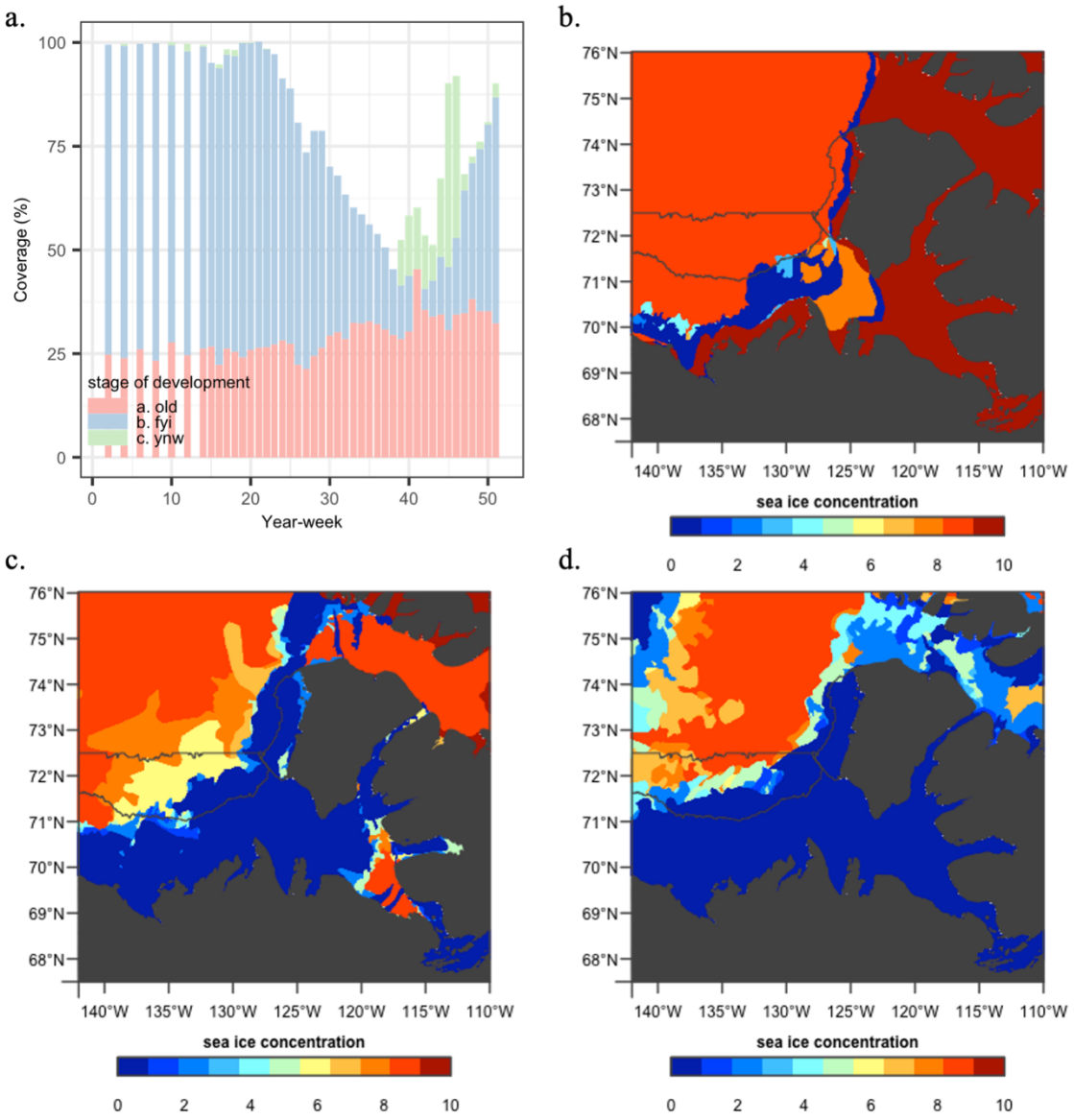

Figure C.12: **(a)** Annual evolution of percent sea-ice coverage by stage of development in 2009, **(b)** minimum sea-ice concentration in year-weeks 18 to 25, **(c)** minimum sea-ice concentration in year-weeks 26 to 33, and **(d)** minimum sea-ice concentration in year-weeks 34 to 41 in 2009.

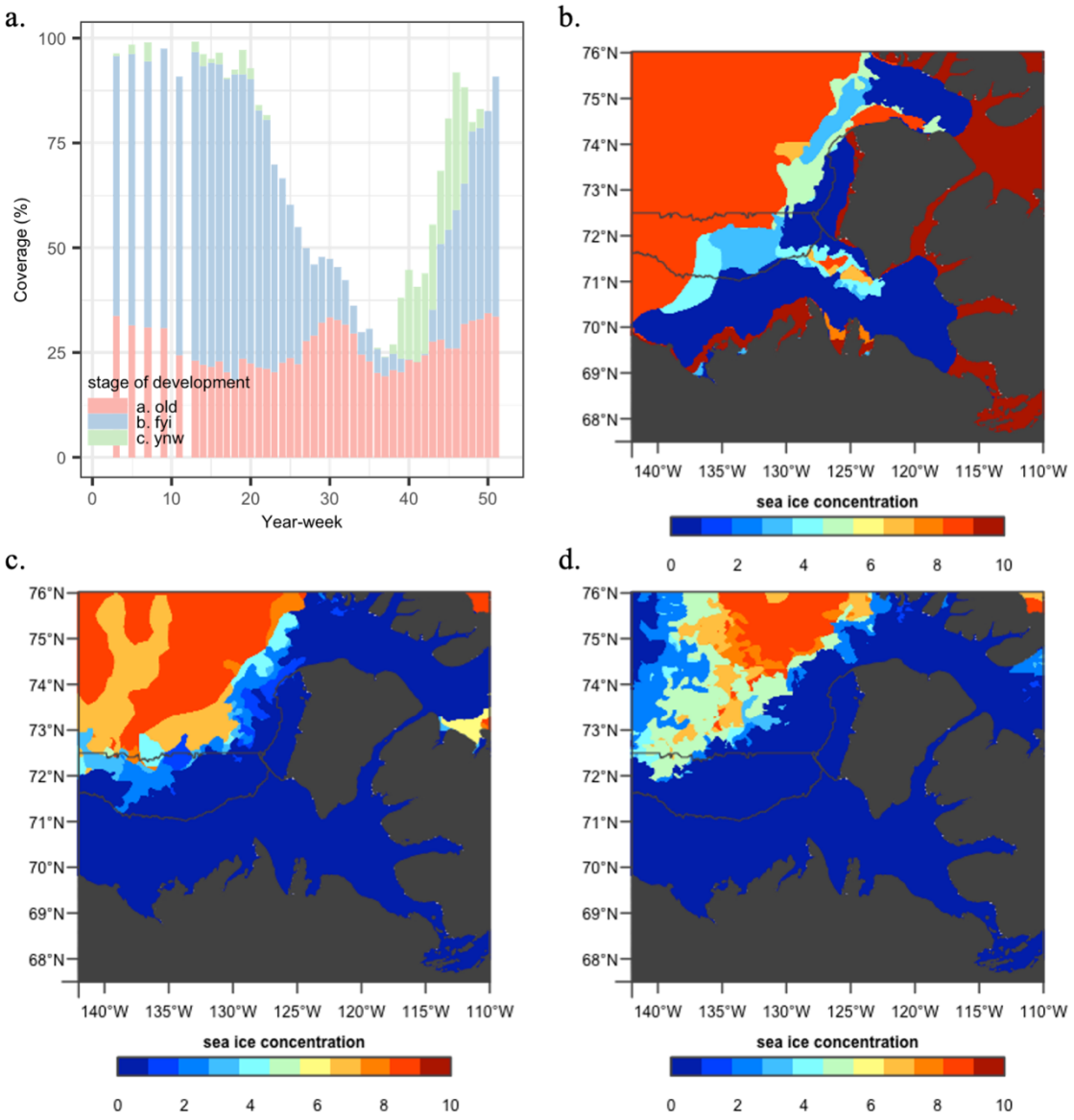

Figure C.13: **(a)** Annual evolution of percent sea-ice coverage by stage of development in 2010, **(b)** minimum sea-ice concentration in year-weeks 18 to 25, **(c)** minimum sea-ice concentration in year-weeks 26 to 33, and **(d)** minimum sea-ice concentration in year-weeks 34 to 41 in 2010.

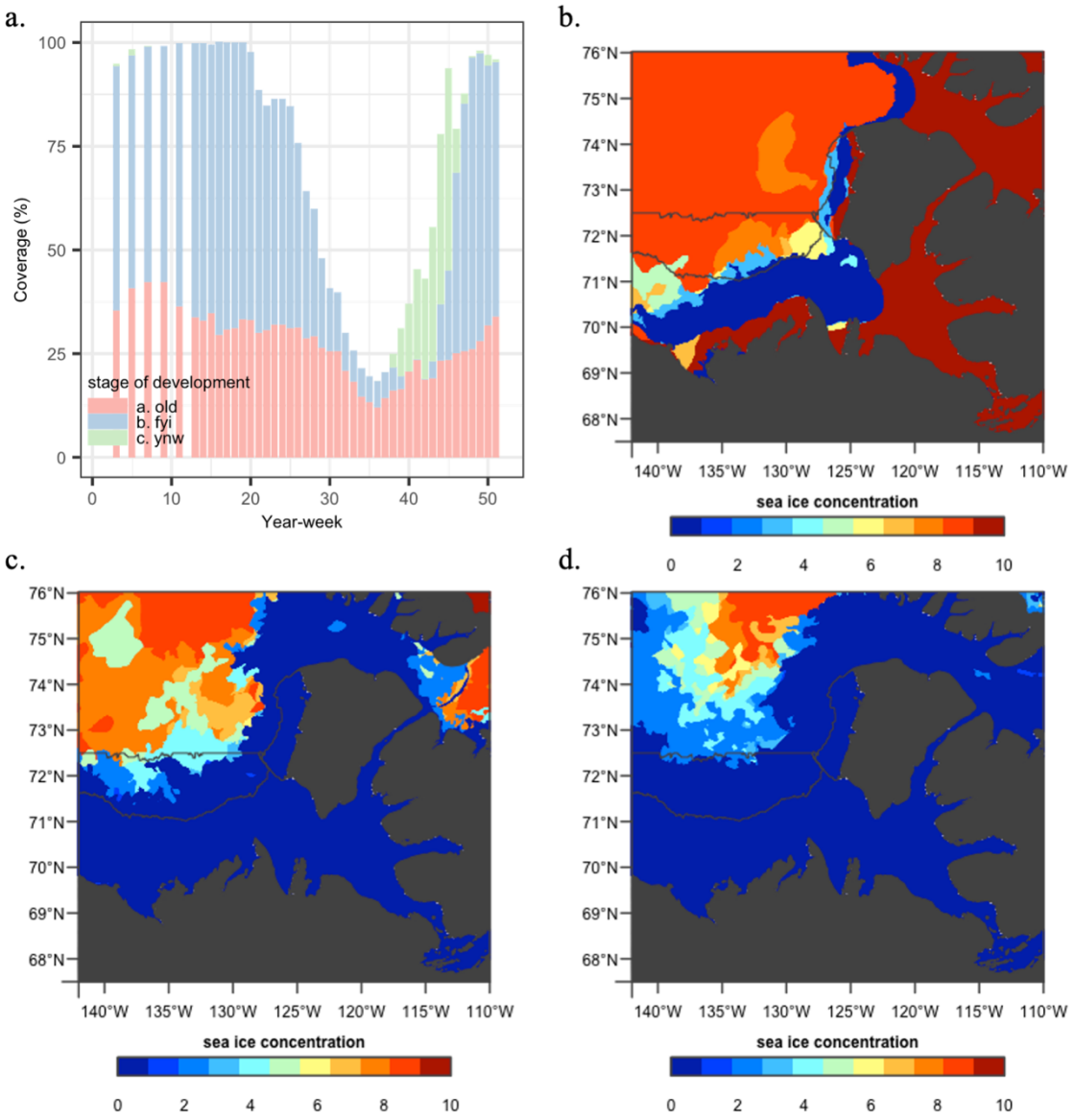

Figure C.14: **(a)** Annual evolution of percent sea-ice coverage by stage of development in 2011, **(b)** minimum sea-ice concentration in year-weeks 18 to 25, **(c)** minimum sea-ice concentration in year-weeks 26 to 33, and **(d)** minimum sea-ice concentration in year-weeks 34 to 41 in 2011.

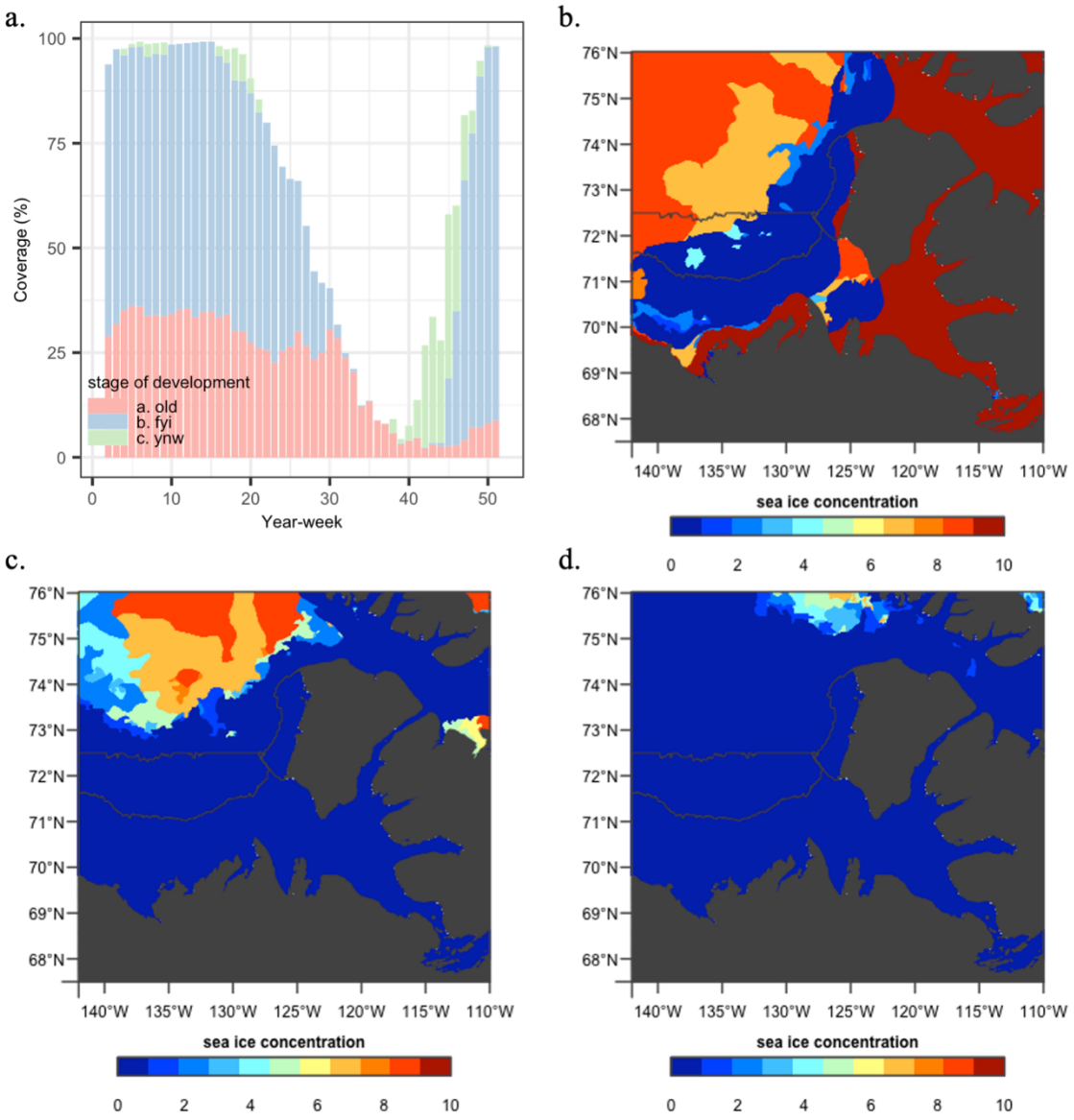

Figure C.15: **(a)** Annual evolution of percent sea-ice coverage by stage of development in 2012, **(b)** minimum sea-ice concentration in year-weeks 18 to 25, **(c)** minimum sea-ice concentration in year-weeks 26 to 33, and **(d)** minimum sea-ice concentration in year-weeks 34 to 41 in 2012.

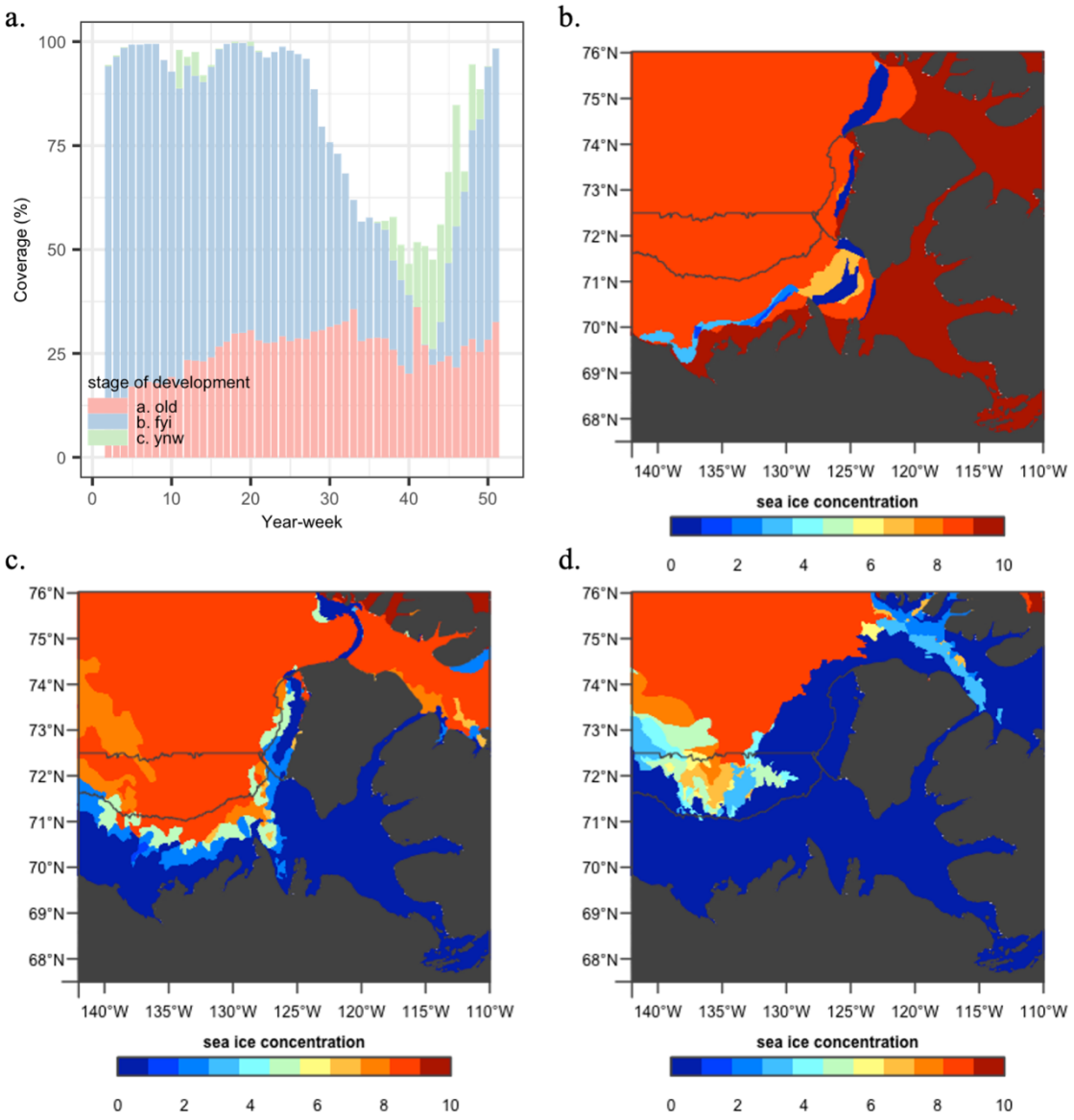

Figure C.16: **(a)** Annual evolution of percent sea-ice coverage by stage of development in 2013, **(b)** minimum sea-ice concentration in year-weeks 18 to 25, **(c)** minimum sea-ice concentration in year-weeks 26 to 33, and **(d)** minimum sea-ice concentration in year-weeks 34 to 41 in 2013.

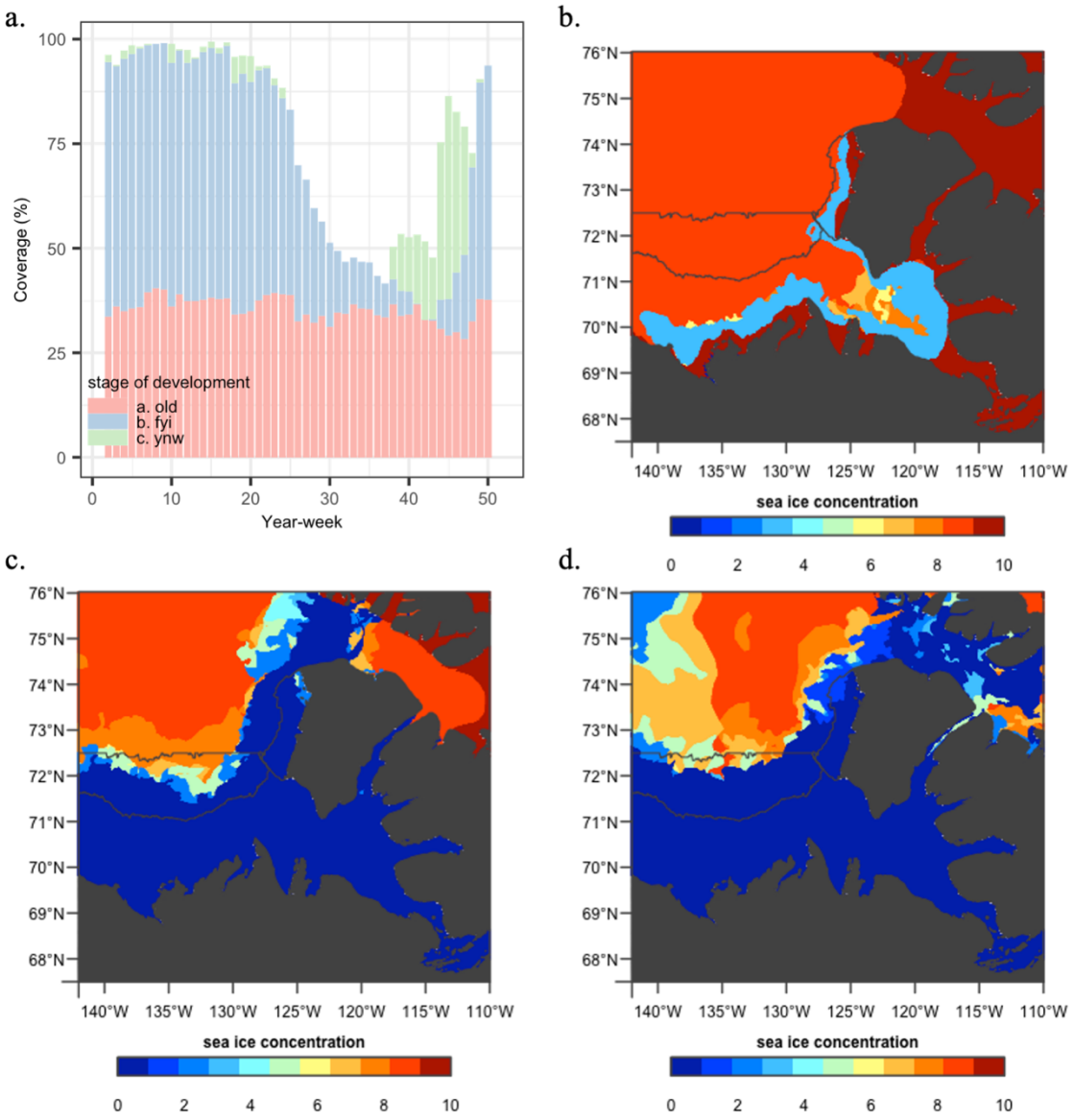

Figure C.17: **(a)** Annual evolution of percent sea-ice coverage by stage of development in 2014, **(b)** minimum sea-ice concentration in year-weeks 18 to 25, **(c)** minimum sea-ice concentration in year-weeks 26 to 33, and **(d)** minimum sea-ice concentration in year-weeks 34 to 41 in 2014.

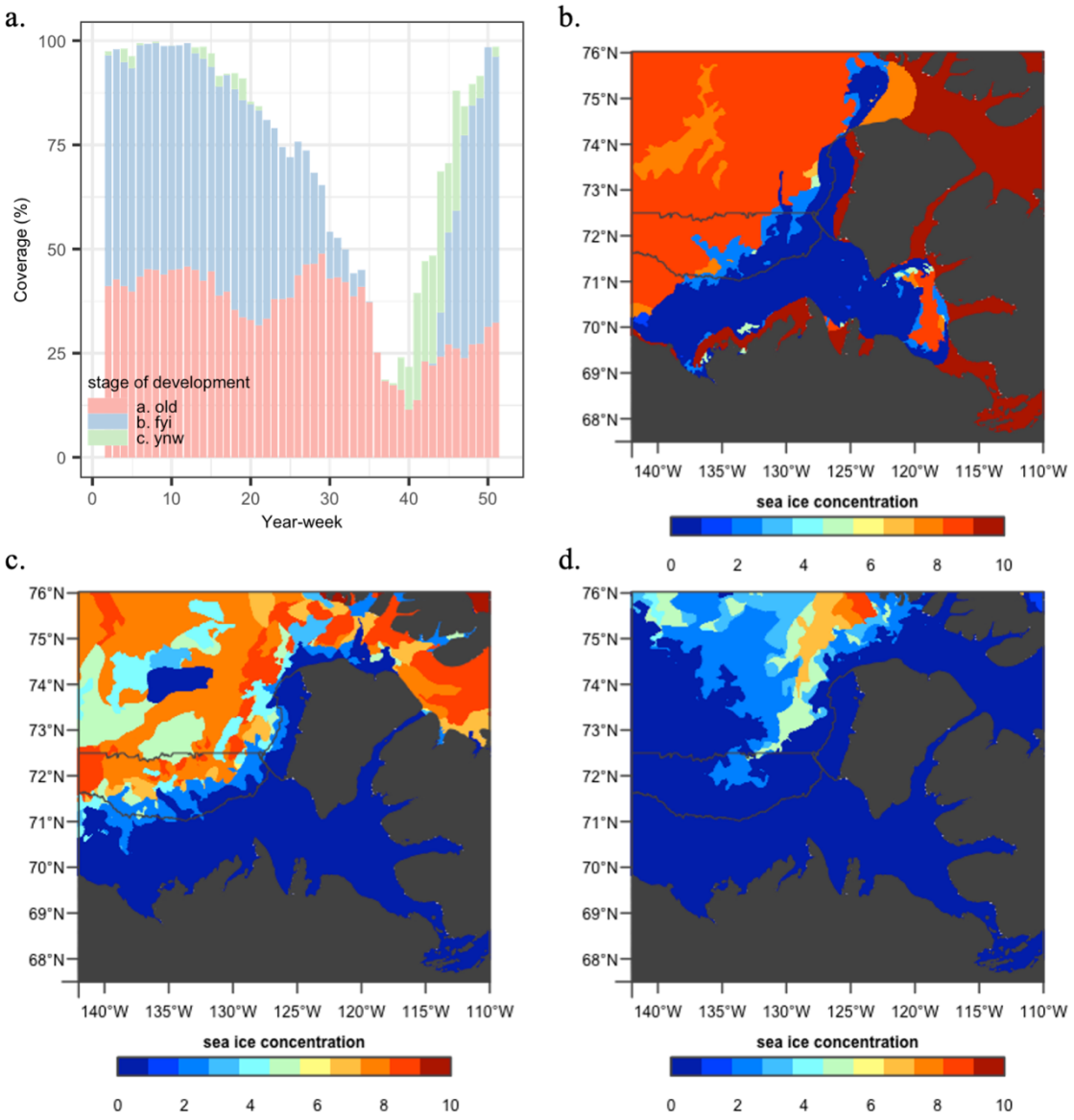

Figure C.18: **(a)** Annual evolution of percent sea-ice coverage by stage of development in 2015, **(b)** minimum sea-ice concentration in year-weeks 18 to 25, **(c)** minimum sea-ice concentration in year-weeks 26 to 33, and **(d)** minimum sea-ice concentration in year-weeks 34 to 41 in 2015.

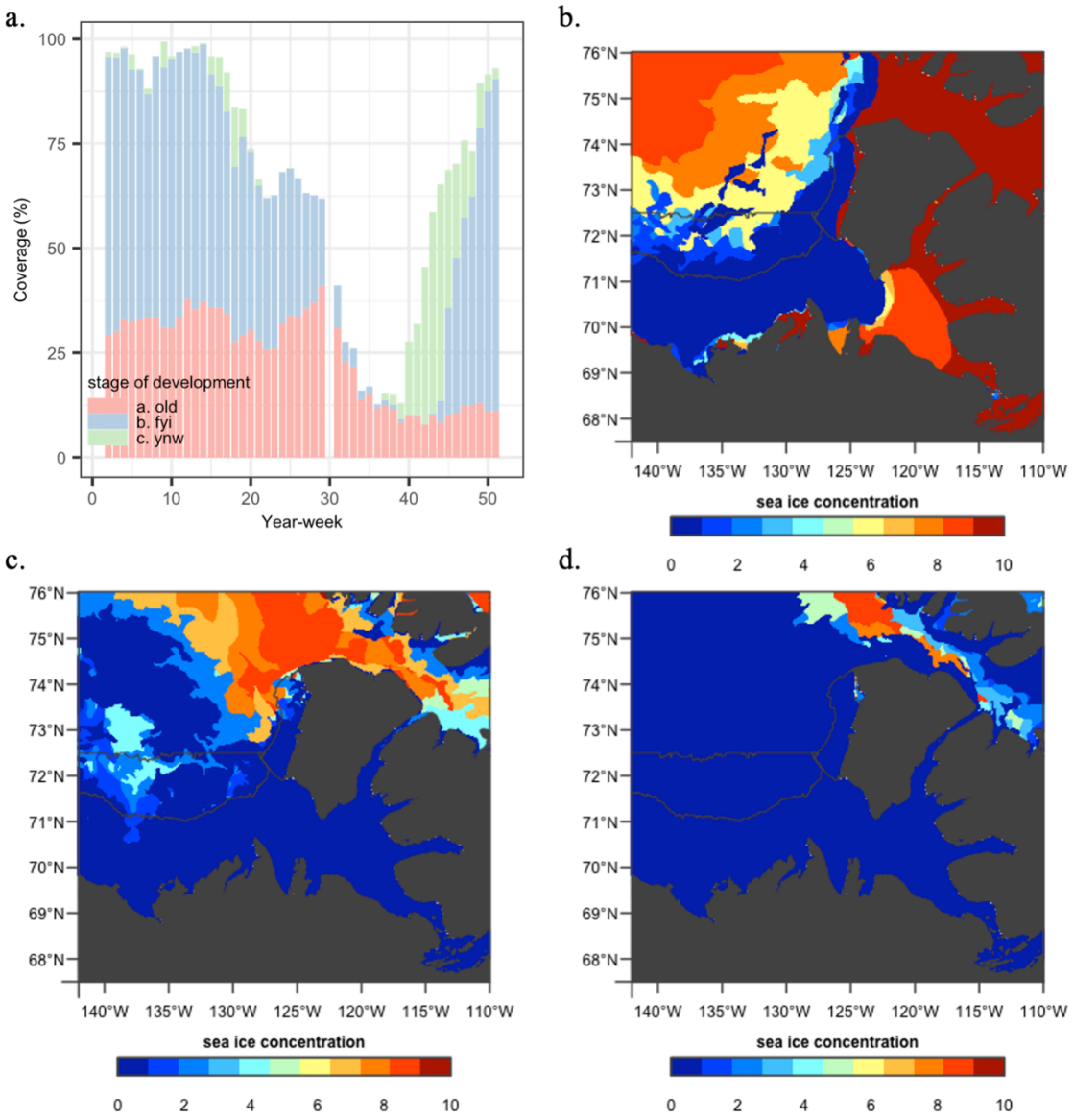

Figure C.19: **(a)** Annual evolution of percent sea-ice coverage by stage of development in 2016, **(b)** minimum sea-ice concentration in year-weeks 18 to 25, **(c)** minimum sea-ice concentration in year-weeks 26 to 33, and **(d)** minimum sea-ice concentration in year-weeks 34 to 41 in 2016.

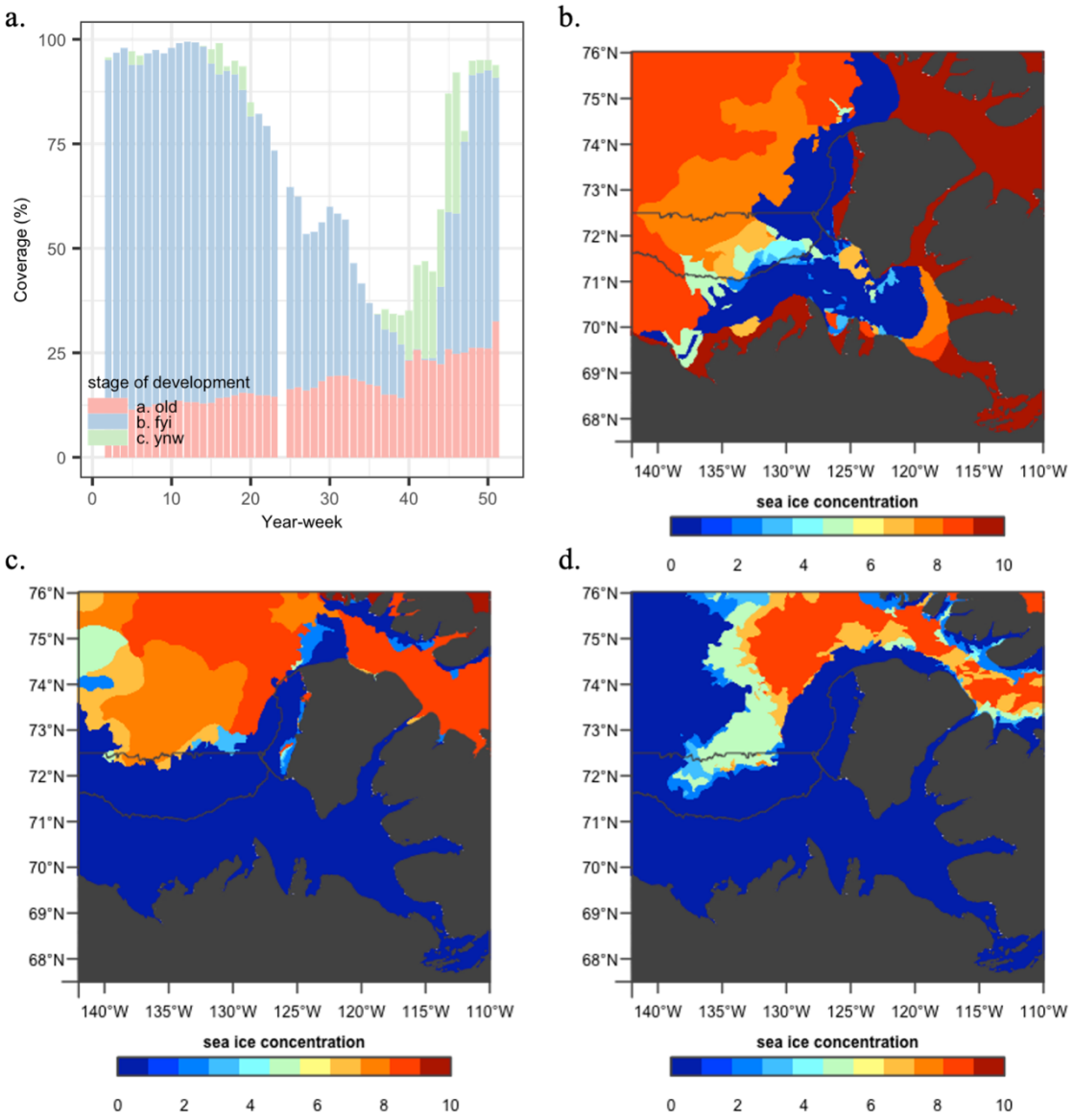

Figure C.20: **(a)** Annual evolution of percent sea-ice coverage by stage of development in 2017, **(b)** minimum sea-ice concentration in year-weeks 18 to 25, **(c)** minimum sea-ice concentration in year-weeks 26 to 33, and **(d)** minimum sea-ice concentration in year-weeks 34 to 41 in 2017.

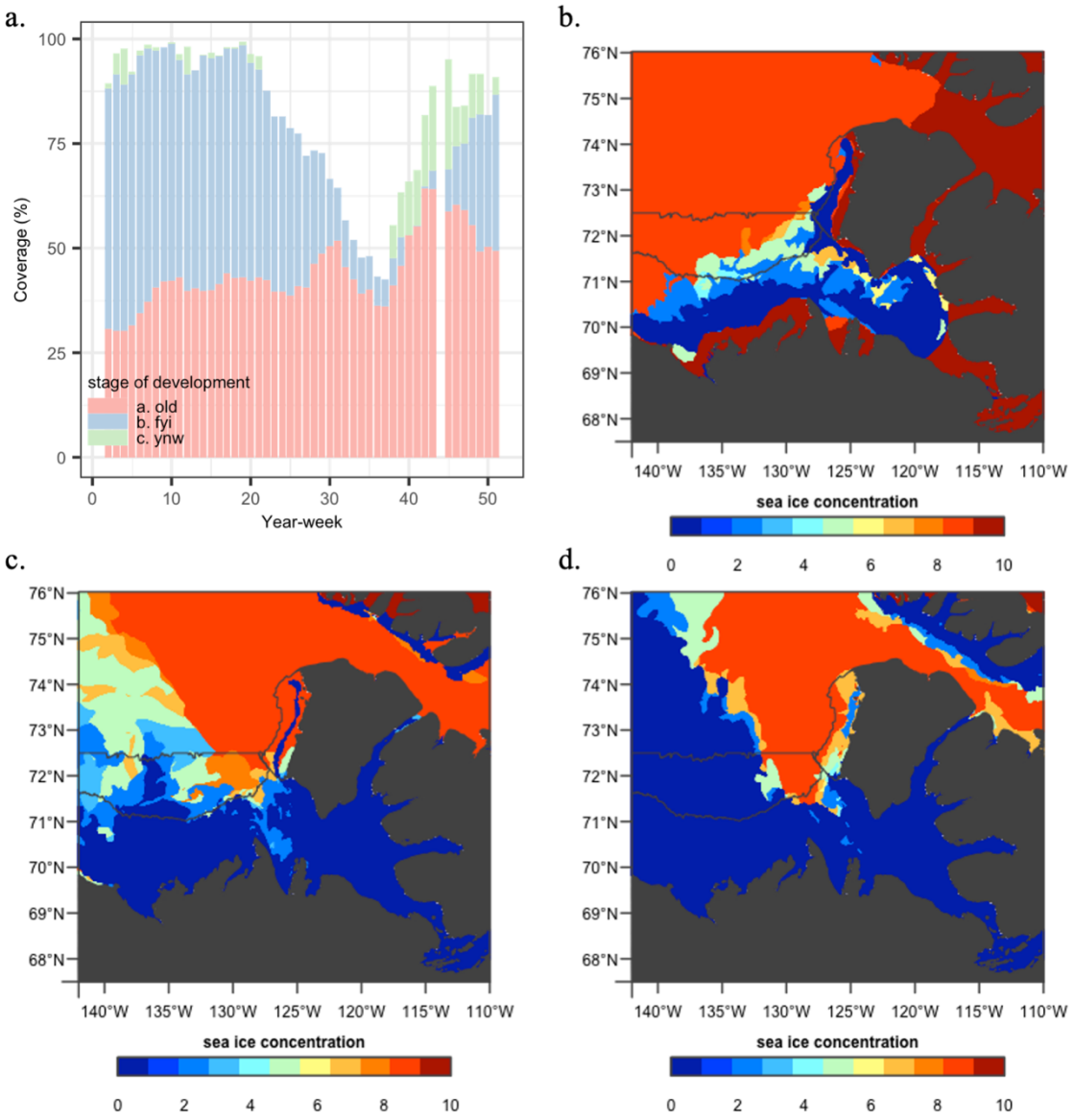

Figure C.21: **(a)** Annual evolution of percent sea-ice coverage by stage of development in 2018, **(b)** minimum sea-ice concentration in year-weeks 18 to 25, **(c)** minimum sea-ice concentration in year-weeks 26 to 33, and **(d)** minimum sea-ice concentration in year-weeks 34 to 41 in 2018.

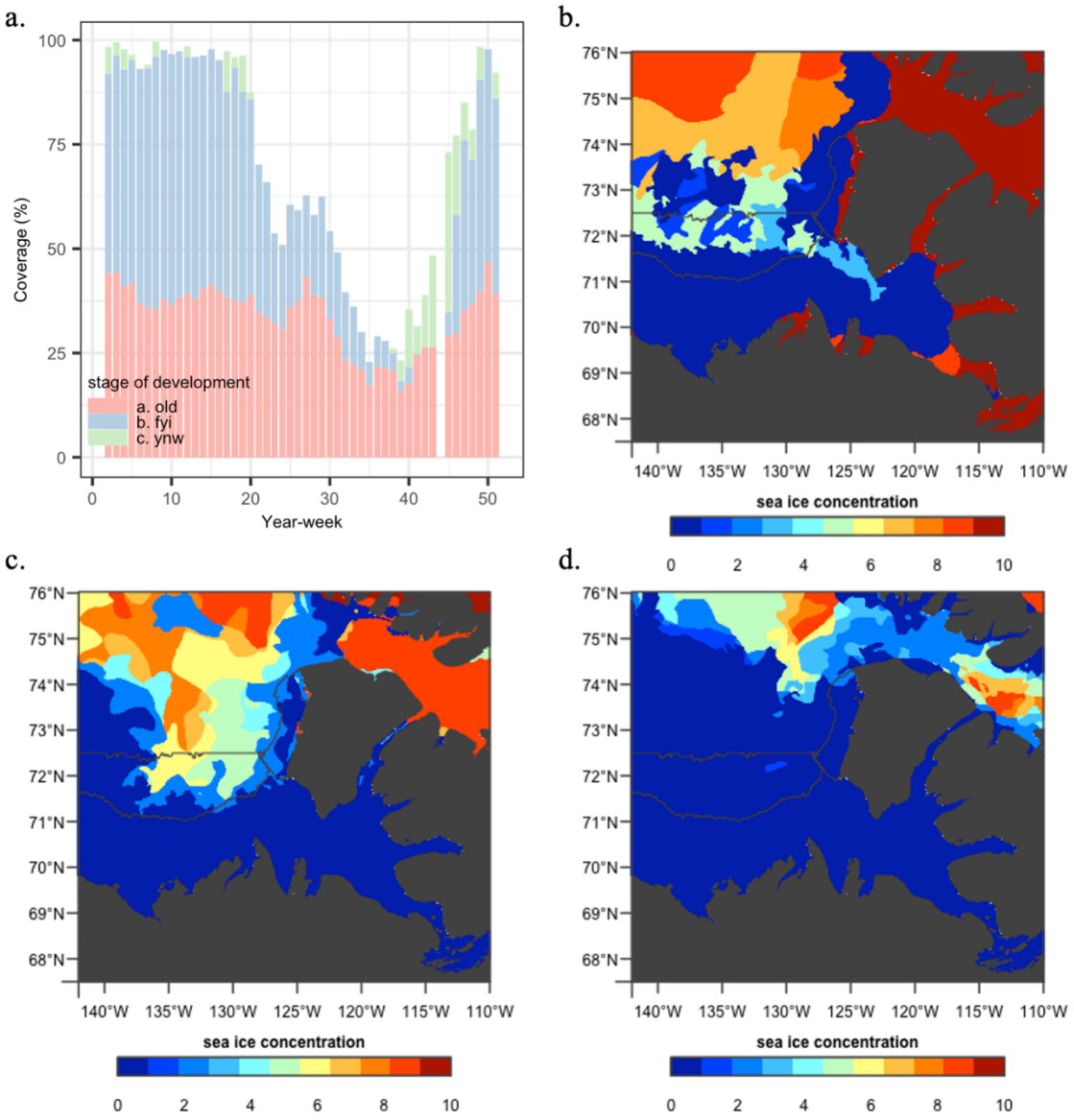

Figure C.22: **(a)** Annual evolution of percent sea-ice coverage by stage of development in 2019, **(b)** minimum sea-ice concentration in year-weeks 18 to 25, **(c)** minimum sea-ice concentration in year-weeks 26 to 33, and **(d)** minimum sea-ice concentration in year-weeks 34 to 41 in 2019.

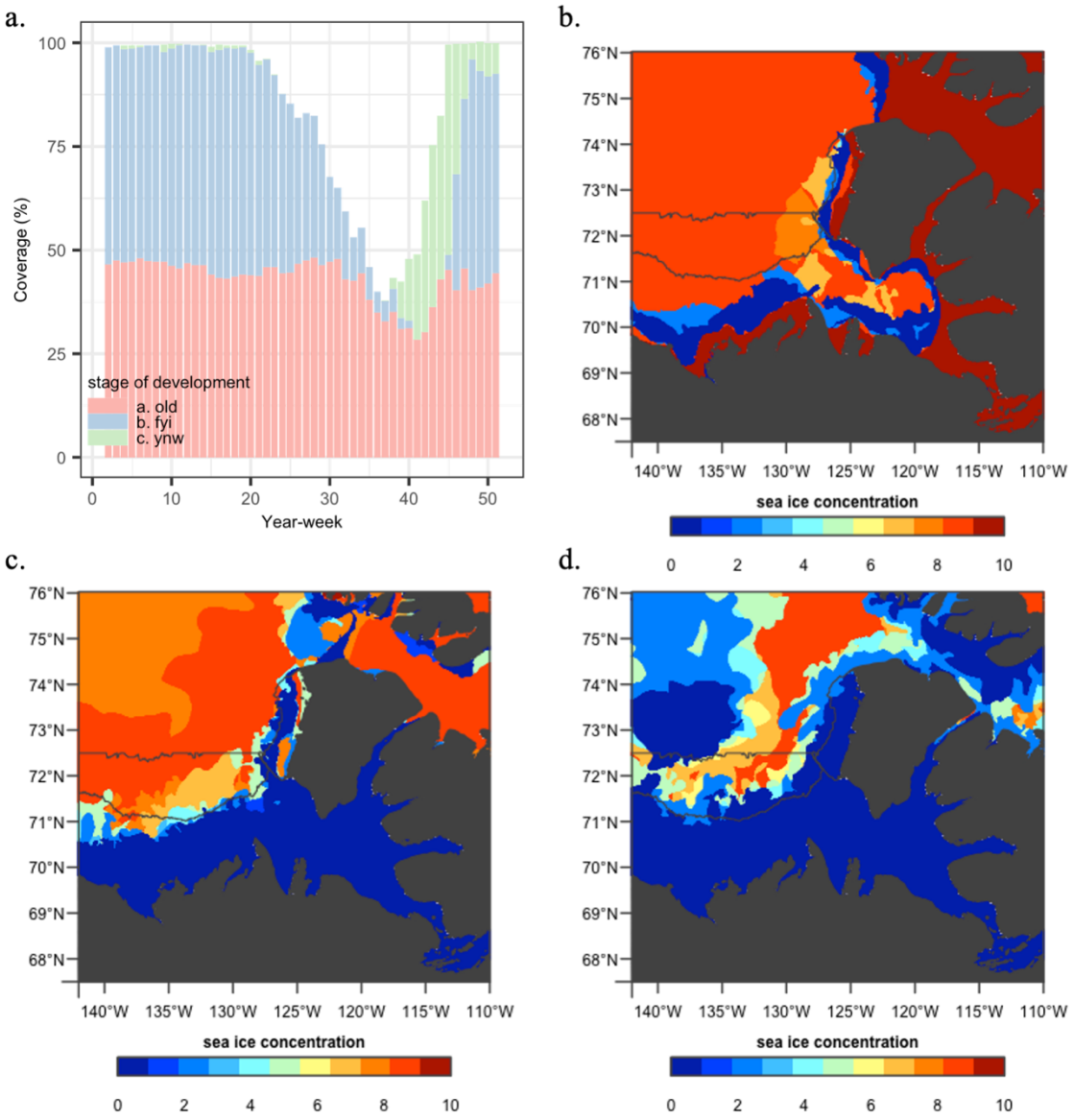

Figure C.23: **(a)** Annual evolution of percent sea-ice coverage by stage of development in 2020, **(b)** minimum sea-ice concentration in year-weeks 18 to 25, **(c)** minimum sea-ice concentration in year-weeks 26 to 33, and **(d)** minimum sea-ice concentration in year-weeks 34 to 41 in 2020.

D Mean sea-ice concentration in the study subregions

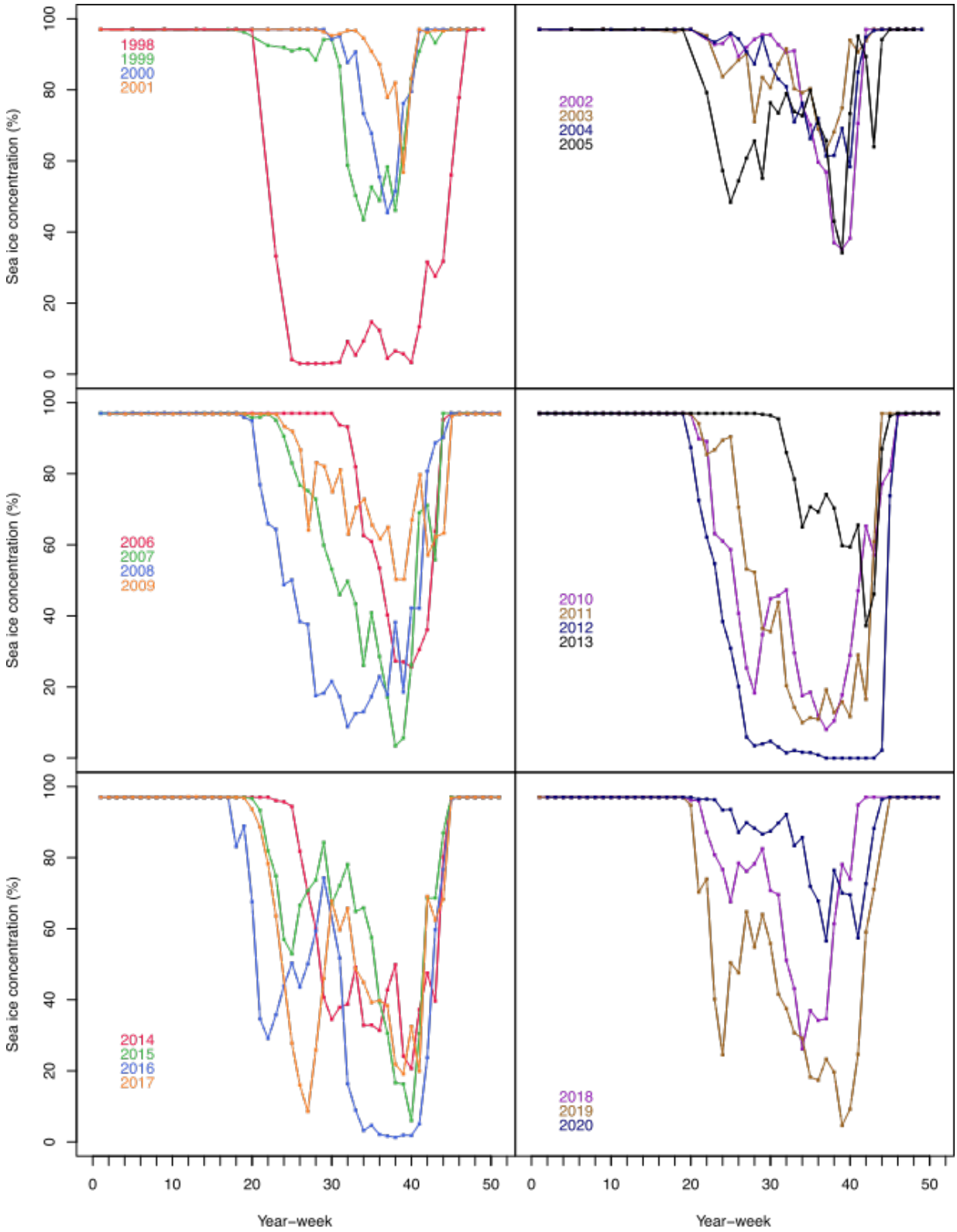

Figure D.1: Annual evolution of the mean sea-ice concentration in the Offshore Beaufort Sea subregion from 1998 – 2020.

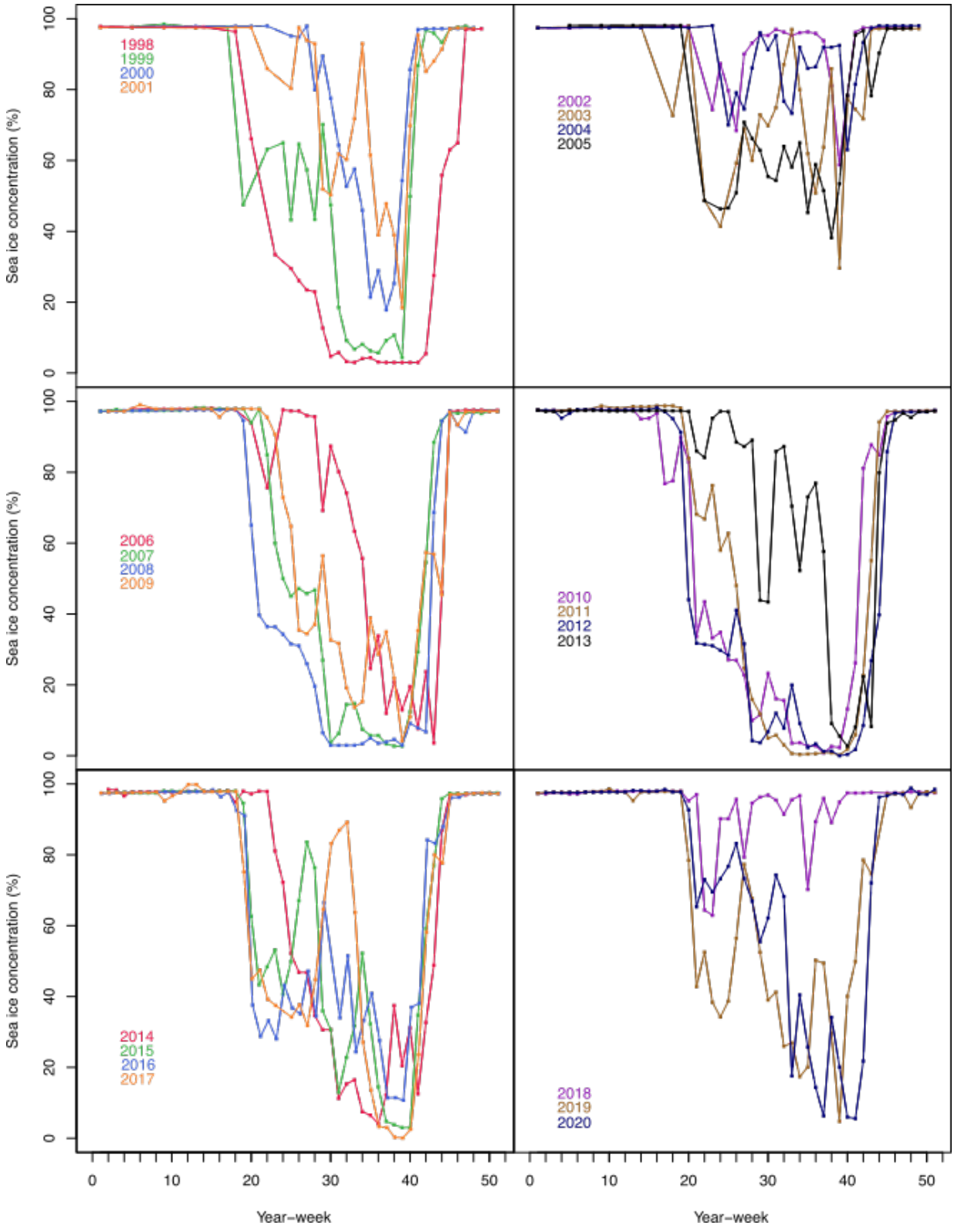

Figure D.2: Annual evolution of the mean sea-ice concentration in the Western Banks Island subregion from 1998 – 2020